Characterisation of the Hyperpolarisation Activated Chloride Current in Rat Superior Cervical Ganglion Neurons.

SAMANTHA AMANDA CLARK

A thesis submitted for the degree of Doctor of Philosophy

Department of Pharmacology
Royal Free Hospital School of Medicine
Rowland Hill Street
London NW3 2PF

1996

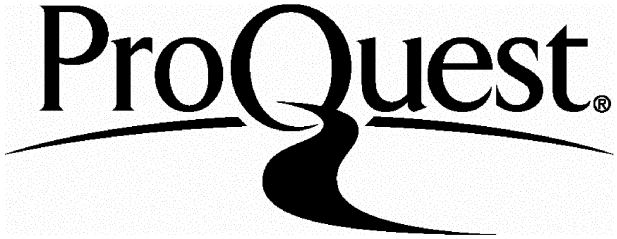

ABSTRACT

Although the cation currents that are found in rat superior cervical ganglia (SCG) neurons have been extensively studied and characterised, the chloride conductances in these neurons have not. The aim of the experiments presented here was to characterise a number of features of the hyperpolarisation activated current that is present in rat SCG neurons.

The current was found to activate at potentials hyperpolarised to -20mV in a time and voltage dependent manner. Current activation was inwardly rectifying. Inactivation was not observed and the activation kinetics were best described by two exponential functions. The current was unaffected by changes in the external potassium and/or sodium concentrations and was not blocked by either 10mM barium or caesium. The reversal potential, however, was approximately 0mV which agreed with the chloride equilibrium potential. The hyperpolarisation activated current was therefore carried by chloride ions and was designated $I_{Cl_{IR}}$. The halide selectivity sequence of $I_{Cl_{IR}}$ was Cl > Br > I.

$I_{Cl_{IR}}$ was blocked in a voltage dependant manner by cadmium, zinc and the organic chloride channel blockers; DIDS, 9AC and NPPB. $I_{Cl_{IR}}$ was not, however, affected by the application of SITS or niflumic acid. Acidification and alkalisation of the external medium resulted in a voltage dependent increase and decrease in the amplitude of $I_{Cl_{IR}}$ respectively. In addition, $I_{Cl_{IR}}$ was found to be sensitive to external hypotonicity.

The properties of $I_{Cl_{IR}}$ described are almost identical to those of ClC-2 and mRNA for ClC-2 was found to be expressed in rat SCG neurons by RT-PCR. It therefore seems very likely that the ClC-2 chloride channel underlies $I_{Cl_{IR}}$ in these cells.

INDEX

List of figures.

Chapter 1: General introduction.

Chapter 2: Methods.

Chapter 3: Biophysical characteristics and ionic selectivity of the hyperpolarisation activated current in rat SCG neurons.

Chapter 4: Pharmacological characterisation of $I_{Cl_{IR}}$

Chapter 5: Effects of changes in the extracellular pH and a reduction in the external osmolarity on $I_{Cl_{IR}}$.

Chapter 6. Is ClC-2 expressed in rat SCG neurons? Analysis of rat SCG neuron mRNA by RT-PCR.

List of tables.

CHAPTER 1: GENERAL INTRODUCTION

This introduction will give an overview of the rat superior cervical ganglion (SCG) and the cationic conductances that can be recorded from SCG neurons. In addition, it will comprehensively review the different types of chloride conductances which have been described to date in both neuronal and non-neuronal cell types. The background to the experiments described in each results chapter will not, however, be covered here but rather in the introductions that precede the descriptions of the results obtained.

The superior cervical ganglion.

The SCG are sympathetic ganglia that are found at the most rostral end of the paravertebral chain. The neurons originating in them innervate the vasculature of the head and neck, the iris and the submandibular glands. All SCG neurons have phasic firing properties. They respond to a depolarising stimulus with a single or a transient burst of action potentials. The synaptic inputs that they receive from preganglionic motor neurons are large and suprathreshold, therefore a single input is capable of initiating an action potential. This taken together with the phasic firing properties indicates that SCG neurons act principally as relay neurons (Wang and Mckinnon, 1995).

Voltage gated currents of SCG neurons.

The pattern of ionic conductances that underlie the electrophysiological properties of SCG neurons is complex. SCG neurons have been shown, using the voltage clamp technique, to possess several different types of potassium conductance and also calcium and sodium conductances. These cation currents have been extensively studied and well characterised. In sharp contrast,

descriptions of voltage gated anion conductances in these cells are limited. The chloride currents that have been described are calcium activated currents that are also voltage sensitive (Sanchez-Vives and Gallego, 1994; Marsh *et al.*, 1995).

The sodium current of SCG neurons.

The sodium conductance of SCG neurons activates around -40mV and reaches a maximum amplitude at approximately 0mV. The channels underlying the conductance exhibit steady state inactivation so that around 50% of the channels are inactivated at -60mV. The current is sensitive to tetrodotoxin (TTX, Adams and Harper, 1995).

Potassium currents present in rat SCG neurons.

Rat SCG neurons possess a transient outward potassium current (I_A, Belluzzi *et al.*, 1985a) and also two delayed outward potassium conductances. The first of these is voltage dependent (I_{Kv}) and the other is activated by calcium ($I_{K(Ca)}$, Belluzzi *et al.*, 1985b). In addition there is a non inactivating current that can be inhibited by muscarine (I_M, Constanti and Brown, 1981).

I_A has rapid activation and inactivation kinetics. It can be activated at potentials between -60 and 0mV, providing there is a hyperpolarising prepulse. Peak current amplitude occurs within a few milliseconds. The prepulse is required because the current is completely inactivated at around -50mV due to steady state inactivation. Since the resting membrane potential is generally more hyperpolarised than -50mV, approximately 50% of the channels are available at rest (Belluzzi *et al.*, 1985a). I_A, although originally thought to be involved in the control of firing frequency is now thought to modulate the response to fast synaptic inputs (Wang and Mckinnon, 1995).

I_{Kv} activates relatively slowly at potentials depolarised to -40mV and once activated it does not show any appreciable inactivation over the time course of the voltage step. Maximal current amplitude is obtained at potentials depolarised to +20mV (Belluzzi *et al.*, 1985b). I_{Kv} contributes to rapid membrane potential repolarisation and also to the after hyperpolarising potential (AHP, Adams and Harper, 1995).

$I_{K(Ca)}$ is a larger current than I_{Kv} and unlike I_{Kv}, $I_{K(Ca)}$ activation is totally dependent on the influx of calcium. In addition however, it also exhibits some dependence on membrane potential depolarisation. $I_{K(Ca)}$ activates at potentials depolarised to -30mV and does so with a fast onset which is followed by a further gradual increase over the voltage step. The time dependent increase in $I_{K(Ca)}$ is not dependent on the continued presence of calcium influx, since the calcium current in these neurons is almost completely inactivated by the time $I_{K(Ca)}$ reaches its steady state amplitude (Belluzzi *et al.*, 1985b).

The M current, I_M, which was first identified in bull frog sympathetic ganglia (Brown and Adams, 1980) is also present in rat SCG neurons (Constanti and Brown, 1981). I_M is a non inactivating potassium current that is activated at potentials between -60 and -30mV. These potentials are more hyperpolarised than those required for activation of the other types of potassium currents in these cells. The M current is usually smaller than 1nA in size but it is has been shown to be responsible for the phasic firing properties of SCG neurons (Wang and McKinnon, 1995). The current activates slowly at depolarised potentials causing the membrane potential to sag towards the potassium equilibrium potential. This reduces the ability of the neurone to fire subsequent action potentials. The M current can be inhibited by the activation of muscarinic cholinergic receptors in a manner that is BAPTA sensitive (Beech *et al.*, 1991) but PTX insensitive. The onset of the inhibition is slow indicating that the effects are due to a diffusible

second messenger but it is not clear what the messenger is (Hille *et al.*, 1995). Injection of antibodies against specific G-protein α subunits has indicated that the G-protein involved is $G_{q/11}$ (Caulfield *et al.*, 1994).

Calcium currents possessed by rat SCG neurons.

The voltage dependent calcium current in rat SCG neurons is carried by N and L type calcium channels (Plummer *et al.*, 1989) with the N type channel carrying approximately 85% of the total current (Regan *et al.*, 1991). The two currents can be separated on the basis of their pharmacology. L type channels are sensitive to dihydropyridines while N type channels can be blocked by ω-conotoxin-GVIA. There may, however, be some overlap in these sensitivities and therefore this method of classification may not be necessarily be definitive. These currents are referred to as high voltage activated calcium currents since they activate at potentials depolarised to -30mV. The N type calcium current tends to inactivate over the course of the voltage step.

Both of these channel types can be modulated by a number of neurotransmitters. The L type channels, like the M current, are inhibited via a slow BAPTA sensitive pathway by muscarine and angiotensin II. The N type channels are also modulated by muscarine via this pathway but in addition, muscarine, along with a number of other neurotransmitters, can inhibit N type channels via a fast, PTX sensitive pathway. These features of the this pathway indicate that it is mediated directly in a membrane delimited manner by G-proteins (Hille *et al.*, 1995). The PTX sensitivity indicates that the G-protein involved is either G_i or G_o (Caulfield *et al.*, 1994). Interestingly it appears that it is the βγ subunits of the G-proteins which are mediating the modulation of N type calcium currents in rat SCG neurons (Ikeda, 1996).

Classification of chloride channels and currents using electrophysiological and molecular biology techniques.

Chloride is the most abundant physiological anion and it moves between the extracellular and intracellular compartments either by the actions of several different types of transporters or through chloride channels. The transporters include the Cl^--HCO^- exchanger and the Na^+-K^+-$2Cl^-$ cotransporter. The lack of primary active chloride transporters in most cell types' results in chloride being distributed close to its electrochemical equilibrium. The internal chloride concentration of a cell is therefore generally less than the extracellular concentration because of the negativity of the inside of the cell. The internal chloride concentration of SCG neurons has been determined by several different methods. Woodward *et al.* (1969) found that the SCG of the rabbit had an internal chloride concentration of 23.5mM by chloride titration. Ballanyi and Grafe (1985) meanwhile, measured the internal chloride ion activity to be approximately 30mM using ion sensitive microelectrodes.

Chloride conductances have been largely ignored over the years but since the advent of the patch clamp technique many different types of chloride channel have been identified and the contribution of chloride currents to physiological processes is starting to be recognised. Chloride currents have numerous functions which include stabilisation of the membrane potential, regulation of cell volume and intracellular pH; and secretion/absorption of salt and water. It is possible to broadly categorise chloride channels as ligand gated, volume sensitive or voltage gated based on their mode of activation. This method of dividing the chloride channels into groups however, is only arbitrary since some chloride channels can be activated by several factors and therefore can be classified as more than one type. The following sections will describe the properties of the different types of channels.

Ligand gated chloride channels.

Ligand gated channels are activated by the binding of either an external or an internal messenger molecule to its appropriate receptor. $GABA_A$, glycine, calcium activated and cAMP gated channels all fall into this category.

$GABA_A$ receptor gated chloride channels.

γ - aminobutyric acid (GABA) is the major inhibitory neurotransmitter of the vertebrate central nervous system. Although GABA can act at three different types of receptor (A, B or C; Bormann, 1988; Drew *et al.*, 1984), it is the $GABA_A$ receptor which is the major mediator of neuronal inhibition. $GABA_A$ receptors are heteromeric complexes which have a chloride channel as part of their structure.

Generally the activation of $GABA_A$ receptors leads to the influx of chloride. This causes hyperpolarisation of the membrane potential and subsequently inhibition of cell excitability. However, the direction of flow of chloride is dependent on the electrochemical driving force which in turn is determined by both the membrane potential and the chloride gradient. Intense activation of $GABA_A$ receptors can increase the internal chloride concentration and this may cause efflux of chloride upon further activation of the $GABA_A$ receptors. The result is depolarisation of the membrane and potentiation of cell excitability (Staley *et al.*, 1995).

Ion channel activation has complex kinetics and it appears that two agonist molecules must bind to the receptor to open the channel. Prolonged application of GABA, however, causes desensitisation which reverses over several minutes. In addition to GABA binding sites, the $GABA_A$ receptor complex can also bind many other compounds such as benzodiazepines, barbiturates, picrotoxin and

some steroids. The benzodiazepines, barbiturates and steroids act allosterically to potentiate the effects of GABA. Picrotoxin meanwhile, directly blocks the chloride channel to inhibit the action of GABA (Bormann, 1988).

$GABA_A$ receptors belong to a superfamily of ligand gated ion channels that also includes glycine and nicotinic cholinergic receptors (Schofield *et al.*, 1987). There are relatively high sequence homologies between the different members of the superfamily. The nicotinic and $GABA_A$ receptors share 15 - 20% homology while glycine and $GABA_A$ receptors share about 30% (Burt, 1994). The different receptors generally gate channels with different selectivities, that is nicotinic gated channels are generally cationic and $GABA_A$ and glycine gated channels are anionic. The selectivity of nicotinic gated channels can be altered, however, from cationic to anionic simply by inserting three amino acid residues into the sequence (Galzi *et al.*, 1992).

The general subunit structure of $GABA_A$ receptors, shown in figure 1.1, is four putative, highly conserved, transmembrane domains (M1-M4) which are preceded by a large extracellular amino terminal. The amino terminal is probably involved in the binding of ligands (Burt, 1994). In addition, there is a large, poorly conserved intracellular loop between M3 and M4 which is thought to be important for subunit specific characteristics and intracellular modification by, for example, protein kinase C (Olsen and Tobin, 1990).

a)

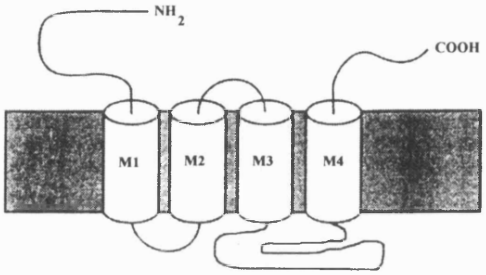

b)

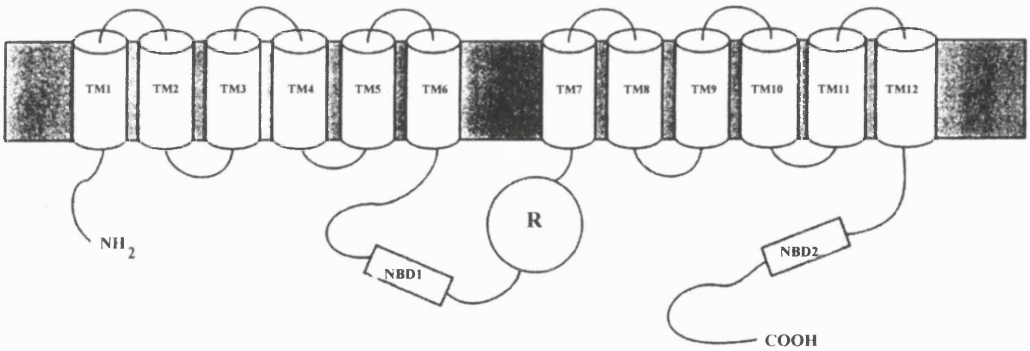

Figure 1.1. Diagrams showing proposed structures of $GABA_A$/Glycine receptor subunits and CFTR. **(a)** $GABA_A$ and glycine receptor subunits have four transmembrane domains (M1-M4). Both the amino and carboxy terminals of the protein are extracellular and there is a large intracellular loop between M3 and M4. Each receptor complex consists of five subunits **(b)** CFTR has two membrane spanning domains (MSD1 and MSD2) which consist of six transmembrane segments each (TM1-TM6 and TM7-TM12 respectively). Situated between MSD1 and MSD2 is the first nucleotide binding domain (NBD1) and the regulatory domain (R). The second nucleotide binding domain (NBD2) is found after MSD2. Both the amino and carboxy terminals of the protein are intracellular. (Figure reproduced from Jentsch (1996))

At least seventeen $GABA_A$ receptor subunits have been identified by homology screening techniques. These subunits belong to five families, $\alpha_{(1-6)}$, $\beta_{(1-4)}$, $\gamma_{(1-4)}$, δ and $\rho_{(1-2)}$. There is approximately 70% amino acid sequence similarity between the individual members of each family and 20-30% between the different families (Delorey and Olsen, 1992). This latter homology is about the same amount as that seen between glycine and $GABA_A$ receptor subunits (Betz, 1990). The subunits, in analogy to the nicotinic receptors which have been well studied, are thought to assemble in groups of five to form the receptor complex (Olsen and Tobin, 1990).

The number of subunit combinations possible with the numerous subunits available is extremely large. It increases further because there are splice variants of the β_2, β_3, β_4 and γ_2 subunits. It is possible that other subunits also have alternative splice variants (Burt, 1994). The exact combinations of subunits which occur in nature and their stoichiometry is not at all clear. Homomeric channels consisting of only one subunit can be functionally expressed and it has been shown that they have a number of the properties of native $GABA_A$ receptors but more subunits are required to obtain all the properties (Burt and Kamatchi, 1991).

α_1 subunits are necessary for the expression of the high affinity, type I benzodiazepine receptor. The other α subunits result in lower affinity binding characteristics and therefore probably make up the type II, low affinity receptor. α subunits are the most abundant of the subunits indicating that there is at least one present per channel complex (Olsen and Tobin, 1990). Benzodiazepine binding also requires a γ_2 subunit (Pritchett *et al.*, 1989) and receptors which are not sensitive to benzodiazepine appear to have a δ subunit instead (Burt and Kamatchi, 1991). In addition, the particular type of β (as well as α subunit) present in the receptor complex appears to determine the affinity of agonist binding (Olsen and Tobin, 1990).

Glycine receptor gated chloride channels.

Glycine is considered to be the major inhibitory neurotransmitter of the spinal cord and brain stem but *in situ* hybridisation has shown that glycine receptors are also expressed throughout the central nervous system (Betz, 1991). In addition, the application of glycine has been reported to have effects on a proportion of rat SCG neurons (Cull-Candy and Mathie, 1986). Glycine receptors have, like $GABA_A$ receptors, a chloride channel as an integral part of their structure. Glycine receptors were first isolated from rat spinal cord (Pfeiffer *et al.*, 1982) and were shown to consist of two polypeptides corresponding to α and β subunits. A third polypeptide was co-purified with these subunits which is now known to be localised to the cytoplasmic face of the membrane. This protein is thought to be involved in synaptic localisation of the receptor or anchoring of the receptor to cytoskeletal elements (Betz, 1990).

Glycine receptor heterogeneity was first detected because neonatal and adult receptors displayed different sensitivities for the convulsive alkaloid, strychnine. There are now known to be several different glycine receptor α subunit isoforms, α1-α4 (Betz *et al.*, 1993) but there has only been one β subunit identified. The number of α subunits increases further because there are splice variants of the α1 and α2 subunits. The α subunits possess the agonist binding site. It is the α2 subunit which exhibits lower sensitivity to strychnine and therefore probably forms part of the neonatal receptor.

Glycine receptors belong to the same ligand gated superfamily as $GABA_A$ and nicotinic cholinergic receptors (Betz, 1990). The subunits share some sequence homology and the subunit structure is believed to be the same (see figure 1.1). The glycine receptor is probably a pentamer which consists of 3 α and 2 β subunits (Betz *et al.*, 1993).

Calcium activated chloride channels.

Calcium activated chloride channels were initially described in cells from the salamander retina (Bader *et al.*, 1982) and *Xenopus* oocytes (Miledi, 1982; Barish, 1983). Since then, they have been reported in a wide range of different cell types including secretory cells, peripheral and central neurons, smooth muscle and cardiac muscle (Scott *et al.*, 1995).

Calcium activated chloride currents are activated by a rise in intracellular calcium close to the membrane and also by membrane depolarisation. The increase in intracellular calcium can occur by influx through voltage and ligand gated ion channels or release from intracellular stores. Both low and high voltage activated calcium channels have been implicated in the activation of chloride currents and it has been suggested that the calcium and chloride channels co-localize (Scott *et al.*, 1995). NMDA receptors are an example of calcium permeable ligand gated ion channels.

The characteristics of calcium activated chloride currents, typified by the current recorded in rat lacrimal gland cells (Evans and Marty, 1986), are relatively slow activation at depolarised potentials, lack of time dependent inactivation, small single channel conductance and a halide selectivity sequence of I > Br > Cl. Although the channels do not inactivate in the continued presence of calcium, they have been shown to deactivate in neurons if calcium is removed by intracellular buffering (Scott *et al.*, 1995). The calcium dependence of these channels is relatively steep which indicates that several calcium ions must bind to the channels for them to activate (Hille, 1992). The activation of calcium activated chloride currents can result in membrane potential depolarisation or hyperpolarisation depending on the relationship between the chloride equilibrium potential (E_{Cl}) and the membrane potential. Therefore calcium activated chloride

currents may have an important role in controlling cell excitability (Hille, 1992; Scott *et al.*, 1995).

Besides the typical calcium activated chloride channels described above there are also other types of chloride currents which exhibit some sort of calcium dependence. *Xenopus* oocytes have been reported to possess an endogenous hyperpolarisation activated chloride current that is dependent on calcium (Peres and Bernardini, 1983). This current is a transient inward current that was found to be abolished by the removal of extracellular calcium. Rat SCG neurons possess a chloride current which requires an increase in the intracellular calcium concentration but also activation of protein kinase C (Marsh *et al.*, 1995). The current is seen some time after the calcium current that is thought to activate it and therefore it appears that the channels are not activated directly by the rise in calcium but through a calcium dependent process. In contrast, a typical calcium activated chloride current has been identified in these neurons but only after axotomization (Sánchez-Vives and Gallego, 1994).

cAMP dependent chloride channels.

Cystic fibrosis transmembrane regulator (CFTR).

Cystic fibrosis is a hereditary disease which is caused by mutations in the CFTR protein that is located in various chloride secreting epithelia. CFTR is a member of the ABC transporter superfamily (Hyde *et al.*, 1990) but there are structural differences between CFTR and other members of the family. Also, the structure of CFTR does not bear any similarity to any known ion channel (Fuller and Benos, 1992). CFTR consists of five domains, as is shown in figure 1.1. There are two membrane spanning regions (MSD1 and MSD2) which have six hydrophobic sequences thought to form transmembrane domains. Located

between MSD1 and MSD2 is the first of two nucleotide binding domains (NBD1) and a highly charged regulatory or R domain. MSD2 is followed by the second nucleotide binding domain (NBD2). Both the amino and carboxy terminals are extracellular (Riordan *et al.*, 1989).

CFTR is a chloride channel that is regulated by cAMP dependant phosphorylation and intracellular ATP. Chloride currents recorded upon expression of CFTR in a number of expression systems all display similar properties (Anderson *et al.*, 1992). Also CFTR has been reconstituted into lipid bilayers and shown to produce a chloride conductance (Fuller and Benos, 1992). In addition, mutations in the membrane spanning regions lead to altered anion selectivity. This suggests that these regions are involved in forming the channel pore (Anderson *et al.*, 1991).

CFTR chloride currents have linear I-V curves, display no time dependant voltage effects and exhibit a Br > Cl > I halide selectivity sequence (Welsh *et al.*, 1994; Anderson *et al.*, 1992). Also the currents are calcium independent, have only a small single channel conductance and are insensitive to stilbene derivatives (Fuller and Benos, 1992). Studies investigating the permeability of the channel have revealed that it exhibits anomalous mole fraction behaviour (Tabcharani *et al.*, 1993).

Channel opening requires the R domain, which has multiple phosphorylation sites for protein kinases A and C, to be phosphorylated. CFTR mutations in which the R domain has been deleted result in constitutively active chloride channels (Cheng *et al.*, 1991). This suggests that the R domain has an inhibitory function, keeping the channel closed unless it is phosphorylated.

ATP also regulates channel function although it can only do so when the channel is already phosphorylated. It is believed that ATP has a permissive role in channel opening (Anderson *et al.*, 1991) but it is not entirely clear whether ATP must be hydrolysed as for other members of the ABC transporter family. ATP and other hydrolysable ATP analogues do however, interact with NBD1 and NBD2. It has been shown that ATP binding to NBD1 enables the channel to open. Binding of ATP to NBD2 appears to stabilise the open channel state and hydrolysis of ATP at NBD2 results in channel closure (Jentsch, 1996). The most common mutation that is responsible for cystic fibrosis is a single amino acid deletion in NBD1. The deletion is thought to interfere with ATP binding. However, there are also many other mutations and these are found in other regions of the protein (Fuller and Benos, 1992).

Besides a role as a chloride channel it has also been proposed that CFTR acts as a membrane transporter, in particular a transporter of ATP. However the evidence is still controversial and requires further study (Jentsch, 1996).

Other chloride currents sensitive to cAMP.

Leydig cells from rat testis possess a hyperpolarisation activated chloride current that is modulated by cAMP and a similar current is observed in other cell types as well (Noulin and Joffre, 1993). The application of cAMP to these cells was found to cause a positive shift and increase in steepness of the current activation curve. In cultured rat cortical astrocytes long term application (1-3 weeks) of a membrane permeable cAMP analogue was shown to lead to the expression of a previously unseen hyperpolarisation activated chloride current (Ferroni *et al.*, 1995). The actions of cAMP on these cells, however, are probably due to cAMP regulated gene expression not a direct action of cAMP on the channel.

In contrast, volume activated chloride currents in chick heart cells, recorded using the whole cell patch clamp method, are prevented from activating by the application of cAMP or cAMP agonists (Hall *et al.*, 1995). The hyperpolarisation activated chloride currents found in Aplysia neurons (Lotshaw and Levitan, 1987) and T_{84} epithelial cells (Fritsch and Edelman, 1996) are also inhibited by cAMP agonists.

Volume sensitive chloride channels.

Most cells need to be able to regulate their volume in response to a hypotonic shock and this is generally achieved by the opening of independent potassium and chloride channels in a process known as regulatory volume decrease. The open channels allow the efflux of potassium and chloride which in turn causes the efflux of water. The volume activated chloride channels have a number of characteristics in common but as yet no volume activated chloride channels have been cloned. It is therefore not possible to determine if the channels belong to one gene family or to several. Volume sensitive chloride currents have been described for many different cell types (Ackerman *et al.*, 1994; Anderson *et al.*, 1992; Arreola *et al.*, 1995, 1996; Nilius *et al.*, 1994) and the typical characteristics of these currents are rapid activation, outward rectification and time dependent inactivation at depolarised potentials. They also tend to have a greater iodide than chloride permeability and a dependence on intracellular ATP (Jentsch, 1996; Ackerman *et al.*, 1994; Nilius *et al.*, 1994).

Other chloride channels exist however which do not have the above characteristics and yet are sensitive to changes in osmolarity. ClC-2 is a voltage activated chloride current that can also be activated by external hypotonicity (Gründer *et al.*, 1992). While the hyperpolarisation activated chloride current in rat osteoblasts is activated not by hypotonicity but by hypertonic external

solutions (Chesnoy-Marchais and Fritsch, 1994). These channels will be discussed in more detail below.

Volume is an extensive parameter and is therefore unlikely to regulate channels directly. Instead it is thought that the change in cell volume causes mechanical stress or alters the concentration of intracellular messengers and it is these parameters which are detected and acted upon (Sarkadi and Parker, 1991).

Activators of endogenous volume activated chloride currents.

P_{ICln}.

P_{ICln} is a protein which was isolated by expression cloning using mRNA from a dog kidney epithelial cell line (Paulmichl *et al.*, 1992). Originally it was thought to form a chloride channel since when it was expressed, it resulted in strongly outwardly rectifying chloride currents. These currents were found to be calcium independent but were inhibited by extracellular nucleotides. Supporting the idea that P_{ICln} was a channel, it was shown that mutations of the nucleotide binding domain caused loss of the inhibition by nucleotides. These mutations, in addition, caused the current to become sensitive to calcium and to exhibit altered voltage dependence (Paulmichl *et al.*, 1992).

However, the protein is not now thought to form a channel itself because of its small size and the lack of any hydrophobic domains that would be able to form α helix transmembrane spanning regions (Paulmichl *et al.*, 1992). In addition, P_{ICln} is now known to be a soluble cytoplasmic protein since it forms complexes with other cytoplasmic proteins such as actin (Krapivinsky *et al.*, 1994).

Since P_{ICln} does not appear to form a channel, it has been proposed that it is an activator of endogenous swelling activated chloride currents instead. Indeed, over expression of P_{ICln} produces a current that has almost identical properties as those reported for native volume activated chloride currents in *Xenopus* oocytes (Ackerman *et al.*, 1994 but see Voets *et al.*, 1996). Also, antisense oligonucleotides generated against the sequence for P_{ICln} suppress the endogenous volume activated chloride current in 3T3 fibroblasts (Gschwentner *et al.*, 1995) and antibodies against P_{ICln} inhibit a similar endogenous current in *Xenopus* oocytes (Krapivinsky *et al.*, 1994).

P-glycoprotein.

The human P-glycoprotein is a member of the ABC transporter superfamily which also includes the cystic fibrosis transmembrane regulator (CFTR). P-glycoprotein acts to transport many different hydrophobic compounds out of cells in a manner that is dependent on ATP hydrolysis. This causes multidrug resistance and as a consequence P-glycoprotein is also known as the multidrug resistance protein or MDR1 (Higgins, 1995). However, expression of P-glycoprotein has also been reported to produce chloride currents that are very similar to currents activated by swelling and to those produced upon expression of P_{ICln} (Valverde *et al.*, 1992). The chloride conductance is known to be distinct and separate to drug transportation since it requires only ATP binding not hydrolysis and mutations which affect the transporter do not affect the chloride current (Gill *et al.*, 1992; Higgins, 1995).

It is now believed that P-glycoprotein is an activator of volume activated chloride channels due to the characteristics of the current produced (outward rectification, fast activation and $I^- > Cl^-$ selectivity) and the observation that it can confer regulation by protein kinase C to endogenous volume activated currents

when injected into cells not expressing it (Hardy *et al.*, 1995; but see Tominaga *et al.*, 1995). It is not essential though, since some cell types possess swelling activated currents but do not express P-glycoprotein.

Voltage gated chloride currents.

Most types of chloride current can be activated to some degree by changes in the membrane potential. It is only if channel opening is solely dependent on membrane potential or if a change in membrane potential is the major activator, that the channels are classified as being voltage activated. There are many chloride channels which can be classified as being voltage dependent.

Native voltage activated chloride currents.

The voltage dependent chloride channel of Torpedo electroplax.

Cells which make up the *Torpedo* electroplax have a high density of voltage gated chloride channels. These channels are found in the non innervated membrane and act to clamp the membrane potential so that large transcellular voltages can develop when the innervated membrane is depolarised. These channels have been extensively characterised by the incorporation of vesicles from the electroplax into planar lipid bilayers (White and Miller, 1979; Miller, 1982; Miller and White, 1984; Richard and Miller, 1990).

A double barrelled structure consisting of two identical protochannels was proposed for the *Torpedo* chloride channel, since when the biophysical properties were investigated, channel openings were found to only occur in bursts and to exhibit two equidistant subconductance states (Miller, 1982). The opening of the *Torpedo* channel was accounted for by a model which involved two voltage

dependent gates (Miller and White, 1984). The first of the gates opens very slowly upon hyperpolarisation, taking between 10 and 40s to reach steady state activation. This slow gate acts on both protochannels simultaneously and closes at an even slower rate so that deactivation, caused by repolarisation of the membrane potential, takes several minutes. The second, fast gate, opens rapidly upon depolarisation and gates each protochannel separately (Miller and White, 1984).

Hyperpolarisation activated chloride currents.

Chloride currents that are activated by hyperpolarisation of the membrane potential have been described for a number of vertebrate and invertebrate, neuronal and non neuronal cell types. These include *Aplysia* neurons (Chesnoy-Marchais, 1983), *Xenopus* oocytes (Peres and Bernardini, 1983), hippocampal neurons (Madison *et al.*, 1986; Staley, 1994), rat osteoblastic cells (Chesnoy-Marchais and Fritsch, 1994), T_{84} epithelial cells (Fritsch and Edelman, 1996), SCG neurons (Selyanko, 1984) and several others (Ferroni *et al.*, 1995; Noulin and Joffre, 1993; Arreola *et al.*, 1996; Dinudom *et al.*, 1993). Most of these currents are slowly activating and do not inactivate over the course of a voltage step.

Aplysia neurons possess a hyperpolarisation activated chloride current.

The slowly activating hyperpolarisation dependent chloride current of *Aplysia* neurons was first identified in 1982 (Chesnoy-Marchais, 1982). This current, which can only be recorded when the neurons are loaded with chloride either by diffusion from the recording microelectrode or by intracellular injection, activates and deactivates with similar kinetics (Chesnoy-Marchais, 1983). It is possible that internal anions may modulate channel gating. Recording the current using the excised patch recording technique revealed that the channel activity

consisted of long bursts and that during the bursts two open channel subconductance states could be observed (Chesnoy-Marchais and Evans, 1986). This type of channel activity which is very like that demonstrated for the *Torpedo* electroplax chloride channel (Miller, 1982) was suggested to be due to the tight coupling of two channel subunits. The hyperpolarisation activated chloride current of *Aplysia* neurons can be modulated by both 5HT and forskolin, a cAMP agonist (Lotshaw and Levitan, 1987). The inhibition, which occurs by a cAMP dependent mechanism, was the result of a change in the voltage dependence of the channel gating.

Hyperpolarisation activated chloride currents found in *Xenopus* oocytes.

As described earlier, one of the hyperpolarisation activated chloride currents that is found in *Xenopus* oocytes is transient and apparently dependent on extracellular calcium (Peres and Bernardini, 1983). The other is a sustained current that is calcium independent (Parker and Miledi, 1988). This current, which was further chracterised by Kowdley *et al.* (1994), was shown to have a halide selectivity sequence of I > Br > Cl. It was also found to be blocked by barium ions but was unaffected by changes in pH. In addition, the current activated at potentials between -30 and -40mV. This current is highly variable in size between different batches of oocytes which would tend to suggest that it does not have a particular function in the *Xenopus* oocyte.

The hyperpolarisation activated current in hippocampal neurons.

In hippocampal pyramidal neurons there is a hyperpolarisation activated chloride current that is inhibited by the activation of protein kinase C (Madison *et al.*, 1986). The current activates at potentials negative to -10mV and so is quite

substantially active at resting membrane potentials. Another study found that this current could also be modulated by activators of protein kinase A (Staley, 1994).

These neurons have $GABA_A$ gated chloride channels, which when activated result in chloride influx and subsequently neuronal hyperpolarisation. However, if the chloride equilibrium potential becomes positive to the membrane potential because of chloride loading via these ligand gated receptors, any further activation can cause depolarisation instead. The hyperpolarisation activated chloride current has non inactivating, inwardly rectifying characteristics and when down regulated by the activation of protein kinase A, GABA binding to $GABA_A$ gated chloride channels to result in excitation. Staley (1994) therefore suggested that the current acts to maintain the relationship between the membrane potential and the chloride equilibrium potential, thereby preventing paradoxical depolarisation.

Other hyperpolarisation activated chloride currents.

The hyperpolarisation activated chloride current in rat osteoblastic cells is, like the currents described above, slowly activating and shows no inactivation (Chesnoy-Marchais and Fritsch, 1994). The current, which activates at potentials negative to -20mV, is unusual however, in that it is also sensitive to the external osmolarity. This sensitivity is the opposite to that normally observed however, in that the current is increased by external hypertonicity rather than hypotonicity.

T_{84} epithelial cells possess a chloride current that activates when the membrane potential is hyperpolarised below -40mV and which has a halide selectivity sequence of $Cl > Br > I$ (Fritsch and Edelman, 1996). This selectivity sequence is different to that reported for other types of chloride currents that have

been described (see earlier). Also as already described, this current can be inhibited by a permeable analogue of cAMP and by activators of protein kinase C.

Rat SCG neurons have been reported to possess a hyperpolarisation activated chloride current (Selyanko, 1984) but the description of its features was very limited and it has not been characterised since it was first identified.

Cloned voltage activated chloride channels.

The ClC family of voltage activated chloride channels.

It is only over recent years that chloride channels have started to be characterised using molecular biology techniques. The use of such techniques has enabled the identification of the ClC superfamily of voltage gated chloride channels. At present, the mammalian ClC family consists of eight members (ClC-0 to ClC-7). These can be subdivided, as is shown in figure 1.2, on the basis of sequence homology. In addition, there are also ClC homologues present in yeast (Greene *et al.*, 1993) and bacteria (Fujita *et al.*, 1994).

It does not appear to be possible to functionally express some members of the mammalian ClC family (ClC-4, ClC-6, ClC-7) and for other members functional expression is controversial (ClC-K (1 and 2), ClC-3). Therefore these members of the family can only be classified as putative chloride channels and it is not possible to assign a function to them. In contrast, ClC-0, ClC-1, ClC-2 and ClC-5 can all be functionally expressed and have defined roles. The expression patterns of the members of the ClC family are different. Some members are almost ubiquitously expressed (ClC-2, ClC-3, ClC-6, ClC-7) but others exhibit restricted expression patterns (ClC-1, ClC-K(1 and 2), ClC-5).

a)

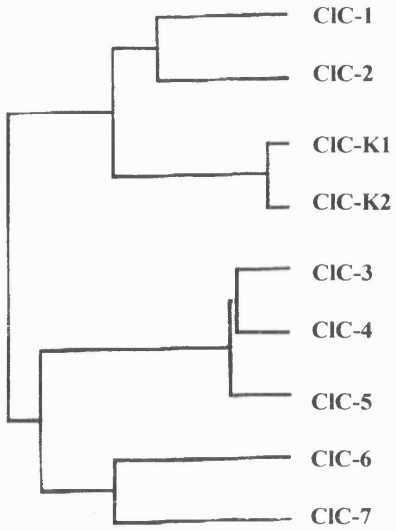

b)

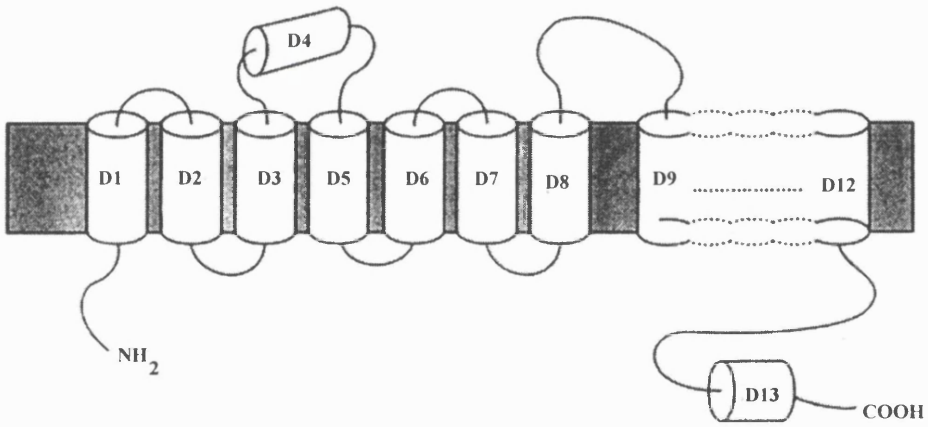

FIGURE 1.2. The ClC family of chloride channels. **(a)** Diagram showing the relationships between the different members of the mammalian ClC proteins. Branches are assigned on the basis of sequence homology. **(b)** Diagram showing the proposed structure of the ClC proteins. There are thirteen hydrophobic domains as determined by hydropathy analysis (D1-D13). The linker between D8 and D9 is glycosylated and therefore must be extracellular. If this is the case then there is a hydrophobic domain amino terminal to this which does cross the membrane. D4 is thought to be that domain because it is poorly conserved among the different members and is only weakly hydrophobic. D13 and therefore the carboxy terminal of the protein is cytoplasmic. (figure reproduced from Jentsch, 1996).

ClC-0, the Torpedo electroplax chloride channel.

ClC-0, the first member of the ClC family to be identified, is the chloride channel of the *Torpedo* electroplax and the cDNA sequence was obtained by negative expression cloning (Jentsch *et al.*, 1990). Shortly after the *Torpedo marmorata* channel was cloned, the chloride channel of *Torpedo californica* was also cloned (O' Neill *et al.*, 1991). It was found to have 97% sequence homology with the *marmorata* channel. ClC-0, besides being strongly expressed in the electroplax, is also present in *Torpedo* skeletal muscle and *Torpedo* brain (Jentsch, 1994). Expression of ClC-0 in *Xenopus* oocytes produces a current which has all the properties of the native channel (Bauer *et al.*, 1991). This confirms that ClC-0 does underlie the *Torpedo* chloride conductance.

An interesting feature of the *Torpedo* channel is that the voltage dependence of gating does not appear to be dependent on some intrinsic gating particle as for certain cation channels. Instead it appears to be due to the permeating anion. Richard and Miller (1990) found that the statistical properties of single channel recordings of the native channel were not symmetrical with time and they therefore suggested that the voltage dependent gating was coupled to the electrochemical gradient of the permeating anion. More recently Pusch *et al.* (1995), have shown, by expression of ClC-0 in *Xenopus* oocytes, that the voltage dependent gating is caused by the permeating anion acting as the gating charge.

ClC-1, the major muscle chloride channel.

Under resting conditions mammalian skeletal muscle has a large chloride conductance which accounts for the greater part of the total membrane conductance (Bretag, 1987). Since *Torpedo* electroplax is evolved from skeletal

muscle the search for the mammalian skeletal muscle chloride channel was carried out by homology screening using the ClC-0 cDNA sequence (Steinmeyer *et al.*, 1991b). The channel which was identified had 55% overall sequence homology with ClC-0 and was named ClC-1. ClC-1 is strongly expressed at very high levels in skeletal muscle but low levels are also found in heart, kidney and smooth muscle (Steinmeyer *et al.*, 1991b). In rat muscle, mRNA encoding ClC-1 increases rapidly during the first few weeks after birth. This agrees with the increase in the chloride conductance that has been previously described for rat skeletal muscle (Conte Camerino *et al.*, 1989).

When expressed in *Xenopus* oocytes ClC-1 causes a chloride conductance which is activated rapidly by depolarisation and which shows inward rectification at positive potentials. At very hyperpolarised potentials the current displays time dependent inactivation so that maximal inward current amplitude is observed at about -100mV (Steinmeyer *et al.*, 1991b). Again, these electrophysiological characteristics are very similar to those reported for the native skeletal muscle chloride conductance (Palade and Barchi, 1977). Attempts to further characterise the current by single channel recording were not successful. A very small single channel conductance for ClC-1 of approximately 1pS was shown by non-stationary noise analysis (Pusch *et al.*, 1994).

The developmental regulation and electrophysiological characteristics of ClC-1 indicate that ClC-1 is the major skeletal muscle chloride channel (Steinmeyer *et al.*, 1991b). Therefore, since the chloride equilibrium potential is close to the resting membrane potential ClC-1 will act to stabilise the skeletal muscle membrane potential.

Skeletal muscle hyperexcitability which results in myotonia or muscle stiffness occurs when there is a slowing in the repolarisation of the membrane

potential that occurs after an action potential. The delay provides time for sodium channels to recover from inactivation whilst the membrane is still depolarised and this results in a series of action potentials instead of just one. A reduction in the resting chloride conductance of skeletal muscle has been reported for two animal models of myotonia (Bryant and Conte Camerino, 1991; Mehrke *et al.*, 1988). In addition, a reduction in chloride conductance occurs with both autosomal recessive (Beckers) and autosomal dominant (Thompsons disease) human myotonias (Pusch and Jentsch, 1994).

Inactivation due to loss of, or mutations in, ClC-1 are now known to account for myotonia. In the ADR (arrested development of righting response) mouse, which is an animal model used in the study of recessive myotonia, ClC-1 is inactivated due to the insertion of a transposon (Steinmeyer *et al.*, 1991a). In Beckers myotonia (Koch *et al.*, 1993) and Thompsons disease (Steinmeyer *et al.*, 1994) point mutations in the sequence of ClC-1 are responsible.

ClC-2, a voltage and volume activated channel.

ClC-2 was identified by homology screening using ClC-1 as a probe (Thiemann *et al.*, 1992) and it was found to have approximately 50% sequence homology to both ClC-0 and ClC-1. Northern analysis showed that it was expressed ubiquitously in all tissues, although *in situ* hybridisation has now shown that ClC-2 is expressed differentially in brain (Smith *et al.*, 1995). When ClC-2 is expressed in *Xenopus* oocytes it results in an inwardly rectifying current that activates in response to strong, unphysiological (greater than -100mV) hyperpolarising voltage steps. Activation of ClC-2 is very slow, with more than twenty seconds being required to reach steady state activation but deactivation occurs much faster (Thiemann *et al.*, 1992).

Besides hyperpolarisation, ClC-2 has also been shown to be activated by hypotonicity (Gründer *et al.*, 1992). When recorded in a hypotonic media, the threshold for activation of ClC-2 is shifted more depolarised and ClC-2 is therefore activated within physiological ranges. ClC-2 has been proposed to function as a regulator of cell volume because of its sensitivity to external osmolarity.

Two amino terminal domains of ClC-2 were found, by extensive mutation studies, to be responsible for channel activation by both hyperpolarisation and hypotonicity (Gründer *et al.*, 1992). One region is essential, in that if it is deleted, channels become unresponsive to both methods of activation. The adjacent region is modulatory and deletions in it result in channels which appear to be partially volume activated. The channels can be further activated by hypotonicity but can also be closed by hypertonicity. The domain incorporating both the essential and modulatory regions is not position dependent as it can be moved to the carboxy terminal of the sequence and still be functional. To explain the properties of this domain, Gründer *et al.* (1992) proposed that it binds to a receptor on the cytoplasmic side of the channel. Hypotonicity or hyperpolarisation reduces the affinity of the receptor for the domain which results in activation of the channel.

ClC-K1, ClC-K2 and ClC-5, kidney chloride channels.

The kidney specific chloride channel, ClC-K1 was isolated by Uchida *et al.* (1993) using RT-PCR with degenerate primers against conserved regions of ClC-0, ClC-1 and ClC-2. It was found to have approximately 40% sequence homology to the other ClC family members. The sequence for a second chloride channel, ClC-K2, was subsequently obtained from rat kidney by Kieferle *et al.* (1994) using a similar approach together with homology screening. In addition, two highly homologous cDNAs were isolated from human kidney which were

named hClC-Ka and hClC-Kb. The rat and human chloride channels were found to have approximately 80% sequence homology to each other but correlation between the rat and human proteins could not be determined because the human channels had more sequence similarity with each other (approximately 90%) than with the rat channels (Kieferle *et al.*, 1994). The second rat chloride channel appears to have two isoforms which have been designated ClC-K2L and ClC-K2S (Adachi *et al.*, 1994).

ClC-K1 and ClC-K2 are differentially expressed in the kidney. ClC-K1 has a restricted distribution with the highest levels being found in the thin ascending limb of the loop of Henle (Uchida *et al.*, 1993), the cortical thick ascending limb and the distal convoluted tubule (Kieferle *et al.*, 1994). ClC-K2 meanwhile has a much broader distribution being found in most segments of the nephron (Kieferle *et al.*, 1994).

There is some controversy as to whether these kidney specific chloride channel proteins can be expressed. Uchida *et al.* (1993) reported that ClC-K1 produced slightly outwardly rectifying, time independent chloride currents when expressed in *Xenopus* oocytes but Kieferle *et al.* (1994) could not obtain any expression despite several modifications of the cDNA designed to make expression easier. In addition, Adachi *et al.* (1994) but not Kieferle *et al.* (1994) could functionally express ClC-K2 and the latter group were also unable to obtain expression of the human kidney chloride channels. It has been suggested that the currents observed by Uchida *et al.* (1993) and Adachi *et al.* (1994) were endogenous *Xenopus* oocyte currents since similar currents were also observed in uninjected oocytes (Jentsch *et al.*, 1995).

ClC-5 was originally cloned from rat brain but it is also strongly expressed in all segments of the rat nephron (Steinmeyer *et al.*, 1995) and it has been

implicated in three human hereditary kidney diseases (Fisher *et al.*, 1994; Lloyd *et al.*, 1996). Nephrolithiasis or kidney stones occurs due to the defective reabsorption of calcium in the proximal tubule. To reabsorb calcium, chloride and water must first be reabsorbed. Since the gene which encodes ClC-5 is partially deleted in this disease it is possible that ClC-5 is the chloride channel responsible for the chloride uptake and that the loss of ClC-5 causes the reduction in calcium reabsorption (Herbert, 1996).

ClC-5 shows a high degree of sequence homology (approximately 80%) to two other members of the ClC family, ClC-3 and ClC-4 but only about 30 % to the rest of the family members (Steinmeyer *et al.*, 1995). It can be functionally expressed in *Xenopus* oocytes to give chloride currents which activate at positive membrane potentials (greater than 20mV) and exhibit strongly outward rectification (Steinmeyer *et al.*, 1995). The depolarised membrane potential required to activate ClC-5 is probably not physiological since such potentials are not believed to be reached in kidney epithelia. It has therefore been suggested that an additional subunit is required (Lloyd *et al.*, 1996). The currents produced upon expression of ClC-5 are reduced or abolished by the mutations which are found in kidney stone disease patients thus providing strong evidence for a causal role in the diseases (Lloyd *et al.*, 1996).

ClC-3, ClC-4, ClC-6 and ClC-7.

ClC-3 was isolated by a PCR cloning strategy using primers based on highly conserved regions of other members of the ClC family (Kawasaki *et al.*, 1994). It has only about 25% sequence homology with the other members. Although it was initially isolated from rat kidney, ClC-3 is most strongly expressed in brain tissue, particularly in neuronal cells.

ClC-3 could only be expressed in *Xenopus* oocytes, when the 5' untranslated region of the sequence was replaced by that of ClC-0 (Kawasaki *et al.*, 1994). The channel expressed appeared to be open at all membrane potentials and chloride currents exhibiting only very slight outward rectification were recorded. ClC-3, however, has also been expressed in stably transfected Chinese hamster ovary cells (Kawasaki *et al.*, 1995) and in these cells the current exhibit very strong outward rectification at positive potentials and a certain degree of time dependence. These recordings were achieved using the inside out patch configuration and nominally calcium free bathing solution which may explain the difference. Interestingly ClC-3 expressed in *Xenopus* oocytes, was found to be modulated by phorbol esters. The channels expressed in the cell line were, in addition, also found to be inhibited by physiological concentrations of calcium in a manner that was voltage dependent (Kawasaki *et al.*, 1995). Another group (Jentsch *et al.*, 1995) has been unable to functionally express ClC-3 and as yet there is no obvious function for this chloride channel.

ClC-4 is a new member of the ClC family that has been cloned from both human (van Slegtenhorst *et al.*, 1994) and rat (Jentsch *et al.*, 1995). The expression of ClC-4 in human and rat is slightly different with human ClC-4 being most strongly expressed in muscle and brain while rat ClC-4 is most strongly expressed in liver and brain. ClC-4 shows approximately 80% sequence homology with ClC-3 and like ClC-3 is only about 30% homologous to the other members of the family (Jentsch *et al.*, 1995). Neither the human nor the rat ClC-4 have yet been functionally expressed (Jentsch *et al.*, 1995) and therefore it is not known if they form chloride channels.

ClC-6 and ClC-7 are the latest members of the ClC family (Brandt and Jentsch, 1995). They share approximately 45% sequence homology to each other but only 30% at most to other members. ClC-6 and ClC-7 are very broadly

expressed being found in most tissue types tested. Functional expression of ClC-6 and ClC-7 has not been achieved whether they are expressed singly or in combination. These members of the ClC family are therefore only putative chloride channels.

Common characteristics of ClC chloride channels.

The ClC family of proteins do not show any sequence similarity with any other types of ion channel. All the members of the ClC family are structurally alike in that they all have similar hydropathy profiles but the transmembrane topology has not been conclusively determined. Hydropathy analysis of ClC-0 indicated that there were twelve or thirteen transmembrane domains (D1 - D13) (Jentsch *et al.*, 1990) but that scheme has since been revised (Jentsch, 1996) because some domains are not particularly hydrophobic and the channels are glycosylated. The revised scheme is shown in figure 1.2. The amino terminal of the protein is hydrophilic, does not have a cleavable signal peptide and is therefore cytoplasmic.

D13, which is highly conserved among the ClC family members, is now known to be cytoplasmic, since the amino terminal domain of ClC-2, which has been shown to be important in activation, can be inserted either before or after it and still be functional (Gründer *et al.*, 1992). This also places the carboxy terminal, as well as the amino terminal of the protein, in the cytoplasm.

All members of the ClC family except ClC-7 (Brandt and Jentsch, 1995) have potential sites for N linked glycosylation in the segment which joins D8 and D9 (Jentsch *et al.*, 1995). The ClC-0, ClC-1, ClC-2 and ClC-K channels have all been found by mutational studies to be glycosylated (Kieferle *et al.*, 1994) and therefore the D8 - D9 linker must be extracellular.

The extracellular location of the D8 - D9 linker means that there is a putative transmembrane domain, amino terminal to this which does not span the membrane. The D4 segment has been proposed to be that segment because it is only weakly hydrophobic and is not very well conserved (Jentsch *et al.*, 1995). In ClC-6 and ClC-7 there is no hydrophobic peak that corresponds to the D4 segment of the other members (Brandt and Jentsch, 1995). The D2 segment has also been suggested as a possible candidate. A splice variant of ClC-K2 (ClC-K2S) can still be functionally expressed despite the D2 and surrounding conserved sequences being deleted (Adachi *et al.*, 1994). This indicates that the D2 segment is not required for channel function and is therefore unlikely to be a transmembrane domain. However, the D2 segment is highly hydrophobic and when it was deleted from ClC-0 no functional expression of the channel was obtained (Jentsch *et al.*, 1995).

Extensive biophysical characterisation of the *Torpedo* chloride channel, reconstituted into planer lipid bilayers, has shown that it has a double barrelled structure which consists of two identical protochannels (Miller and White, 1984; Miller and Richard, 1990). It has not been possible to determine if other members of the family, which have been functionally expressed, also have a similar structure because they have very low single channel conductances (Pusch *et al.*, 1994; Jentsch *et al.*, 1995). The high degree of sequence homology between the different ClC proteins, however, makes this a possibility.

It is not clear if a single protein or several ClC proteins are required to form a functional channel but evidence seems to indicate that they are multimeric structures. Mutations in ClC-1 have been shown to be the cause of both recessive (Koch *et al.*, 1993) and dominant (Steinmeyer *et al.*, 1994) myotonic diseases. This can only be explained by the channels being multimeric structures consisting of several subunits and mutant subunits being able to combine with wild type ones

to cause dominant negative effects (Steinmeyer *et al.*, 1994). The extent of inactivation due to dominant negative effects is dependent on the number of subunits. Steinmeyer *et al.* (1994) investigated the effects of two mutations that are found in dominant myotonia by coinjecting constant amounts of wild type channel and increasing amounts of mutant channel. They found that the chloride current was dose dependently reduced by the mutants and titration experiments suggested that there were either three or four subunits. The double barrelled structure of ClC-0 leads them to favour the tetrameric structure.

Most of the members of the ClC family that have been functionally expressed have the same halide selectivity. ClC-0 (Jentsch *et al.*, 1990), ClC-1 (Steinmeyer *et al.*, 1991b), ClC-2 (Thiemann *et al.*, 1992) and ClC-5 (Steinmeyer *et al.*, 1995) all have Cl > Br > I selectivity sequences. In contrast, ClC-3 has a selectivity sequence of I > Cl > Br (Kawasaki et al., 1994) and the ClC-K channels have a Br > I > Cl selectivity (Uchida *et al.*, 1993; Adachi *et al.*, 1994). Interestingly, there is some controversy over whether ClC-3 and the ClC-K channels can be functionally expressed (Kieferle *et al.*, 1994; Jentsch *et al.*, 1995). It has been suggested that the currents recorded upon expression of these proteins may be endogenous to the expression system. If this is the case then it may account for the different halide selectivity.

Phospholemman.

Phospholemman is a small protein consisting of 72 amino acids that is the major target for phosphorylation by protein kinase A and protein kinase C in the myocardium (Palmer *et al.*, 1991). The expression of phospholemman is not restricted to the heart, it is also found in liver and muscle but not in brain or kidney. Hydropathy analysis shows that phospholemman has only one hydrophobic domain that is capable of forming a transmembrane domain,

however, expression of the protein in *Xenopus* oocytes results in a hyperpolarisation activated chloride current (Moorman *et al.*, 1992). This current, which is calcium independent, is increased by acidification of the external medium and is inhibited by barium ions. Moorman *et al.* (1992) found that mutations in the putative transmembrane domain caused changes in the kinetics of the current and suggested that phospholemman formed a chloride channel upon expression.

It has also been suggested, however, that phospholemman is a regulator of endogenous chloride channels because similar currents are observed in uninjected oocytes (Parker and Miledi, 1988) and overexpression of a dead ClC-1 mutant was also reported to produce hyperpolarisation activated chloride currents (Steinmeyer *et al.*, 1994). This indicated that it was the overexpression of a non specific protein that caused the current.

The endogenous *Xenopus* oocyte current is similar to the current produced upon expression of phospholemman but it is not identical (Kowdley *et al.*, 1994). The endogenous current displays different activation kinetics, pharmacology and is insensitive to changes in the extracellular pH. The strongest evidence, however, for phospholemman forming a chloride channel comes from experiments where phospholemman was incorporated into planer lipid bilayers and shown to produce anion selective currents (Moorman *et al.*, 1995). In such studies the protein is completely isolated and therefore can not be modulating another one. In the same study similar currents were also recorded in excised patches from phospholemman expressing oocytes. In addition, both intact oocytes expressing phospholemman and phospholemman incorporated into bilayers displayed a high taurine permeability. This latter property lead the group to suggest that phospholemman may be involved in cell volume regulation.

Aim of this study.

There is only a very short description of a hyperpolarisation activated chloride current in rat SCG neurons (Selyanko, 1984) and extensive characterisation of the current has not been reported to date. The aim of the experiments reported here was to characterise a number of features of this current. This was done by employing the whole cell and perforated patch clamp techniques together with RT-PCR. The biophysical properties the current and its block by pharmacological agents were studied. In addition, the effects of changes in the external pH and osmolarity were investigated. RT-PCR was carried out using primers for the cloned chloride channel ClC-2, to determine if mRNA for ClC-2 is expressed in rat SCG neurons.

CHAPTER 2: METHODS

The acute dissociation of Superior Cervical Ganglia (SCG) neurons.

7-8 day old Sprague Dawley rats of either sex were killed by decapitation close to the base of the neck and the superior cervical ganglia were removed under sterile conditions. The head was placed onto a Sylgard-lined petri dish, dorsal surface down, and pinned firmly with two pins. The exposed trachea was then separated from the surrounding tissue with dissecting scissors, reflected rostrally and kept in position by a third pin. The ganglia which are white, slightly transparent elongated structures which overlie the carotid artery bifurcation (see figure 2.1), were located under a dissecting microscope by reflecting the bands of longitudinal muscle found either side of the midline. Using a pair of No. 5 watchmakers' forceps and a fine pair of spring iridectomy scissors the ganglia were carefully but rapidly dissected out into a 35mm culture dish containing 3mls of iced Hanks solution (composition/L : 200mg KCl, 30mg KH_2PO_4, 4g NaCl, 60mg $Na_2HPO_4.12H_2O$, 500mg d-Glucose, 596mg N-[2-Hydroxy ethyl] piperazine-N'-[2-ethane sulphonic acid] (HEPES), pH 7.4).

The ganglia were cleaned of extraneous tissue and transferred to a 15ml Falcon tube containing 3mls of Hanks solution supplemented with 41 units of papain and 0.4mg/ml L-cysteine. They were then incubated at 37°C in a water bath for 20 minutes. After this time the papain solution was removed and replaced with 3mls of Hanks solution containing 1.3mg/ml collagenase and 12mg/ml dispase. The ganglia were incubated for a further 30-45 minutes and triturated every 15 minute with a 5ml Gilson pipette to aid cell dissociation. Following this, 3mls of cold Liebovitz L-15 medium were added to the tube and the dissociated ganglia were centrifuged at 1200rpm for 5 minutes to form a loosely bound pellet. The supernatant was carefully drawn off and the pellet was resuspended in another

3mls of L-15 medium. After a further 5 minute centrifugation at 1200rpm the supernatant was removed and replaced with 1ml of medium. The resultant cell suspension was maintained at 4°C and all recordings were obtained from individual neurons, within 10 hours of removal of the ganglia from the animals. Typical examples of cells from which recordings were made are shown in figure 2.2.

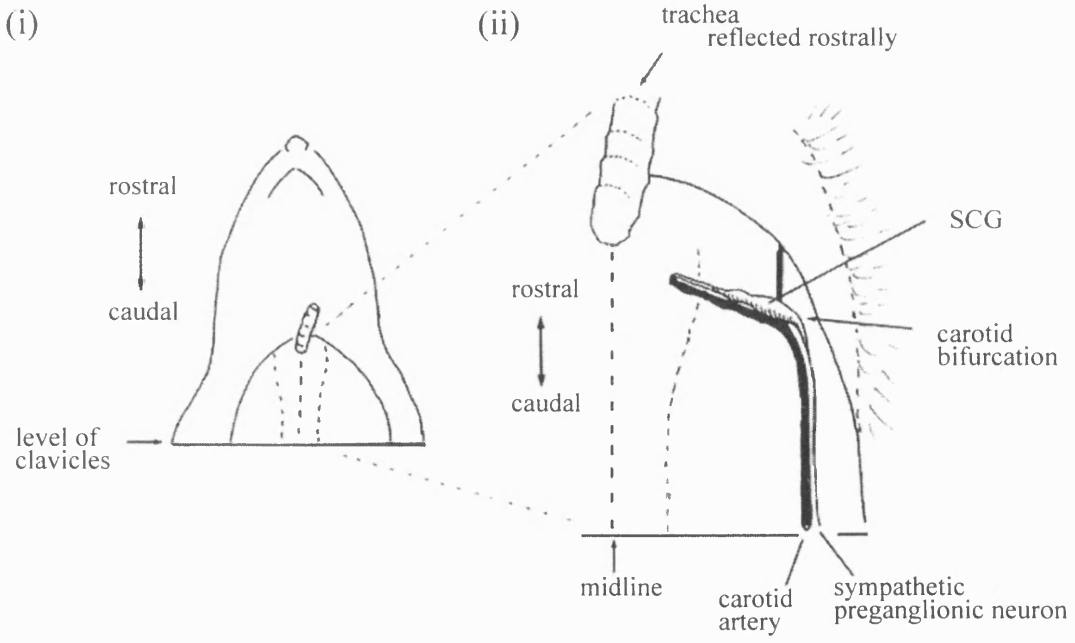

Figure 2.1. Dissection of Superior Cervical Ganglia. **(i)** Diagrammatic representation of the ventral view of the decapitated head. **(ii)** Expanded view that shows the lateral position of the ganglia with respect to the longitudinal muscle bands and the close association of the ganglia with the carotid artery, (Modified from Stansfeld and Mathie, 1993).

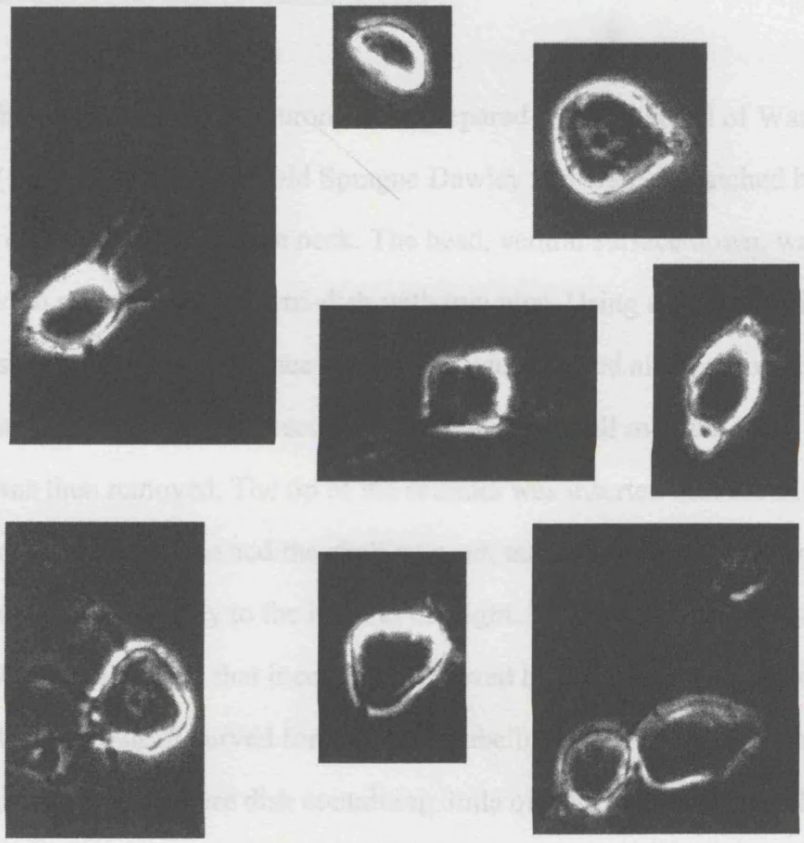

Figure 2.2. Examples of SCG neurons obtained by dissociation. The pictures shown are phase contrast images of a selection of dissociated neurons. As can be seen from the images some neurons have processes while some are spherical. Others have obviously been damaged by the dissociation procedure and are granular in appearance. Only those neurons which were smooth in appearance and were phase bright were recorded from. Cells were approximately 15 - 20 μM in diameter.

The preparation of Cerebellar granule neurons.

Cerebellar granule (CG) neurons were prepared by the method of Watkins and Mathie (1994, 1996). 7-8 day old Sprague Dawley rats were dispatched by decapitation close to the base of the neck. The head, ventral surface down, was firmly pinned to a Sylgard-lined petri-dish with two pins. Using a fine pair of scissors the skin on the dorsal surface of the head was bisected along the midline, reflected away from the skull and secured with pins. The skull over the cerebellum was then removed. The tip of the scissors was inserted into the skull at the point where the plates fuse and the skull was cut, taking care not to damage the tissue underneath, laterally to the left and the right. The caudal plate was then bisected down the midline so that it could be removed by reflection away from the cerebellum. Using a pair of curved forceps the cerebellum was removed in one go and placed into a 35mm culture dish containing 3mls of Earles medium (g/ml: 6.8 NaCl, 2.2 $NaHCO_3$, 0.16 NaH_2PO_4, 0.4 KCl, 0.2 $MgSO_4$, 0.2 Glucose) which had been supplemented by 0.08mg/ml DNase, 0.25mg/ml soybean trypsin inhibitor and 3mg/ml bovine serum albumin (BSA).

The meninges and any extraneous tissue were removed from the cerebellum which was then chopped into small pieces with fine scissors. The solution and chopped tissue were transferred to a 15ml Falcon tube and triturated with a fire polished Pasteur pipette to achieve a milky cell suspension. The suspension was allowed to settle for 5 minutes and then the supernatant was removed into a second Falcon tube to be centrifuged at 500 rpm for 5 minutes. The pellet was resuspended in culture medium (minimum essential medium, 10% FCS, 25µl/ml chick embryo extract, 50IU penicillin, 50µg/ml streptomycin).

50µl aliquots of cell suspension were then placed into the centre of 13mm, poly-l-lysine coated, glass coverslips. After being incubated for one hour at 35°C

in humidified air (5% O_2/95% CO_2) the coverslips were flooded with 0.5 mls of growth medium. All recordings and RT-PCR experiments were carried out on neurons 48-72 hours after they were plated out.

Electrophysiological recording.

All the data presented were recorded using the conventional whole cell configuration of the patch clamp technique (Hamill *et al.*, 1981) or the amphotericin B perforated patch technique (Rae *et al.*, 1991). All experiments were conducted at room temperature (21-25°C). The membrane potential was voltage clamped using an Axopatch 1-D amplifier (Axon instruments) and the currents were low pass filtered at 5kHz. Data were sampled and captured on line to a Viglen 486 computer via a TL-1 DMA interface. Voltage protocol generation and data acquisition were achieved using pClamp 5.5 or pClamp 6.0.2 software (Axon Instruments). In the conventional whole cell mode, compensation of the capacity transients gave a mean whole cell capacitance of 21.3 ± 0.7pF and a mean series resistance of 7.6 ± 0.4MΩ (n = 167). Compensation of the capacity transients in the perforated patch mode gave a mean whole cell capacitance of 20.3 ± 2.3pF and a mean series resistance of 20.8 ± 2.3MΩ (n = 16).

Voltage protocols.

The following voltage protocols were used in experiments:

1. To obtain a current-voltage relationship the membrane potential was held at either 0 or -30mV and the potential was stepped between -10 and -120mV in a series of 10mV steps lasting 3000ms. The membrane was then depolarised to -60mV for 800ms before being returned to the holding potential. The currents were sampled at 500Hz and the inter-episode duration was 10s.

2. The second type of voltage protocol that was used was the same as the first except that only one step to -90mV was applied and the currents were sampled at 250Hz.

3. Tail currents, which were used to obtain the reversal potential of the current, were generated in early experiments by applying a 2000ms prepulse to -110mV from a holding potential of -30mV and then stepping in 10mV steps between -60 and +40mV for 1400ms. The inter-episode duration was 10s and currents were sampled at 500Hz. In later experiments the reversal potential was determined by applying a 4058ms prepulse to -90mV from a holding potential of 0mV and then stepping for 4750ms to potentials between -60 and +60mV in a series of 20mV steps. The inter-episode duration was 12s and currents were sampled at 250Hz for the prepulse step and 200Hz for the depolarisation steps. This latter protocol was established because it was less harsh on the cells.

The currents generated by the above voltage protocols were not leak subtracted at the time of recording but by subtracting the instantaneous current from the steady-state current the leak current was subtracted from the data at the time of analysis.

Parameter measurement and analysis.

Parameter measurements were carried out using clampfit analysis software (Axon). Figure 2.3 indicates how current parameters were determined. The instantaneous current was defined as the amplitude of the current measured approximately 25ms after the start of the voltage step (A, figure 2.3). The amplitude of the steady-state current was measured towards the end of the voltage step, approximately 2900ms into the voltage step (B, figure 2.3). The magnitude of the time dependent current was defined as the difference between the two (B-

A). In the results chapters the current amplitude (unless otherwise mentioned) refers to the time dependent current amplitude as determined by this method. To determine the reversal potential of the current, the tail current amplitude was plotted against command potential. In the early experiments, the peak tail current was plotted, that is the current measured at C. In the later experiments the time dependent tail current was plotted. This was defined as the difference between the peak and the end tail current amplitudes (C-D).

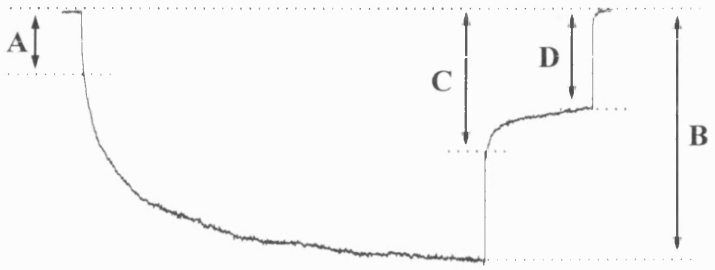

Figure 2.3. Diagram illustrating how current parameters were determined. The amplitude of the instantaneous current was measured as shown by A and the amplitude of the steady-state current was measured as shown by B. Subtracting the instantaneous current from the steady-state current (B-A) gave the time dependent current amplitude. The current measured at C gave the peak tail current, while the difference between C and D gave the amplitude of the time dependent tail current.

Once parameters had been measured, the data obtained was manipulated using Excel spread sheets and graphically presented using Origin software. Specific details of analysis are explained at the relevant points in the individual results chapters. Statistical comparison was achieved with either a paired or unpaired Students t test, as appropriate. The exception to this was the comparison of current amplitudes measured using different internal chloride concentrations. The test used for that comparison was an unpaired Welch (alternate) t test. The data, where applicable, are presented as mean ± standard error of the mean (sem), with n being the number of neurons from which the currents were recorded.

The manufacture of electrodes.

Electrodes were manufactured from thick walled boroscilicate glass capillary tubing (Plowdon and Thompson, 1.4-1.6mm (outer diameter) x 0.8-1.0mm (inner diameter) with 2mm fibre) using a vertical two stage List medical L/M-3P-A or a Flaming/Brown (model P-87, Sutter Instrument Co.) micropipette puller. They were fire polished as necessary using a Narishige MF-83 micro forge. The electrodes were filled with the appropriate internal solution (see below) and were then coated with sigma-cote (Sigma Chemicals Ltd.). The resistance of the filled electrodes was between 3 and 6MΩ.

Composition of the pipette and external solutions.

Pipette solution composition.

The standard pipette solution used was a CsCl based solution, the composition of which was (in mM): 125 CsCl, 5 HEPES, 5 $MgCl_2$ and 0.1 Bis (2-aminophenoxy)-ethane-N, N, N', N' tetraacetate (BAPTA) .This solution was titrated with CsOH to pH 7.4. In addition the osmolarity was measured with a Wescor 5500 Vapor pressure osmometer (Chemlab scientific products Ltd.) and corrected to between 300 and 310 mmol/kg with sucrose. The effects of internal BAPTA on the inhibition of the current by zinc were investigated using a modified CsCl based solution, composition (in mM): 115 CsCl, 5 $MgCl_2$, 5 HEPES and 10 BAPTA. To study the effect of reducing the internal chloride concentration 120mM of the CsCl was replaced by 120mM Cs acetate or K aspartate.

Composition of the external solutions.

Once cells had been clamped they were continually perfused with control external solution. The perfusion system consisted of six reservoirs from which solutions of different composition were gravity fed into the bath. The inflow for the perfusion system was placed approximately 2mm from the cell, close to the surface of the culture dish. The outflow was positioned behind the electrode, at the surface of the bath fluid and inline with the inflow pipe. The flow of solution was maintained at approximately 4-5ml/min. The effect of a change in external solution was generally observed 50 to 150s after the solution had been changed.

In early experiments the external solution was one which was suitable for measuring calcium currents (external 1) and had the following composition (in mM): 108.5 NaCl, 2.5 KCl, 10 $BaCl_2$, 2 $MgCl_2$, 8 glucose, 10 HEPES. The solution was titrated with KOH to pH 7.4. This solution, however, resulted in contamination by calcium currents upon depolarisation of the membrane potential so the solution was modified to allow the hyperpolarisation activated current to be studied in relative isolation. The modified external solution (external 2) consisted of (in mM): 117.5 NaCl, 2.5 KCl, 2.4 $MgCl_2$, 0.1 $CaCl_2$, 8 glucose, 10 HEPES, 10 Tetraethylammonium (TEA), 0.005 Tetrodotoxin (TTX). Together with the CsCl based internal solution this external solution should have effectively blocked the Ca^{2+}, K^+ and Na^+ currents present in rat SCG neurons. However, when the membrane potential was depolarised at the end of a command step there was still an unidentified current present. This current was found to be reduced when external K^+ was removed and therefore a further modification to the external solution was made, namely all external KCl was substituted with an equimolar amount of NaCl and the solution was titrated with NaOH to pH 7.4. This solution (external 3) enabled tail currents and hence reversal potentials to be measured more accurately.

In all experiments where the ionic composition of the external solution was altered, the replacement ion was always substituted by replacing NaCl with the sodium salt of the replacement ion or by equimolar substitution of NaCl. The exception to this was the N-methyl-D-glucamine (NMDG) substituted solution where both the NaCl and KCl were replaced. The solution was titrated with HCl to pH 7.4 and this resulted in the Cl^- concentration remaining approximately the same. The osmolarity of the external solution was measured and adjusted to between 310 and 325 mmol/kg with sucrose. To study the effects of external hypotonicity the osmolarity of external 3 was left uncorrected. The osmolarity of such a solution was between 255 and 263 mmol/kg.

Liquid junction potentials.

The liquid junction potentials generated between the solutions used in the experiments described here, were calculated where possible using ion concentrations and the generalised Henderson equation. The values calculated were relatively small (see table 1, appendix 1) and as a result the data have not been corrected for them.

Reverse Transcription-polymerase chain reaction (RT-PCR).

Preparation of SCG and CG neurons for RT-PCR experiments.

Cell suspensions of SCG neurons were obtained as described above. A suspension of CG neurons was obtained by triturating the neurons from the coverslips after they had been in culture for two days. The cell suspension that was obtained was centrifuged at 1000rpm and the pellet was then resuspended in Liebovitz L-15 medium. For both cell types the cell suspension was then maintained at 4°C for 30-60 minutes to enable the cells to recover from the dissociation process. Before use the cell suspensions were centrifuged at 1000 rpm for 5 minutes and the supernatant removed. The cell pellet was then used in the preparation of mRNA.

The primers used in the RT-PCR experiments.

The sequences of the two primer pairs used in the RT-PCR reactions were identical to those used by Smith *et al.*, (1995). Both sets of primers probed for regions at the amino terminal of the ClC-2 sequence where sequence similarity with other members of the ClC family was least. The ClC primers probed for a 755bp sequence while ClCS probed for a 238bp sequence. The ClCS sequence was amino terminal to that probed by the ClC primers. It was necessary to use the ClCS primers rather than the ClC primers in experiments in which Actin primers were also used because the actin primers probed for a sequence of almost identical length to that probed for by the ClC primers. It would therefore have been impossible to determine if both the ClC-2 and Actin sequences had been detected.

The primers which were used to probe for ClC-2 were as follows (the figures in brackets refer to the base pair sequence of ClC-2):

ClC.for	5'-GTACCC***C***ATGTAGCCCTCAGC-3' (1948-1969)
ClC.rev	5'-CCGGAGCTCCTTTAGGGTGAC-3' (2703-2683)
ClCS.for	5'-GGAAGGGATGGAGCCTCGAG-3' (207-226)
ClCS.rev	5'-CCCTGGACACTAGGAACTTGT-3' (445-425)

Actin is ubiquitously expressed in all cell types and the reverse transcription and amplification of its mRNA was employed as an internal control. The primer pairs used had the following sequences and probed for a 763bp sequence.

ACTIN.for	5'-TTGTAACCAACTGGGACGATATGG-3' (1554-1577)
ACTIN.rev	5'-GATCTTGATCTTCATGGTGCTAGG-3' (2869-2846)

The purification of cell mRNA.

To separate the mRNA from other RNAs present in cells magnetic oligo-dT beads (Dynabeads, Dynal) were employed. These polystyrene beads are 2.8μm in diameter and have 25 nucleotide long chains of deoxy-thymidine covalently attached to them by a 5' linker group. These beads can isolate up to 2μg of polyA-RNA under the appropriate conditions.

The cells, prepared as described above, were gently triturated with 50μl of lysis buffer (Dynal) so that the cell membranes were disrupted and the total cell RNA released. The success of the trituration in disrupting the cells was judged by the viscosity of the solution which indicated the presence of strands of DNA. Once the cells were sufficiently disrupted the solution was centrifuged at 2150

rpm for 5 minutes to sediment the cell debris. The supernatant was removed and added to 50µl of prewashed magnetic oligo-dT beads in a PCR reaction tube. This mixture was incubated at room temperature for 10 minutes to enable the mRNA to bind to the beads. After this time the tube was placed on ice and the beads were washed with 3 volumes of wash buffers I and II (Dynal) and 3 volumes of 1x RT buffer (see table 2.1). This was to ensure that there was as little genomic DNA present in the sample as possible. Before draining the final RT buffer wash the beads were split as necessary into separate PCR reaction tubes.

Reverse Transcription (RT) of mRNA to cDNA.

Once the beads had been drained of RT buffer, 10µl of RT incubation mixture (see table 2.1) was added to each tube. The reagents required for reverse transcription were made up as a master mix because of the small volumes and therefore the possible error that would be involved if the reagents were added separately to individual tubes. To prevent evaporation of the reagents during repeated heating and cooling the reaction mixture was overlaid with 20µl of mineral oil (Sigma Chemical Ltd.). The reagents were heated to 64 or 70°C (see results) by placing the tubes in a thermal cycler (Techne, cyclogene) previously heated to that temperature and they were then incubated for 30 minutes to enable the mRNA to be transcribed into cDNA. The reaction was stopped by placing the tubes on ice.

Solution	Composition
Lysis Buffer	100mM Tris-HCl, 500mM LiCl, 10mM EDTA, 1% LiDS, 5mM DTT, pH 8.
Wash Buffer I	10mM Tris-HCl, 150mM LiCl, 1mM EDTA, 0.1% LiDS, pH 8.
Wash Buffer II	10mM Tris-HCl, 150mM LiCl, 1mM EDTA, pH 8.
RT Buffer (10x)	10mM Tris-HCl, 90mM KCl, pH 8.3.
Chelating Buffer (10x)	5% glycerol, 8mM Tris-HCl, 80mM KCl, 0.04% Tween 20, 0.6mM EGTA, pH 8.3.
RT Master Mix	200μM dNTPs, 0.25U/μl rTth, 1x RT buffer, 1mM $MnCl_2$, 0.75μM Reverse primer(s).
PCR Master Mix	1x Chelating buffer, 1.5mM MgCl2, 0.25U/μl rTth, 0.15μM forward primer(s).

Table 2.1. Composition of the solutions used in the reverse transcription polymerase chain reaction. EDTA (Ethylenediaminetetraacetic acid), EGTA (Ethyleneglycol-bis(β-aminoethyl)-N,N,N',N'-tetraacetic acid), dNTPs (di-nucleotide-tri-phosphates), TRIS HCl (tris (hydroxymethyl) aminomethane, HCl), rTth (rTth DNA polymerase), LiDS (lithium n-Dodecyl sulphate), DTT (dithiothreitol)

Amplification of cDNA by the Polymerase chain reaction (PCR).

After completion of the RT step, amplification of the resultant cDNA was carried out using the polymerase chain reaction. 40µl of PCR incubation mixture (see table 2.1) was added through the mineral oil layer and the mixture was brought to 95°C by placing the tubes in a preheated thermal cycler block. The tubes were incubated for two minutes at this temperature so that the cDNA was denatured and ready for amplification. The amplification process consisted of a series of denaturing (heating to 95°C for 1 minute) and annealing/ extending steps (cooling to 62°C for 2 minutes). The process was completed by incubating the reaction tubes for a further 7 minutes at 62°C. The tubes were then placed on ice.

Manufacture of agarose gel.

A 2% agarose gel was cast by melting 1g of agarose in 50mls of TBE (Tris-borate, EDTA (45mM tris-borate, 1mM EDTA)) electrophoresis buffer until a clear, transparent solution was achieved. The agarose was then cooled to 60°C, poured into an electrophoresis tank and allowed to harden. Once this had occurred the gel was covered to a depth of about 2mM with TBE.

Preparation of samples, obtained from the RT-PCR procedure, for electrophoresis.

2µl of gel loading buffer (6x: 0.25% bromophenol blue, 0.25% xylene cyanol FF, 30% glycerol in water) was added to 10µl of each of the samples. 2µl of DNA size markers (100bp fragments, 50ng/ml, Sigma) was diluted with 10µl of 1x gel loading buffer. 10µl of the prepared samples and DNA size markers were then transferred to individual wells of the gel. The gel was run at 70V for approximately 40 minutes.

Visualisation of the cDNA bands.

The gel was gently shaken in a 30μg/ml solution of ethidium bromide (Sigma) for 15-20 minutes. The bands were then visualised with an ultra violet light source. A Polaroid photograph was taken of the illuminated gel to give a permanent record of the results. If the amount of DNA was expected to be low then the gel was incubated in ethidium bromide for 20-30 minutes and afterwards it was destained by placing it in a solution of 1mM $MgSO_4$ for 30-40 minutes.

Materials.

Cell dissociation was achieved with collagenase (type I) purchased from Sigma Chemicals Ltd. and dispase (type II) from Boehringer Mannheim. Liebovitz L-15 medium was obtained from GIBCO-BRL. All salts used to make internal and external solutions, unless otherwise stated were of AnalaR standard and were purchased from BDH. BAPTA, HEPES, sucrose, TTX, TEA, 4,4'-Diisothiocyanato-stilbene -2,2'-disulphonic acid (DIDS), 4-Acetamido-4'-isothiocyanato-stilbene-2,2'-disulfonic acid (SITS), Antracene-9-carboxylic acid (9AC), $CdCl_2$, $ZnCl_2$ and niflumic acid were all purchased from Sigma Chemicals Ltd. 5-Nitro-2-(3-phenylpropylamino) benzoic acid (NPPB) was purchased from Research Biochemicals International (RBI).

RT-PCR primers were purchased from Perkin-Elmer. The other components of the reaction mixtures required for the RT-PCR experiments were kindly provided by Dr. Maureen Docherty.

CHAPTER 3

Biophysical characteristics and ionic selectivity of the hyperpolarisation activated current in rat SCG neurons.

INTRODUCTION.

An increase in conductance upon hyperpolarisation and a decrease in conductance upon depolarisation of the membrane potential was first demonstrated in frog skeletal muscle fibres (Katz, 1949). The term used to describe this phenomenon was anomalous or inward rectification. Subsequently there have been numerous studies which have identified other hyperpolarisation activated inwardly rectifying currents in a variety of both vertebrate and invertebrate cell types.

Three main types of inwardly rectifying currents have been described. The first of these are cationic currents and these have been described in cells of the olfactory cortex (Constanti and Galvin, 1983), in starfish eggs (Hagiwara and Takahashi, 1974), tunicate embryos (Miyazaki *et al.*, 1974) and skeletal muscle (Hodgkin and Horowicz, 1959). These currents are solely permeable to potassium ions and it has been found that the activation threshold is dependant on the difference between the membrane and potassium equilibrium potentials (Hagiwara and Takahashi, 1974). These currents are rapidly activating and voltage dependent (e.g. Constanti and Galvin, 1983). The currents activate at potentials hyperpolarised to the potassium equilibrium potential and switch off at potentials depolarised to this. They are blocked by both barium and caesium ions at concentrations of less than 1mM and between 0.3-10mM respectively (e.g. Constanti and Galvin, 1983, Gay and Stanfield, 1977, Hagiwara *et al.*, 1978). Inwardly rectifying potassium channels have recently been cloned (IRK1, Kubo *et al.*, 1993; HIR, Perier *et al.*, 1994; HRK1, Makhina *et al.*, 1994) and they have

been functionally classified as strong inward rectifiers (Hille, 1992) owing to the steepness of the slope conductance at potentials hyperpolarised to the potassium equilibrium potential. The inward rectification observed was originally thought to be due to intrinsic gating properties and a voltage dependent block by magnesium (Hille,1992). However, it now appears that some if not all the inward rectification is the result of the actions of spermines, in particular spermidine (Lopatin *et al.*, 1994).

The second group of hyperpolarisation activated currents are also cationic but they tend to be equally permeable to both sodium and potassium and activate only slowly. Currents which fall into this category include I_f, (Brown and DiFrancesco,1980), I_h (Bader *et al.*, 1982; Crepel and Penit-Soria, 1986; Mayer and Westbrook, 1983), I_Q (Halliwell and Adams, 1982) and I_{AR} (Spain *et al.*, 1987; Araque and Buño, 1994). These currents are steeply voltage dependent but the voltage dependence of current activation is not determined by the extracellular potassium concentration (Hille, 1992). This type of current is also blocked by low concentrations of caesium ions (0.2-10mM) but they are insensitive to barium (Crepel and Penit-Soria, 1986; Di Francesco, 1982).

The final group of hyperpolarisation activated, inwardly rectifying currents, which have been described are chloride currents. Until recently, very little characterisation of hyperpolarisation activated chloride currents had been carried out, one possible exception being the current found in *Aplysia* A neurons (Chesnoy-Marchais, 1983). However, a number of chloride channels were recently cloned which when expressed in *Xenopus* oocytes resulted in hyperpolarisation activated chloride conductances (see chapter 1 for details). They are ClC-0 (Jentsch *et al.*, 1990) and ClC-2 (Thiemann *et al.*, 1992), which belong to the ClC family of voltage gated chloride channels and phospholemman, which is a major target for protein kinase phosphorylation in the heart (Moorman *et al.*,

1992). Since the discovery and successful expression of these channels the number of hyperpolarisation activated chloride currents that have been identified has increased. Hyperpolarisation activated chloride currents have now been found in a wide range of cells. They have been identified in invertebrate cell types which include *Aplysia* neurons (Chesnoy- Marchais, 1983) and *Xenopus* oocytes (Parker and Miledi, 1988; Kowdley *et al.*, 1994). They have also been described in both neuronal and non-neuronal mammalian cell types such as hippocampal pyramidal neurons (Madison *et al.*, 1986; Staley, 1994), T_{84} epithelial cells (Fritsch and Edelman, 1996), rat osteoblastic cells (Chesnoy-Marchais and Fritsch, 1994), mouse mandibular cells (Dinudom *et al.*, 1993), cortical astrocytes (Ferroni *et al.*, 1995), rat leydig cells (Noulin and Joffre, 1993) and rat parotid acinar cells (Arreola *et al.*, 1996)

Rat SCG neurons were first shown to possess a hyperpolarisation activated current by Selyanko (1984). It was reported to be a chloride current since it was augmented if recorded with a KCl or CsCl microelectrode solution rather than an acetate based solution. However, no further characterisation was carried out and no detailed information on the current is known. Recently, it has been shown that rat SCG neurons also possess a hyperpolarisation activated potassium current (Wang and McKinnon, 1996). This current has properties that appear to have most in common with the strong inward rectifier type currents and, as will be detailed in the following section, does not appear to be the current which has been described here.

The experiments which are presented in this chapter were designed to enable a more detailed description of the biophysical properties and ionic selectivity of the hyperpolarisation activated chloride current to be obtained.

RESULTS.

General features of the hyperpolarisation activated current in rat SCG neurons.

Figure 3.1a shows typical data traces obtained by stepping from a holding potential of -30mV to command potentials between -10mV and -120mV in 10mV steps. Currents, which activated slowly with hyperpolarising voltage steps, consisted of an instantaneous current jump followed by a time dependent relaxation. The current recorded at hyperpolarised potentials was due to an increase rather than a decrease in conductance since the instantaneous current measured at the end of the voltage step was larger than that measured at the beginning. For example, in figure 3.1a, the current at the end of the voltage step to -120mV was -576pA while that at the start of the step was only -223pA. A hyperpolarisation activated current could be recorded in all neurons but the amplitude of the current was variable between individual cells. The amplitude of the time dependent current activated by stepping to -90mV from a holding potential of -30mV ranged from -20 to -310pA (n = 98). The current amplitude did not appear to depend on the cell size since the range of whole cell capacitance values was much tighter than the range of current amplitudes (see methods). All the experiments in this thesis are from neurons dissociated from 7-8 day old rats, the current could also be recorded in neurons dissociated from adult rats.

In figure 3.1b the instantaneous current, which is the current amplitude measured immediately after the start of the voltage step (closed squares, figure 3.1a), is plotted together with the amplitude of the steady state current (the current at the end of the voltage step, open circles, figure 3.1a). The amplitudes of both the instantaneous current and the steady state current show strong voltage dependence.

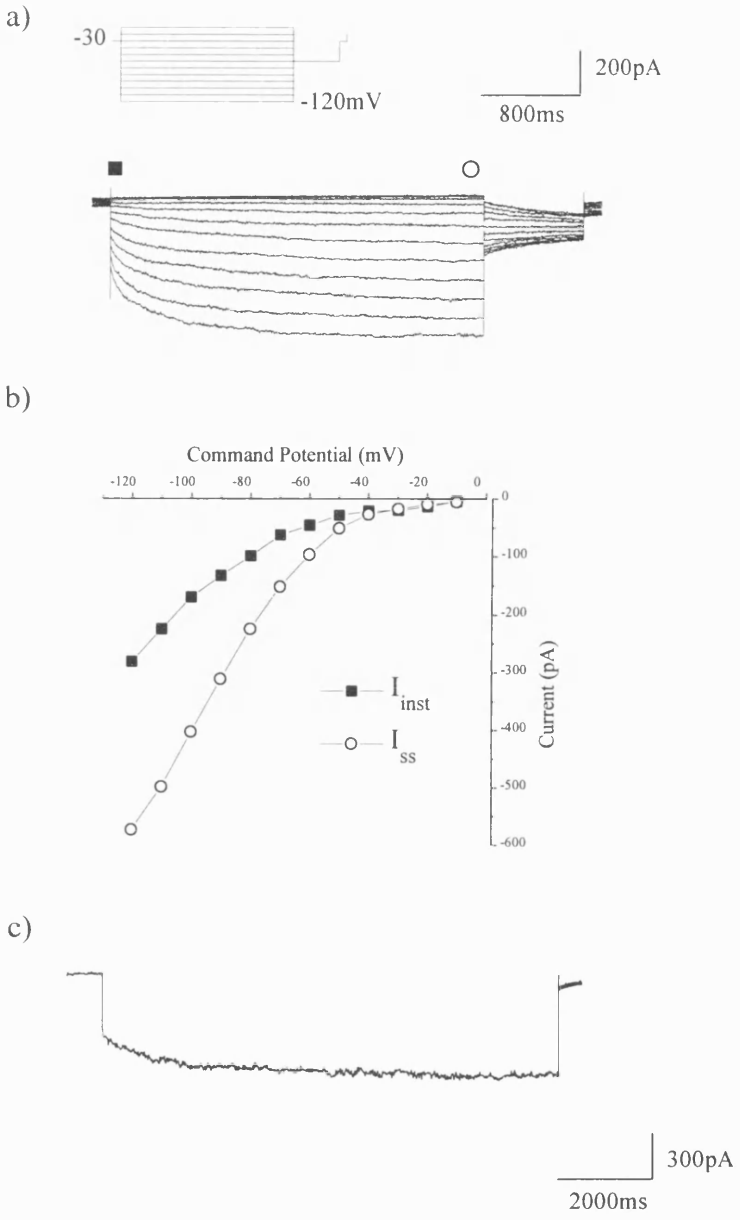

FIGURE 3.1. A hyperpolarisation activated current. **(a)** Typical data traces which are generated by applying 10mV voltage steps to between -10 and -120mV from a holding potential of -30mV. **(b)** The instantaneous current amplitude, (I_{inst}, closed squares) measured at the point shown by the closed squares in (a), is plotted together with the steady-state current (I_{SS}, open circles), which is measured at the point shown by the open circles in (a). **(c)** A typical data trace recorded by applying a single voltage step to -90mV from a holding potential of -30mV for 10s, note the difference in time scale in (a) and (c).

A feature of the currents shown in figure 3.1a is that they do not appear to show any time dependent inactivation over the time course of the voltage steps that were typically used. This was further confirmed by applying a single hyperpolarising voltage step to -90mV for 10s (n = 2). Even over this time course the current showed no inactivation, indeed the current amplitude continued to increase slightly during the voltage step (figure 3.1c).

Comparison of the currents activated from holding potentials of -30 and 0mV.

The instantaneous component of the current showed inward rectification when currents were generated by stepping from a holding potential of -30mV (figure 3.1b). There are a number of possible explanations for this. The first is that there is more that one current present under the recording conditions. The other more likely reason however, is that some of the channels underlying the current are open at -30mV and the current jump at the start of the voltage step is due to an increase in driving force.

Figure 3.2a shows typical current traces generated by stepping between -10mV and -110mV from a holding potential of 0mV. As can be observed from the data traces the instantaneous current is much reduced. The instantaneous current and steady state current amplitudes (measured at closed squares and open circles respectively, figure 3.2a) are plotted in figure 3.2b. The instantaneous current measured using this voltage protocol is linear, at least over the voltage range studied and therefore probably represents a leakage current. The steady state current still shows strong inward rectification.

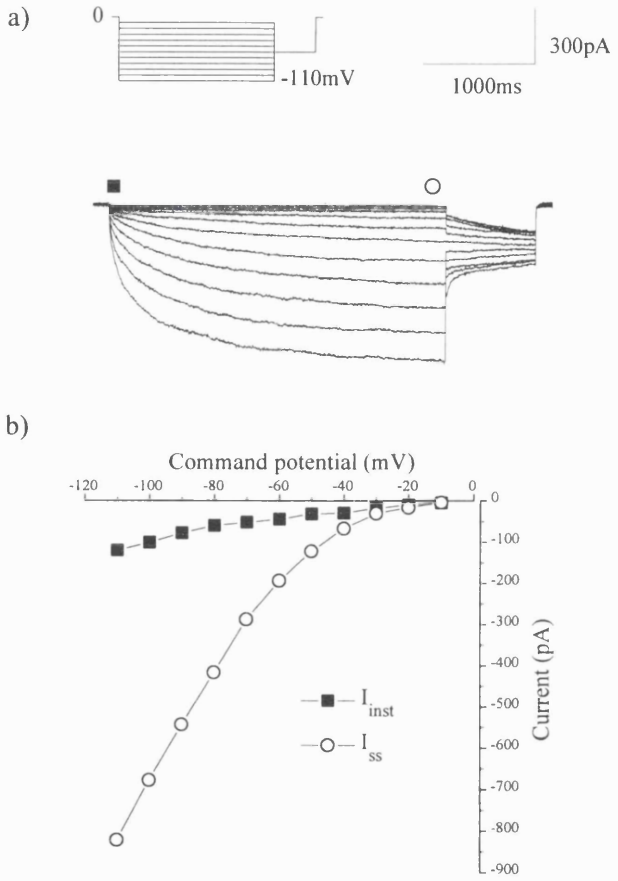

FIGURE 3.2. The hyperpolarisation activated current activated from a holding potential of 0mV. **(a)** Typical data traces recorded by applying hyperpolarising voltage steps to between -10 and -110mV from a holding potential of 0mV. **(b)** The instantaneous and steady-state current amplitudes plotted against command potential for the current shown in (a). The current amplitudes were measured as described for FIGURE 1.

Subtracting the instantaneous component of the current from the steady state current gives the amplitude of the time dependent relaxation. The amplitude of the time dependent current generated from a holding potential of -30mV or 0mV is shown in figure 3.3. The data shown are the mean ± sem, n = 7 for all data points. Figure 3.3 illustrates that there is an apparent increase in the time dependent current with the more depolarised holding potential such that at -110mV the mean current amplitudes are -176.8 ± 28.6pA and -356.4 ± 118.3pA for the -30mV and 0mV holding potentials respectively. Using a holding potential of 0mV it can be seen that the time dependent current activates at potentials hyperpolarised to -20mV. Therefore, when a holding potential of -30mV was used the current was already activated and stepping the potential hyperpolarised resulted in a large instantaneous component due to an increase in the driving force for the open channels. The large instantaneous component masked the initial portion of the time dependent current resulting in an apparent reduction in observed time dependent current amplitude.

The magnitude of the hyperpolarisation activated current increases with recording time.

Figure 3.4 is a graph of the amplitude of the time dependent current, which was activated by a voltage step to -90mV from a holding potential of 0mV, plotted against the approximate time into the recording. As can be seen from the graph, the amplitude of the current increases with recording time. There is an approximately 3-fold increase in current size over the time course shown. For example, at 1 minute into the recording the current amplitude was -56.3 ± 15.3pA (n = 5) while 14 minutes into the recording it was -206.6 ± 22.4pA (n = 5).

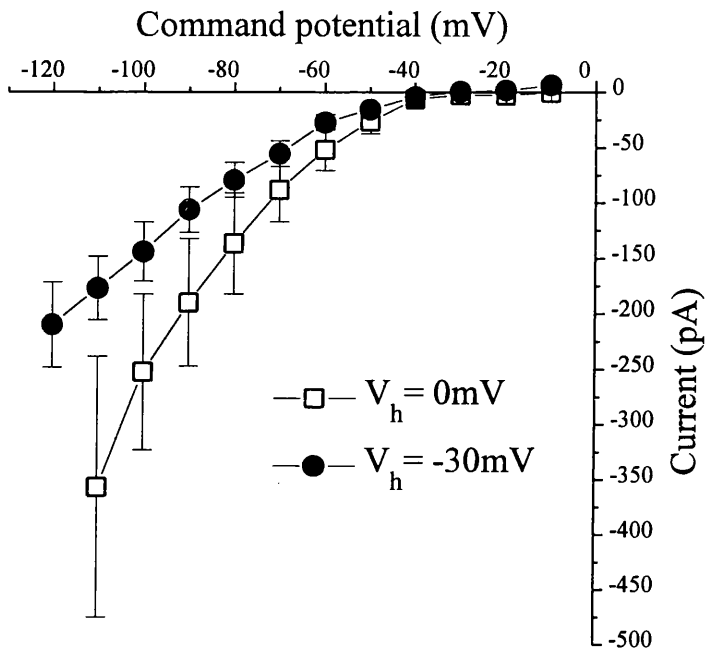

FIGURE 3.3. Comparison of the amplitudes of the currents generated from holding potentials of -30 and 0mV. The data plotted are the mean current amplitudes recorded as a result of the application of a series of voltage steps from holding potentials of -30mV (closed circles) and 0mV (open squares). The data shown are mean ± sem, n = 7.

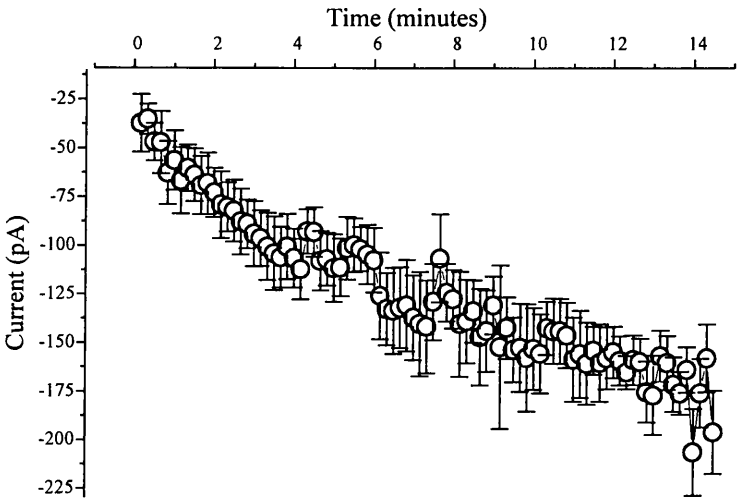

FIGURE 3.4. The amplitude of the hyperpolarisation activated current increases with time into the recording. The amplitude of the time dependent current, generated by a single step to -90mV from a holding potential of 0mV, is plotted against approximate time into the recording. The data shown are the mean ± sem (n = 5).

Fitting of a double exponential by the method of exponential peeling.

The activation of the currents in six neurons was studied in more detail by the fitting of exponential functions. Initially this was attempted using the fitting programmes which are part of the Axon clampfit and Origin software, however while the fitting programmes clearly indicated that the current activation was better fitted with a double rather than a single exponential function, the time constant and amplitude values obtained were neither reasonable nor repeatable between individual cells. Because of these difficulties a method of exponential peeling was employed.

Exponential peeling is a method by which the individual components of the double exponential function are separated. Figure 3.5 illustrates how the data was successfully fitted with a double exponential function using the exponential peeling method. Figure 3.5a shows the time dependent current in isolation. The data trace shown is one generated by stepping to -110mV from a holding potential of 0mV. The current amplitude was made positive by adding the maximum steady state current amplitude to the total current, hence the steady state current has an amplitude of approximately 0pA while the current amplitude at the start of the voltage step is about 400pA. This transformation was essential for the next step where the natural logarithm of the current amplitude was taken. The next step was to take the natural logarithm of the current amplitude and fit a straight line (arrow 1, figure 3.5b) to the second part of the transformed current trace. This fitted line was then subtracted from the total current to give the data trace shown in figure 3.5c (the current amplitude is now plotted on a linear scale). This data trace was reliably fitted with a single exponential equation (arrow 2) using the Origin fitting programme. The values obtained by fitting this single exponential were then put into a double exponential equation which was used to fit the total time dependent current as shown in figure 3.5d (arrow 3).

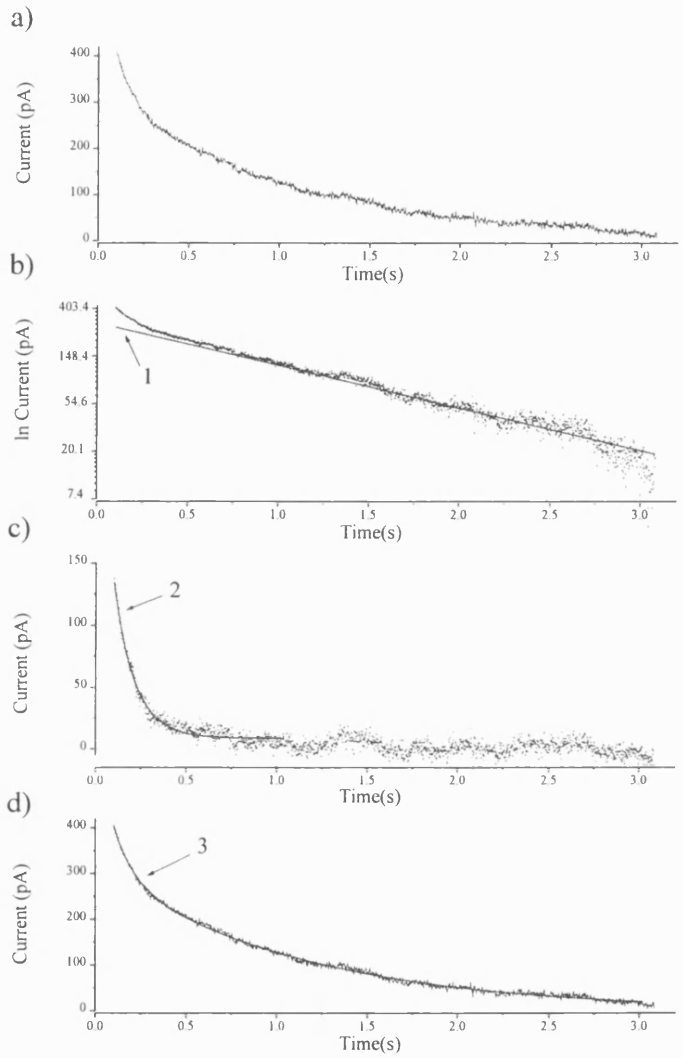

FIGURE 3.5. The fitting of a double exponential function by the method of exponential peeling. **(a)** The time dependent current only is plotted. The current has been made positive by the addition of the steady-state current amplitude to the data trace, that is 400pA was added to each sample point. **(b)** The natural logarithm of the current amplitude is taken (ln current, y-axis). A straight line is then fitted to the second part of the transformed data trace (shown by arrow 1). **(c)** The straight line is subtracted from the total current and a single exponential function is then fitted to the initial part of the remaining current (shown by arrow 2). Note that the current amplitude axis is linear. **(d)** The time constant and current amplitude values obtained by fitting the single exponential are put into a double exponential equation which is then used to fit the total current (shown by arrow 3). The current trace shown is one that was generated by a hyperpolarising voltage step to -110mV.

Using this method double exponential functions could be reliably fitted to current traces generated by hyperpolarising voltage steps to between -80 and -110mV. The results of this fitting procedure are illustrated in figure 3.6. The time constants (τ_1 and τ_2) both decreased with increasing hyperpolarisation. τ_1 (figure 3.6a) decreased, although not significantly ($p > 0.5$), from 0.33 ± 0.04s ($n = 5$) at -80mV to 0.20 ± 0.02s ($n = 6$) at -110mV. τ_2 (figure 3.6b) was significantly ($p < 0.002$) reduced from 2.3 ± 0.2s ($n = 5$) at -80mV to 1.3 ± 0.1s ($n = 6$) at -110mV. τ_2 was approximately seven times slower than τ_1 at all potentials. The respective amplitudes A_1 and A_2 are shown in figures 3.6c and 3.6d. Both amplitudes significantly increased with increasing hyperpolarisation such that at -80mV A_1 was 45.2 ± 1.5pA and A_2 was 143.5 ± 10.9pA while at -110mV A_1 was 112.1 ± 7.7pA and A_2 was 270.6 ± 35.1pA ($p < 0.003$, $p < 0.02$, for A_1 and A_2 respectively). A_1 expressed as a fraction of the total current amplitude (A_1+A_2) is plotted in figure 3.6e. It did not significantly change with command potential ($p > 0.2$). At -80mV the A_1 as a fraction was 0.24 ± 0.01 ($n = 5$) while at -110mV it was 0.31 ± 0.04 ($n = 6$).

In figure 3.6f the goodness of the fits obtained by exponential peeling was determined. The total amplitude (A_1+A_2) obtained by the fitting procedure was plotted (open circles) together with the current amplitude as measured by subtracting the instantaneous current from the steady state current (closed squares). As can be seen from the graph there does not appear to be any substantial difference in the current amplitudes determined by the two methods. This confirms that the fits obtained by exponential peeling are reasonable.

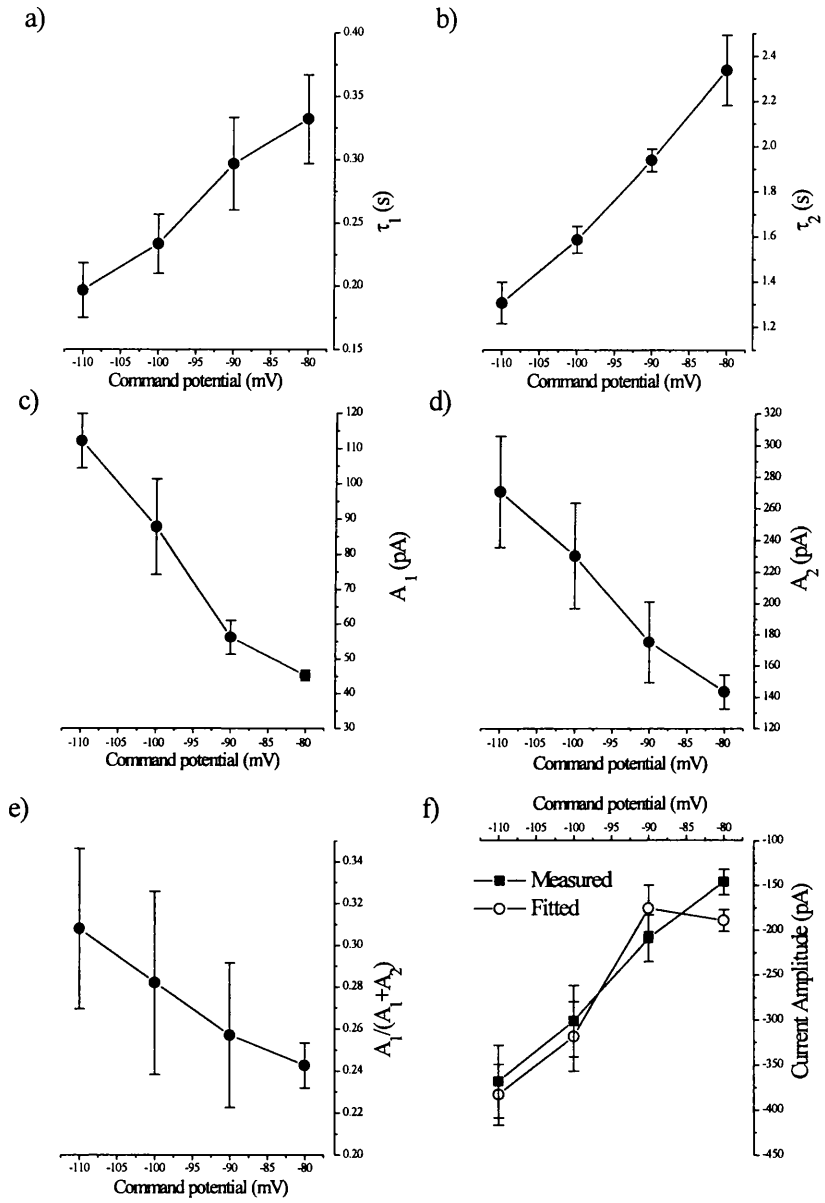

FIGURE 3.6. A double exponential function could be fitted to current traces generated by voltage steps to between -80 and -110mV. **(a)** and **(b)** Plots of the time constants, t_1 and t_2, determined by exponential peeling, against the command potential. **(c)** and **(d)** The amplitudes A_1 and A_2 plotted against the command potential. **(e)** A_1 expressed as a fraction of the total current amplitude ($A_1 + A_2$). **(f)** The total current amplitude measured by exponential peeling ($A_1 + A_2$, open circles) is plotted together with the amplitude of the current as determined by subtracting the instantaneous current from the steady-state current (closed squares). The data presented are the mean ± sem, n = 6 except for the data points obtained at -80mV where n = 5.

Evidence that the hyperpolarisation activated current in SCG neurons is not carried by cations.

This current on first examination has characteristics which are similar to those of hyperpolarisation activated cation currents such as I_f (Brown and Di Francesco, 1980), I_Q (Halliwell and Adams, 1982) and I_h (Bader, Bertrand and Schwarz, 1982; Crepel and Penit-Soria, 1986; Mayer and Westbrook, 1983). These currents are blocked by caesium and/or barium and in addition their amplitude and activation are altered by changes in the external potassium concentration.

Effect of raising the external potassium concentration.

Figure 3.7 shows the effect of raising the external potassium concentration from 2.5mM (control) to 25mM. In figure 3.7a the current traces generated under the two conditions are shown and the respective current voltage relationships are plotted in figure 3.7b. At -90mV the current amplitude was -171 ± 21pA in control and -175 ± 77pA (n = 6) in 25mM potassium. Raising the external potassium concentration was without effect on the current amplitude at all potentials tested.

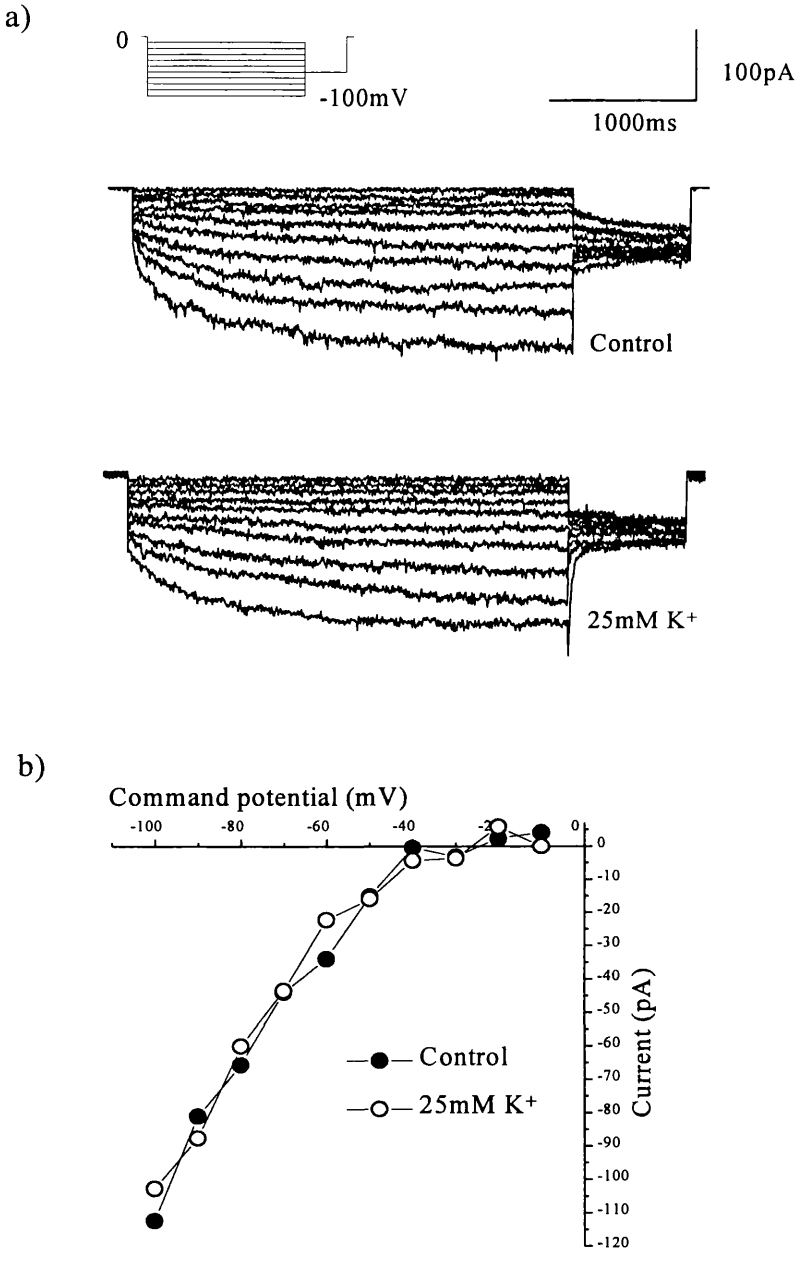

FIGURE 3.7. The effect of raising the external potassium concentration from 2.5 to 25mM. **(a)** Data traces obtained in 2.5mM potassium (control) and 25mM potassium containing external solutions. Currents were generated by applying a series of voltage steps to between -10 and -100mV from a holding potential of 0mV. **(b)** The amplitudes of the time dependent components of the currents obtained in 2.5mM (control, closed circles) and 25mM potassium (open circles) plotted against command potential.

Effect of substituting NMDG for the external potassium and sodium.

Similarly replacing all the potassium and sodium in the external medium with NMDG was also without effect. The current amplitude at -90mV was -133.2 ± 42.2pA in control solution and -95.3 ± 25.9pA (n =10) in NMDG substituted solution. There was no significant difference ($p > 0.07$). Current traces generated in control and NMDG substituted external solutions are shown in figure 3.8a. The respective current voltage relationship plots are shown in figure 3.8b. There was no effect observed at any of the potentials tested.

Effect of replacing the external potassium with sodium.

Also without effect was the replacement of the external potassium with sodium. Figure 3.9a shows the current traces generated in control and potassium free external media and in figure 3.9b the mean current amplitudes ± sem (n = 7 for control and n = 24 for potassium free) obtained at each potential are shown. These current traces were obtained by hyperpolarising voltage steps from a holding potential of 0mV.

Effect of barium and caesium ions.

Figure 3.10 illustrates the lack of effect of both barium and caesium ions. The data traces shown were generated by a single step to -90mV from a holding potential of -30mV. The concentration of each ion was 10mM. This is a concentration which would be enough to abolish a hyperpolarisation activated cation current.

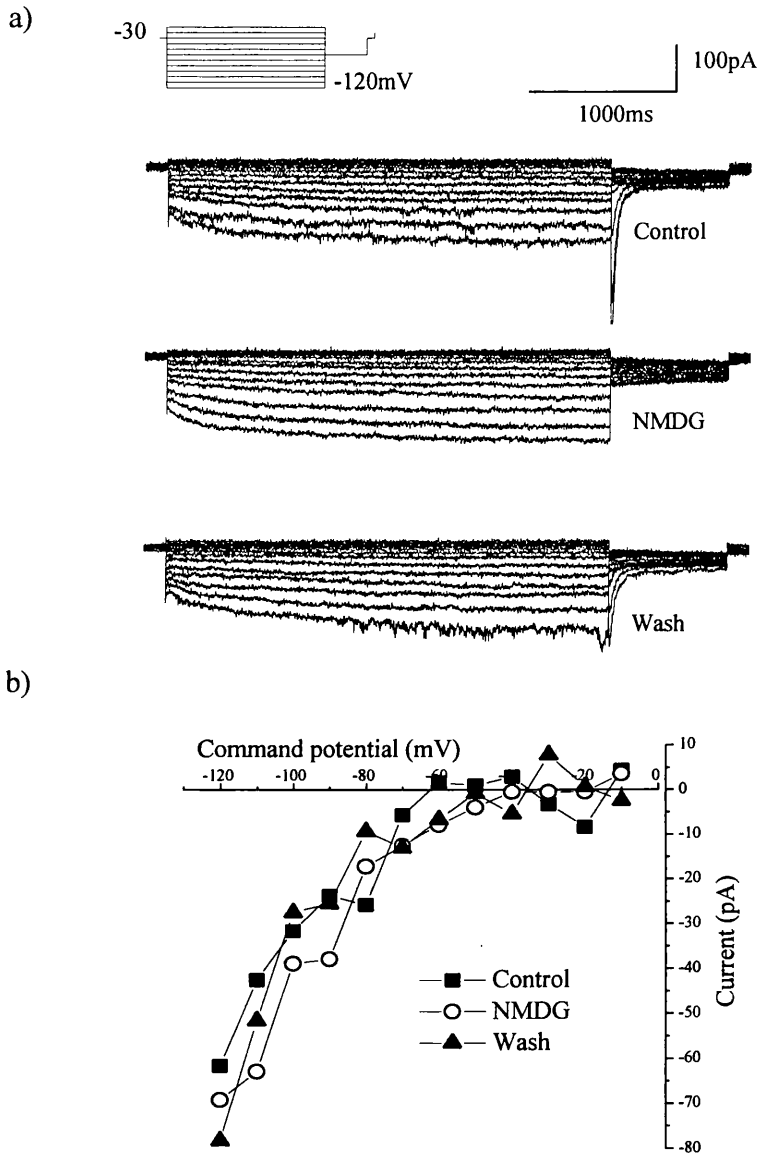

FIGURE 3.8. Substituting NMDG for the potassium and sodium in the external solution was without effect on the magnitude of the current. **(a)** Current traces recorded in control (potassium and sodium containing) and NMDG substituted solutions. Currents were generated by stepping to potentials between -10 and -110mV from a holding potential of -30mV. **(b)** The current voltage relationships for the current traces shown in (a). The current amplitudes obtained in control (closed squares), NMDG substituted solution (open circles) and wash (closed triangles) are plotted against command potential.

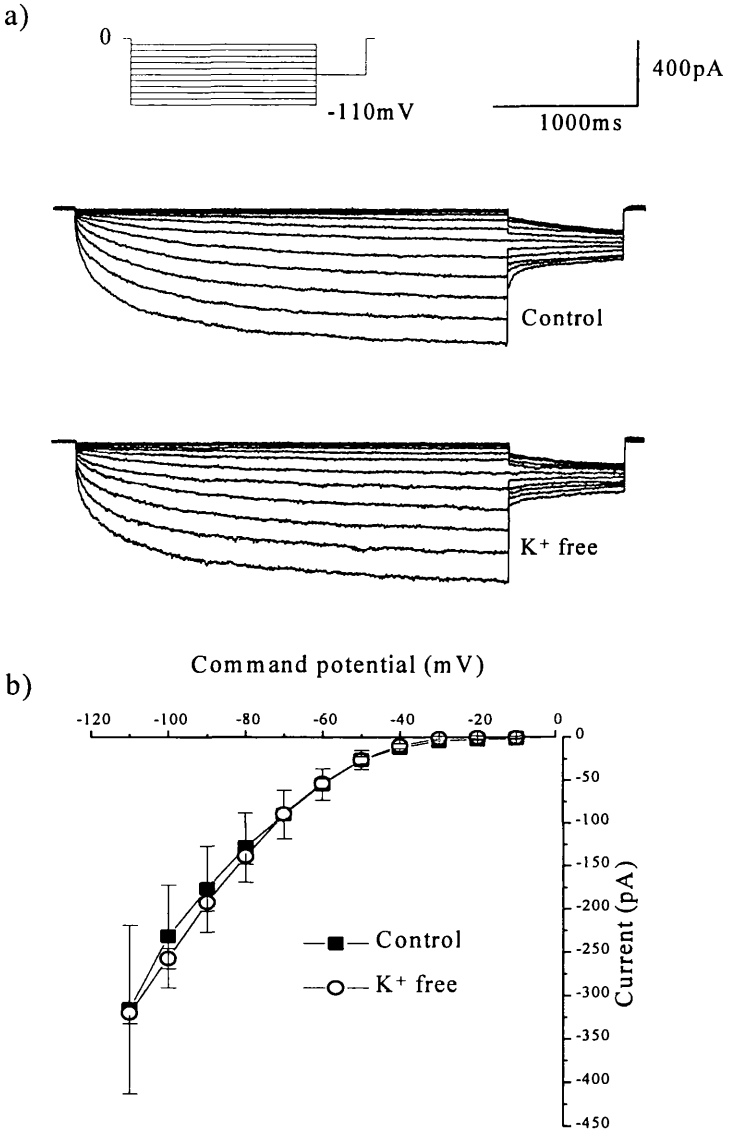

FIGURE 3.9. Removing all external potassium by replacing it with sodium had no effect on the current amplitude. **(a)** Current traces, recorded in control (potassium containing) and potassium free (K^+ free) external solutions were generated by applying hyperpolarising voltage steps to between -10 and -110mV from a holding potential of 0mV. **(b)** Mean current voltage relationships obtained in control (closed squares) and potassium free (K^+ free, open circles). The data presented are the mean ± sem, (n = 7 for control and n = 24 for potassium free).

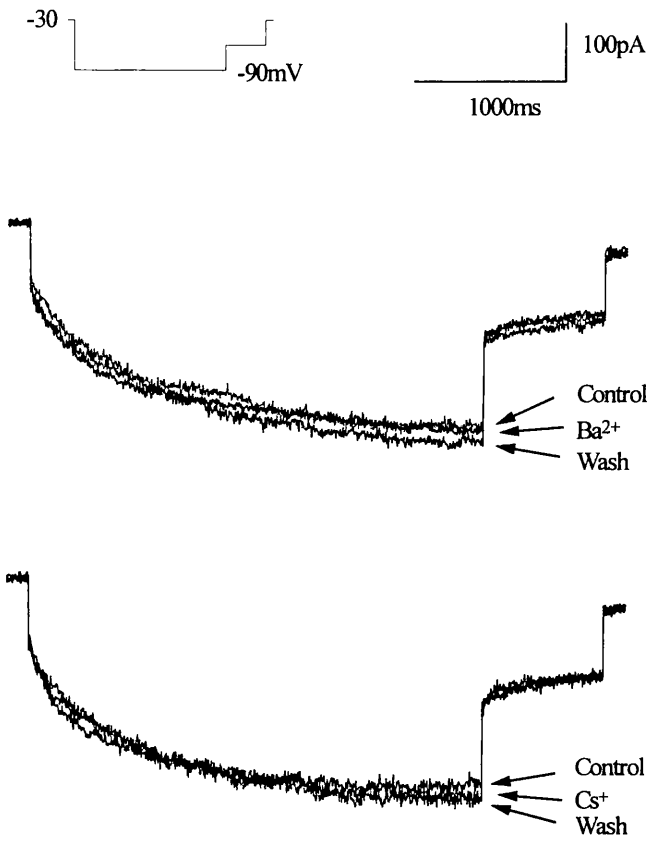

FIGURE 3.10. Effect of 10mM $BaCl_2$ and 10mM CsCl on the hyperpolarisation activated current. Data traces were generated by a single step to -90mV from a holding potential of -30mV. The upper current traces illustrate the lack of effect of barium ions (Ba^{2+}) on the amplitude of the current while the lower traces show a similar lack of effect of caesium (Cs^{+}) ions.

The lack of effect of the various changes in external potassium concentration and both 10mM caesium and 10mM barium indicated that this current could not be regarded as a hyperpolarisation activated cation current.

Evidence for the current being carried by chloride.

An inward current can be due to the inward movement of positively charged ions or the outward movement of negatively charged ions. So, having carried out experiments which revealed that the current was not carried by cations further experiments were performed to determine if the charge carrier was chloride.

Effect of changing the internal chloride concentration.

If the inward current is the result of the outward movement of chloride ions then a decrease in the current amplitude would be expected upon reducing the internal chloride concentration. The patch pipette chloride concentration was reduced to 15mM by partially substituting Cs acetate for CsCl. Figure 3.11a shows typical current traces obtained with CsCl and Cs acetate pipette solutions. Both current traces were recorded approximately 80s after achieving the whole cell configuration. With a Cs acetate pipette solution the mean current amplitude at 80s was -12 ± 11pA (n = 9) compared to a mean current amplitude of -91 ± 26pA (n = 13) measured with a CsCl pipette solution. The substitution of acetate for chloride resulted in a significantly smaller current ($p < 0.05$) at any given time into the recording (figure 3.11b). In addition the current did not increase in size with recording time.

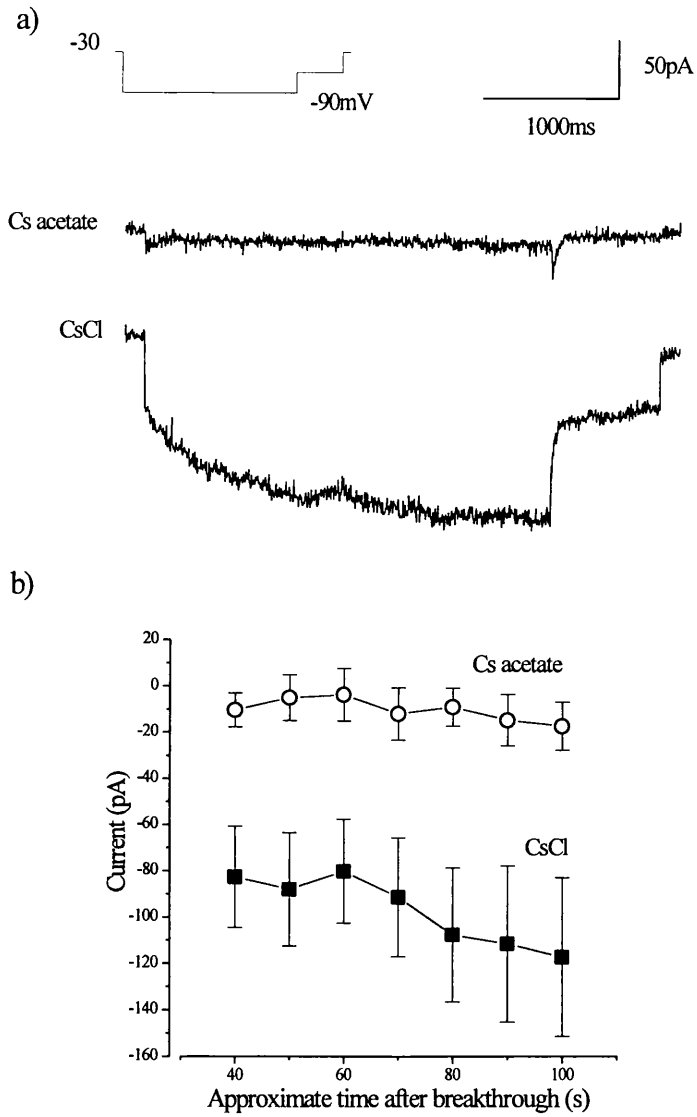

FIGURE 3.11. Effect of reducing the internal chloride concentration. **(a)** Typical data traces generated by a single step to -90mV from a holding potential of -30mV and measured with Cs acetate (upper trace) or CsCl (lower trace) pipette solutions. The currents shown were recorded from two different cells, approximately 80s after obtaining the whole cell configuration. **(b)** Mean current amplitudes measured with CsCl (closed squares) and Cs acetate (open circles) pipette solutions. The current amplitudes are plotted against approximate time after obtaining the whole cell configuration (capacitance compensation was estimated to take 30s). Each data point represents the mean ± sem, (n = 8 and n = 13 for CsAcetate and CsCl solutions respectively).

The whole cell capacitance and series resistance of the cells from which currents were recorded using a Cs acetate pipette solution were not significantly different to those where a CsCl pipette solution was used. The mean whole cell capacitances were 14.6 ± 1.6pF (n = 9) and 15.8 ± 3.9pF (n = 14) respectively, and the mean series resistances 4.7 ± 0.4MΩ (n = 11) and 4.5 ± 0.5MΩ (n = 13) respectively. Therefore the effects observed cannot be explained by different cell sizes and incomplete ion exchange.

In a further four cells, K aspartate was used to replace the CsCl in the internal solution and a reduced current amplitude was also observed. The mean amplitude at -90mV was -2.1 ± 0.4pA (n = 4) with a K aspartate internal solution. This indicates that the reduced current amplitude observed with a Cs acetate pipette solution can not simply be attributed to a non specific effect of acetate.

Determination of the reversal potential of the hyperpolarisation activated current in rat SCG neurons.

Determination using potassium containing external solution.

Using external solution 2 the reversal potential of the current was determined by generating tail currents. The current was first activated with a hyperpolarising voltage step to -120mV and then the membrane potential was stepped to between -50mV and +40mV in 10mV steps. The upper current traces in figure 3.12a are typical current traces recorded using this voltage protocol. The mean peak tail current amplitudes are plotted against command potential in figure 3.11b (closed squares) and gave a mean reversal potential of approximately -10mV (n = 5).

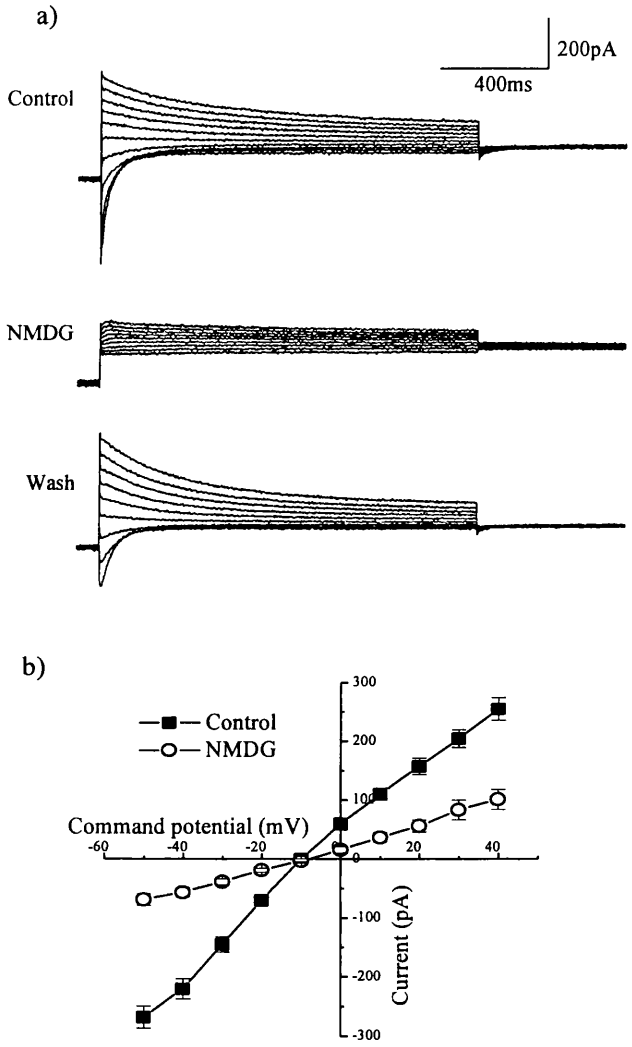

FIGURE 3.12. Reversal potential of the hyperpolarisation activated current measured in control and NMDG substituted solutions. **(a)** Tail currents were generated in control and NMDG substituted external solutions by activating the current with a hyperpolarising prepulse to -120mV and then applying 10mV depolarising voltage steps to between -50 and +40mV. **(b)** The peak tail current amplitudes obtained in control (closed squares) and NMDG substituted solution (open circles) are plotted against command potential. The data are mean ± sem, n = 5.

As can be observed from the current traces shown in figures 3.7,3.8 and 3.9, while the amplitude of the time dependent current was not affected by changes in the external potassium concentration there were obvious effects on the tail currents produced upon repolarising the membrane potential to -60mV. Raising the external potassium concentration from 2.5 to 25mM resulted in a substantial increase in tail current amplitude, while replacing external potassium and sodium with NMDG caused the large tail currents to disappear. This effect is shown more clearly in figure 3.12a where the much reduced tail current amplitudes and the change in kinetics recorded in NMDG substituted solution are very obvious. The mean peak tail current amplitudes are plotted in figure 3.12b and it is interesting to see that while the current amplitudes are reduced there is no apparent change in the reversal potential. The mean reversal potential was about -10mV (n = 5) in NMDG substituted solution which agrees with that obtained in control.

Although NMDG substituted solution had no effect on the reversal potential, the effects caused by changes in the external potassium on the tail current amplitudes possibly indicate that there is a second contaminating current present when the membrane is depolarised from a hyperpolarised prepulse. Because of this possibility the experiments to determine the reversal potential of the current were repeated using potassium free external solution. As already mentioned this change in the external was without effect on the time dependent current amplitude.

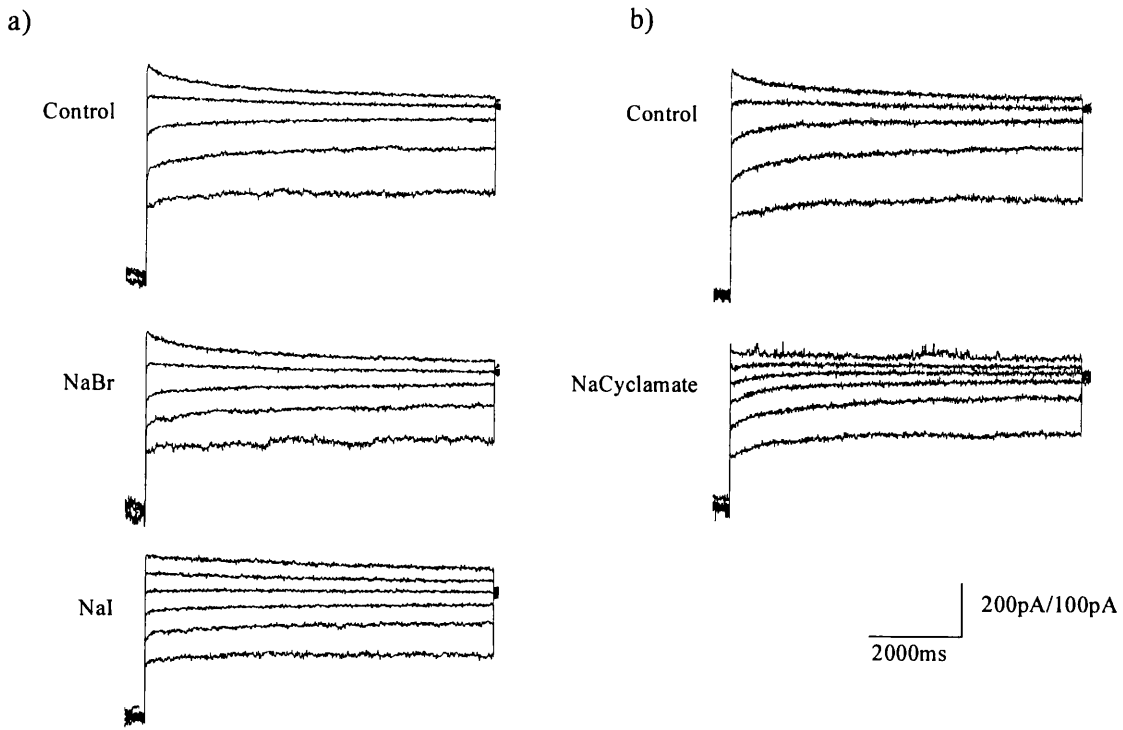

FIGURE 3.13. Reversal potential of the hyperpolarisation activated current measured in potassium free and anion substituted external solutions. **(a)** Tail currents were generated in control (potassium free), bromide substituted (NaBr) and iodide substituted (NaI) external solutions, by first hyperpolarising the membrane potential to -90mV and then applying depolarising command voltage steps to between -60 and either +20 or +40mV, in 20mV steps (see protocol 3, methods). The dotted line illustrates the zero current level. **(b)** Tail currents recorded, using the same voltage protocol as in (a), in control (potassium free) and cyclamate substituted (Na cyclamate) solutions. Zero current level is shown by the dotted line.

Determination of the reversal potential using potassium free external solution.

Using the potassium free external solution (external 3) the reversal potential was again determined by generating tail currents. To activate the current a hyperpolarising voltage step to -90mV was applied and this was followed by depolarising potentials to between -60 and +20 or +40mV in 20mV steps. The upper data traces in figure 3.13a and b illustrate typical tail currents recorded using this voltage protocol. The zero current level is shown by the dotted line. The current traces indicate that the current appears to reverse at approximately 0mV. This is confirmed in figure 3.14a where the mean amplitude of the time dependent component of the tail currents ± sem are plotted against the command potential.

The data shown by the closed squares were obtained from tail currents generated approximately 5 minutes after obtaining the whole cell configuration. At that time in the recording the current reversed at approximately -15mV (n = 5). However, when the tail currents were recorded again between 20 and 40 minutes after going whole cell (open circles) the current reversed at approximately 0mV (n = 5). This is in good agreement with the predicted equilibrium potential for chloride. The reversal potential of the current therefore indicates that the charge carrier is chloride. The current will be called $I_{Cl_{IR}}$ for the rest of this thesis.

Determination of the anion selectivity of $I_{Cl_{IR}}$.

The anion selectivity of the channel underlying the current was determined by replacing the NaCl in the external solution with the sodium salt of either bromide (NaBr), iodide (NaI) or cyclamate (Na cyclamate, cyclamate is a large organic anion). The tail currents recorded in these substituted solutions are shown in figures 13a and b. The zero current level is indicated in each case by the dotted line. The NaBr substitution did not appear to greatly affect the reversal potential

of the current but both NaI and in particular Na cyclamate caused a change in the reversal potential (note that the current in cyclamate substituted solution only just reverses over the voltage range studied). These effects are shown more clearly in figure 3.14. The effects of the bromide, iodide and cyclamate substitutions are shown in figures 3.14b, c and d respectively. In each case the time dependent tail current amplitude, measured from the current traces in figure 3.13, is plotted against the command potential. In the examples given, bromide caused a shift in the reversal potential from -7 to -3mV, iodide shifted the reversal potential from -7 to 0mV and cyclamate caused a shift from 0 to +30mV. The mean changes in reversal potential were 2.2 ± 1.4mV (n = 6), 8.8 ± 3.9mV (n = 4) and 23.6 ± 2.1mV (n = 5) for bromide, iodide and cyclamate substituted solutions respectively. Putting these values into the Goldman, Hodgkin, Katz equation,

Equation **3.1.**

$$\Delta E_{rev} = -RT/F . \ln\left[\frac{[Cl]_o + P_A/P_{Cl}[A]_o}{[Cl]_i}\right]$$

Where $[Cl]_o$ is the external chloride concentration (15mM), $[A]_o$ is the concentration of the replacement anion (120mM), $[Cl]_i$ is the internal chloride concentration (135mM) and R, T and F have their usual meanings.

gave relative permeability values of 0.91, 0.67 and 0.32 for bromide, iodide and cyclamate respectively. Therefore the halide selectivity sequence for $I_{Cl_{IR}}$ appears to be $Cl \geq Br > I$.

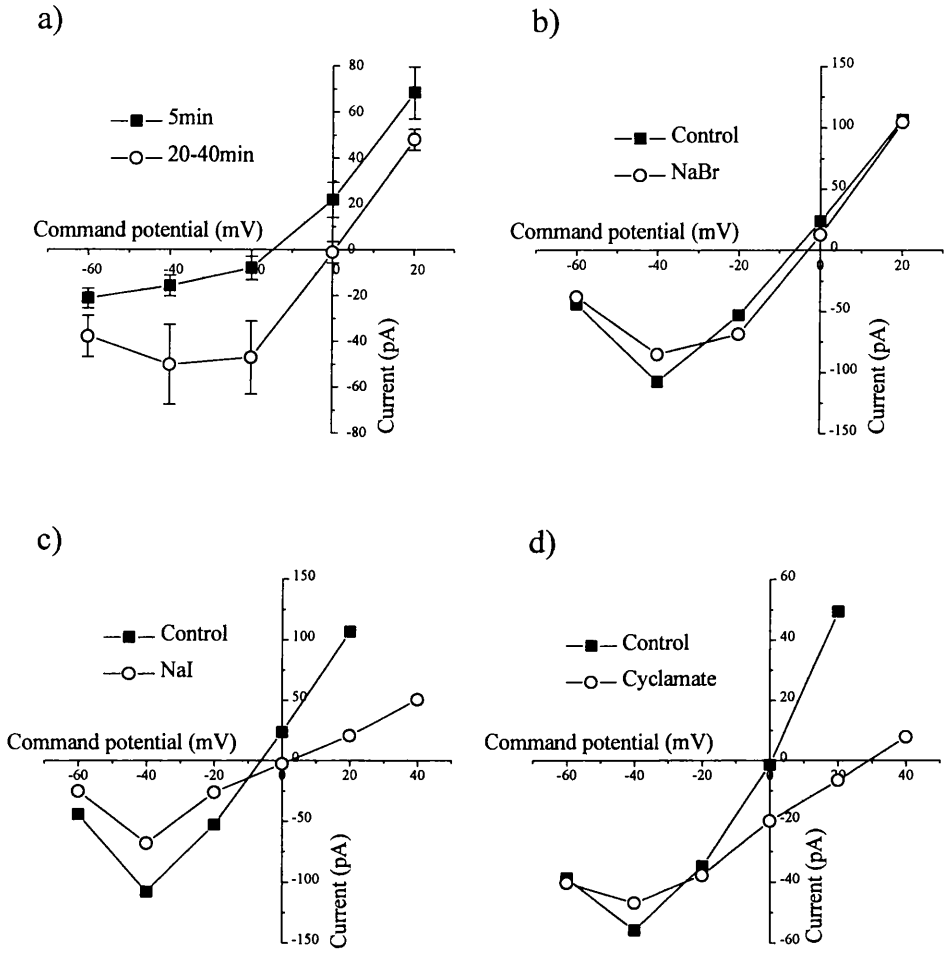

FIGURE 3.14. Graphs showing the effect of time and anion substitution on the reversal potential of the hyperpolarisation activated current. **(a)** The time dependent tail current amplitudes measured 5 minutes (closed squares) or between 20 and 40 minutes (open circles) after obtaining the whole cell configuration are plotted against the command potential. The data are the mean ± sem (n = 5). **(b)** Tail current amplitudes, measured from the current traces shown in FIGURE 12a, are plotted against the command potential, (control, closed squares and bromide substituted, open circles). **(c)** Same as in (b) except that the amplitude of the tail currents in control (closed squares) and iodide substituted (open circles) solutions are plotted. **(d)** The amplitudes of the tail current traces, shown in FIGURE 12b, generated in control (closed squares) and cyclamate substituted (open circles) solutions are plotted against command potential.

Anion substitution of the external solution results in a reduction in current size.

The replacement of the external chloride with another anion not only caused a shift in the reversal potential but also resulted in reductions in the current amplitude. In figure 3.13 which shows the current traces generated in the substituted solutions it can be seen that the current amplitude immediately before the depolarising command step is reduced by all three anion substituted solutions. Bromide caused a 29.6 ± 6.4% (n = 6) reduction in control current at -90mV, while iodide and cyclamate caused 45.3 ± 6.2% (n = 4) and 40.9 ± 8.4% (n = 5) inhibition of control current respectively.

The reduction in current amplitude caused by iodide and cyclamate substitution of external chloride is also evident in figure 3.14. A depolarised shift in the reversal potential would be expected to cause an increase in the driving force and therefore an increase in current amplitude at hyperpolarised potentials. The results show, however that the current amplitude does not change at the hyperpolarised potentials. In addition the current at depolarised potentials is reduced. This indicates that the substitute anions are causing a block of the current as well as a shift in the reversal potential.

DISCUSSION

The results of the experiments described in this chapter have shown that rat SCG neurons possess a hyperpolarisation activated chloride current ($I_{Cl_{IR}}$) which has a halide selectivity sequence of $Cl^- \geq Br^- > I^-$. This current is activated at potentials hyperpolarised to -20mV and at potentials between -80 and -110mV the activation could be described by the sum of two exponential functions. The amplitude of $I_{Cl_{IR}}$ in many cases was small at the start of recording but it increased over time. Experiments showed that the current was not a hyperpolarisation activated cation current but there was a contaminating, probably cationic current, present upon repolarisation of the membrane potential.

Identity of the contaminating current present upon repolarisation.

Recording $I_{Cl_{IR}}$ using potassium containing external solutions, resulted in a large and fast inward tail current being generated when the membrane potential was repolarised to -60mV. The kinetics of the tail current appeared to be much faster than the activation kinetics of $I_{Cl_{IR}}$, therefore it did not seem likely that the tail currents were solely due to the deactivation of $I_{Cl_{IR}}$. Also such changes in solution did not affect the activation or amplitude of $I_{Cl_{IR}}$ observed during the preceding hyperpolarising voltage step. The large tail current was not seen if the external potassium and sodium were replaced with NMDG or if the potassium chloride was replaced with sodium chloride. This seems to suggest that there was an additional current component present at -60mV and that it was probably carried by potassium.

Since the high or zero potassium external solutions had no effect on current amplitude during the hyperpolarising voltage step, the large tail currents are probably not due to the deactivation of another current present during that

voltage step. Although rat SCG neurons have been reported to possess a hyperpolarisation activated potassium current (Wang and McKinnon, 1996) no evidence for the presence of this current was found in the experiments presented here. Also with the recording solutions used, that is an external solution containing TEA and an internal solution that was CsCl based, other types of potassium current that are found in rat SCG neurons (Belluzzi *et al.*, 1985a, 1985b) should not be present. The external calcium concentration used was low (0.1mM) so that neither voltage activated calcium currents or currents activated by a rise in calcium would have been activated. The identity of the contaminating component is therefore not obvious and remains to be elucidated.

Activation of $I_{Cl_{IR}}$.

Activation of $I_{Cl_{IR}}$ upon hyperpolarisation of the membrane potential resulted in a time and voltage dependent inward current. The activation of the time dependent current was best fitted by a double exponential function and the two time constants became faster with increasing hyperpolarisation. The fit by a double exponential function indicates that the activation process can not be described by a simple two state model where the underlying channels are either open or closed. Such a model was proposed for the hyperpolarisation activated chloride current in *Aplysia* neurons since both the activation and deactivation kinetics could be fitted with a single exponential function (Chesnoy-Marchais, 1983). In addition, both the activation and deactivation time constants in *Aplysia* neurons were the same. The possible presence of a contaminating current prevented detailed investigation of the deactivation of $I_{Cl_{IR}}$ in rat SCG neurons.

To acquire more detailed information on channel kinetics it would be necessary to obtain single channel recordings. To date there have not been many reports characterising the channel activity which underlies hyperpolarisation

activated chloride currents but interestingly the channels which have been described all appear to exhibit similar behaviour. The chloride channels which have been best characterised are those of the *Torpedo* electroplax. Recordings, made from lipid bilayers in which vesicles of the *Torpedo* electroplax had been incorporated, revealed that they exhibit bursting activity consisting of two equal subconductance states (Miller, 1982). To explain this behaviour a model in which each channel consisted of two identical protochannels was proposed. Channels of *Aplysia* neurons display similar activity (Chesnoy-Marchais and Evans, 1986) as do the chloride channels of collecting duct basolateral membrane (Sansom *et al.*, 1990). It would be interesting to see if the channels underlying $I_{Cl_{IR}}$ exhibited the same bursting activity and therefore whether this type of channel activity was a feature of hyperpolarisation activated chloride currents in general. Of course it is possible that the single channel conductance may be too small to be resolved by single channel recording. The single channel resistance of ClC-2 has been found, by noise analysis, to be between 3-5pS (Pusch and Jentsch, 1994).

The amplitude of $I_{Cl_{IR}}$ did not reach a maximum over the voltage range that was typically used and applying even more hyperpolarised potentials generally resulted in large spurious currents and frequently cell death. Therefore when conductance was plotted against potential no point of inflection was seen in the curve and a Boltzmann equation could not be fitted to the data (see figure 4.5 in the next chapter). The inability to fit the data meant that parameters of activation, such as the voltage at which $I_{Cl_{IR}}$ was half activated ($V_{1/2}$) and the steepness of the voltage dependence of activation, could not be determined.

Development of $I_{Cl_{IR}}$.

One of the features of $I_{Cl_{IR}}$ is that its magnitude increased during the period of time over which it was recorded. The increase in current amplitude

occurred in all cells but the time course of current development was variable between them. There are several possible explanations for the time dependent increase in $I_{Cl_{IR}}$. The first and perhaps most obvious, is that the increase in current reflects an increase in the chloride concentration of the cell caused by diffusion of chloride out of the pipette. This explanation is supported by the results obtained when the current was recorded with either an acetate or aspartate based internal solution since when using these solutions the current was very reduced in amplitude and did not increase with recording time. Also, the hyperpolarisation activated chloride currents of both *Aplysia* neurons (Chesnoy-Marchais, 1983) and mouse mandibular gland cells (Dinudom *et al.*, 1993) require chloride loading to reach any appreciable size.

The amplitude of the current in many cases, however, continued to increase even when sufficient time had elapsed to allow the chloride concentration of the cell to equilibrate with that in the pipette solution (approximately five minutes). If the current development was due to the increase in chloride concentration, once equilibrium had been achieved it would be expected that the current would remain at a steady amplitude. Such an observation was made for the hyperpolarisation activated chloride current of T_{84} epithelial cells (Fritsch and Edelman, 1996). Therefore it appears that there may be another factor contributing to the development of $I_{Cl_{IR}}$.

There is a possibility that $I_{Cl_{IR}}$ is tonically inhibited by an intracellular regulator molecule and that once the whole cell configuration of the patch clamp technique is achieved the molecule diffuses out of the cell causing $I_{Cl_{IR}}$ to develop. A similar mechanism was proposed for the hyperpolarisation activated chloride current in rat hippocampal neurons (Staley, 1994). In these neurons the current although initially small, increased with time. In addition, activators of protein kinase C inhibited the current but only when they were applied near the

start of recording, that is, before any substantial diffusion had occurred. As a result it was suggested that protein kinase C downregulated the current under normal conditions. It would be interesting in the future to investigate, not only the effects of activators of protein kinase C but also other intracellular molecules such as cAMP, so that it could be determined if $I_{Cl_{IR}}$ is tonically regulated. Results from experiments where ATP was either included or omitted from the pipette solution indicated that $I_{Cl_{IR}}$ is not dependent on ATP.

The final explanation for the increase in magnitude of $I_{Cl_{IR}}$ is that it is sensitive to osmolarity. Even though the osmolarity of both the internal and external solutions was corrected by the addition of sucrose to reduce the chance of cell swelling, it is possible that a small change in cell size due to osmotic effects did occur during the course of the recordings and that this caused the amplitude of the current to increase (for further discussion see chapter 5).

Comparison with other hyperpolarisation activated currents.

The results presented in this chapter clearly show that the hyperpolarisation activated current is not carried by cations. Inward rectifiers (e.g. Constanti and Galvin, 1983) and hyperpolarisation activated cation currents such as I_f (Brown and DiFrancesco, 1980), I_Q (Halliwell and Adams, 1982) and I_h (e.g. Mayer and Westbrook, 1982) are affected by changes in the external potassium concentration and are inhibited by caesium and/or barium. The current in rat SCG neurons was not affected by either increasing the concentration of potassium or by totally removing the external potassium. In addition both caesium and barium at concentrations which would abolish the cation carried currents were ineffective.

The lack of inhibition of $I_{Cl_{IR}}$ by barium ions also shows that this current can not be the same as that recorded upon expression of phospholemman in

Xenopus oocytes (Moorman *et al.*, 1992). The phospholemman induced current is blocked by barium with an IC_{50} of 0.36mM. In addition, it has been shown that the threshold for activation of the current recorded upon expression of phospholemman is much more hyperpolarised than that for $I_{Cl_{IR,}}$ -80mV versus -20mV respectively. Also phospholemman is not expressed in brain (Palmer *et al.*, 1991) and therefore is probably not expressed in SCG neurons.

The properties of $I_{Cl_{IR}}$ studied in this chapter are, however, similar to other hyperpolarisation activated chloride currents such as those that have been recorded in rat osteoblastic cells (Chesnoy-Marchais and Fritsch, 1994), T_{84} epithelial cells (Fritsch and Edelman, 1996) and *Aplysia* neurons (Chesnoy-Marchais, 1983). The threshold for activation of $I_{Cl_{IR}}$ is around -20mV which is within the range observed for the other currents and all of these currents exhibit inward rectification. In addition, the halide selectivity sequence found for $I_{Cl_{IR}}$, $Cl^- \geq Br^- > I^-$, is the same as that determined for the current in T_{84} epithelial cells (Fritsch and Edelman, 1996). ClC-2 when expressed in *Xenopus* oocytes activates at potentials much more hyperpolarised than $I_{Cl_{IR}}$ but the current looks qualitatively the same and the two currents have the same halide selectivity sequence (Thiemann *et al.*, 1992).

CHAPTER 4

Pharmacological characterisation of $I_{Cl_{IR}}$.

INTRODUCTION.

Ion channel blockers are used to aid in the identification and characterisation of ion channel conductances. Chloride channels can be blocked by both organic and inorganic agents.

The divalent cations cadmium and zinc are inorganic chloride channel blockers. Zinc has well documented effects on $GABA_A$ gated chloride channels found in rat SCG neurons (Smart and Constanti, 1990; Smart, 1992; Aguayo and Alarcón, 1993) but has also been found to be effective at blocking the hyperpolarisation activated chloride current in hippocampal pyramidal neurons (Staley, 1994), the current that occurs upon expression of ClC-2 in *Xenopus* oocytes (Jentsch, personal communication), reconstituted cardiac chloride channels (Townsend and Rosenberg, 1995) and chloride efflux from skeletal muscle (Spalding *et al.*, 1990). In hippocampal pyramidal neurons, zinc was reported to act at an intracellular site since no block occurred if a high concentration of EGTA or BAPTA was present in the pipette solution (Staley, 1994).

Cadmium completely blocks the hyperpolarisation activated chloride current in hippocampal pyramidal neurons at a concentration of 100μM (Madison *et al.*, 1986). At concentrations greater than 300μM, cadmium has also been found to block the hyperpolarisation activated chloride currents in rat osteoblastic cells (Chesnoy-Marchais and Fritsch, 1994) and T_{84} epithelial cells (Fritsch and Edelman, 1996). Selyanko (1994) reported that the hyperpolarisation activated current in rat SCG neurons was blocked by 200μM cadmium and the ClC-2

induced current is sensitive to cadmium as well (Jentsch, personal communication). Although cadmium has been identified as a blocker of the hyperpolarisation activated chloride currents found in many cell types, it is ineffective as a blocker of the current that occurs upon expression of phospholemman (Kowdley *et al.*, 1994).

Figure 4.1 shows the structures of some of the organic chloride channel blockers. The compounds belong to three different groups; Anthracene -9-carboxylic acid (9AC) and 5-Nitro-2-(3-phenylpropylamino) benzoic acid (NPPB) are carboxylic acid analogues. 4-Acetamido-4'-isothiocyanato-stilbene-2,2'-disulfonic acid (SITS) and 4,4'-Diisothiocyanato-stilbene -2,2'-disulphonic acid (DIDS) are disulphonic stilbene derivatives. Niflumic acid is nicotinic acid analogue.

9AC is a well known blocker of skeletal muscle chloride currents. Bryant and Morales-Aguilera (1971) found that 9AC caused myotonia when applied to the resting muscle chloride conductance and 9AC has subsequently been found to be a potent blocker of ClC-1, the chloride channel that underlies the conductance (Steinmeyer *et al.*, 1991b). In addition 200μM 9AC completely inhibited chloride currents recorded after the incorporation of vesicles from skeletal muscle transverse tubule into planar lipid bilayers (Ide *et al.*, 1995).

Besides skeletal muscle chloride channels 9AC can block calcium-activated chloride currents of smooth muscle (Baron *et al.*, 1991; Hogg *et al.*, 1993, 1994) and chloride transporters in epithelia (Oberleithner *et al.*, 1983). 9AC is a partial blocker of the currents produced upon expression of ClC-K1 (Uchida *et al.*, 1993), ClC-2 (Thiemann *et al.*, 1992) and phospholemman (Kowdley *et al.*, 1994). However, there are also other chloride currents which are virtually unaffected by the application of 9AC. These include the chloride conductance of

mouse mandibular gland cells (Komwatana *et al.*, 1994), the hyperpolarisation activated chloride current of rat leydig cells (Noulin and Joffre, 1993) and the currents produced upon expression of ClC-3 (Kawasaki *et al.*, 1994) and ClC-5 (Steinmeyer *et al.*, 1995).

NPPB was developed after extensive testing of carboxylic acid derivatives on chloride channels of the thick ascending loop of Henle (Wangemann *et al.*, 1986). It was the most potent blocker of the group and has subsequently been applied to many other types of chloride channels. NPPB can inhibit chloride currents of epithelial cells (Tilmann *et al.*, 1991; Singh *et al.*, 1991) and rat peritoneal mast cells (Matthews *et al.*, 1989). It can also inhibit calcium activated chloride currents (Ishikawa and Cook, 1993) and volume activated chloride currents in numerous cell types (Nilius *et al.*, 1994). NPPB has, in addition, been applied to hyperpolarisation activated chloride currents (Arreola *et al.*, 1996; Chesnoy-Marchais and Fritsch 1994; Fritsch and Edelman, 1996) and been found to cause a partial inhibition. NPPB was ineffective at inhibiting ClC-5 (Steinmeyer *et al.*, 1995) and the current of mouse mandibular gland cells (Komwatana *et al.*, 1994).

The stilbene derivatives SITS and DIDS which are known to inhibit several anion transporters (Passow, 1986) also block chloride channels. In particular the effects of DIDS and SITS on the chloride channel of the electroplax have been extensively studied (White and Miller, 1979; Miller and White, 1984). In these studies *Torpedo* electroplax chloride channels were incorporated into planar lipid bilayers and the application of either SITS or DIDS was found to result in their inhibition. However, this only occurred if they were applied from the *cis* or intracellular side of the membrane. In addition, while the effects of SITS were fully reversible the inhibition caused by DIDS was not.

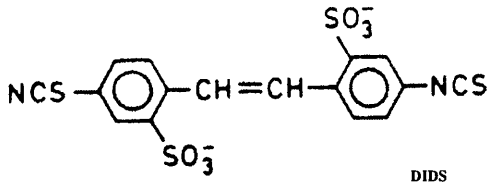

DIDS

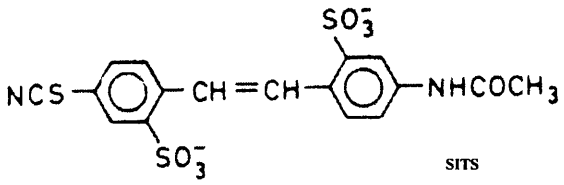

SITS

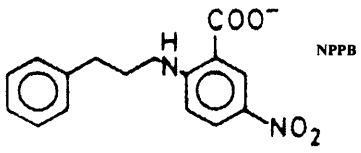

NPPB

9AC

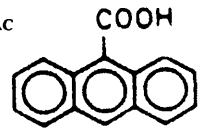

Niflumic acid

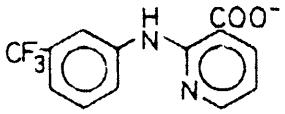

FIGURE 4.1. Chemical structures of some chloride channel blockers. DIDS (4,4'-Diisothiocyanato-stilbene -2,2'-disulphonic acid), SITS (4-Acetamido-4'-isothiocyanato-stilbene-2,2'-disulfonic acid), NPPB (5-Nitro-2-(3-phenylpropylamino) benzoic acid), 9AC (Anthracene 9 carboxylic acid).

SITS had no effect on the hyperpolarisation activated chloride current of *Aplysia* neurons (Chesnoy-Marchais, 1983; Lotshaw and Levitan, 1987) but has been shown to be able to inhibit phospholemman induced chloride currents (Kowdley *et al.*, 1994), calcium activated smooth muscle chloride currents (Hogg *et al.*, 1994) and skeletal muscle chloride currents (Ide *et al.*, 1995). In addition, SITS appears, in particular, to be a good inhibitor of volume activated chloride channels (e.g. Arreola *et al.*, 1995; 1996 and the references therein).

DIDS is also able to block a wide range of different chloride channels. Inhibitory effects of DIDS have been reported for the cloned chloride channels ClC-K1 (Uchida *et al.*, 1993), ClC-K2 (Adachi *et al.*, 1994) and ClC-3 (Kawasaki *et al.*, 1994). Also, skeletal muscle transverse tubule chloride channels (Ide *et al.*, 1995), calcium activated chloride currents (Baron *et al.*, 1991; Hogg *et al.*, 1994; Ishikawa and Cook, 1993), chloride currents of rat leydig cells (Noulin and Joffre, 1993), rat peritoneal mast cells (Matthews *et al.*, 1989), phospholemman (Kowdley *et al.*, 1994) and the hyperpolarisation activated chloride currents of rat osteoblastic cells (Chesnoy-Marchais and Fritsch, 1994) and *Aplysia* neurons (Chesnoy-Marchais, 1983) are blocked by the application of DIDS. The effects of DIDS on the chloride current of *Aplysia* neurons were however, only observed, when it was injected into the cells (Chesnoy-Marchais, 1983). Therefore, DIDS inhibition of *Torpedo* and *Aplysia* chloride channels appears to occur by a similar mechanism. DIDS, like the other types of chloride channel blockers, does not block all chloride channels since it was not found to inhibit ClC-5 (Steinmeyer *et al.*, 1995), the current recorded upon expression of ClC-2 (Thiemann *et al.*, 1992) or the hyperpolarisation activated currents in T_{84} epithelial cells (Fritsch and Edelman, 1996) and mouse mandibular gland cells (Komwatana *et al.*, 1994).

Niflumic acid is an inhibitor of the band 3 transporter (Falke and Chan, 1986) but is most often used as a blocker of calcium activated chloride channels in

such cell types as rat sensory neurons (Currie *et al.*, 1995), Xenopus oocytes (White and Aylwin, 1990), smooth muscle cells (Janssen and Sims, 1994, 1995; Hogg *et al.*, 1994; Pacaud *et al.*, 1989) and mouse pituitary cells (Korn *et al.*, 1991). In addition, niflumic acid blocks the calcium activated chloride current induced in SCG neurons by axotomy (Sanchez-Vives and Gallego, 1994). A few osmolarity sensitive chloride currents have been reported to be blocked by niflumic acid (Bakhranov *et al.*, 1995; Kelly *et al.*, 1994), as is phospholemman (Kowdley *et al.*, 1994) but most other types of chloride current are not. The niflumic acid insensitive chloride currents include the hyperpolarisation activated chloride currents found in Aplysia neurons (Chesnoy-Marchais, 1983) and rat osteoblastic cells (Chesnoy-Marchais and Fritsch, 1994) and the chloride currents produced upon expression of ClC-5 (Steinmeyer *et al.*, 1995) and ClC-K2 (Adachi *et al.*, 1994). Niflumic acid is therefore relatively specific for calcium activated chloride currents.

The aim of this chapter was to obtain a pharmacological profile for $I_{Cl_{IR}}$. Four different types of compounds, which have been shown previously to block a variety of chloride currents, were applied. The concentrations used were similar to those which have been shown to have near maximal effects on other current types. The four groups of putative blockers tested, were the divalent cations cadmium and zinc, the carboxylic acid derivatives 9AC and NPPB, the calcium activated chloride channel blocker niflumic acid and the stilbene derivatives SITS and DIDS.

RESULTS

Effects of the divalent cations cadmium and zinc on the amplitude of $I_{Cl_{IR}}$.

The data traces in figure 4.2 illustrate the effect of 10μM cadmium on $I_{Cl_{IR}}$. In the presence of 10μM cadmium the current amplitude was reduced. For the example shown, the amplitude of the time dependent current recorded at -110mV was decreased from 520pA in control to 217pA in the presence of 10μM cadmium. A reduction in current amplitude was also seen when currents were recorded in external solution containing 10μM zinc. Current traces generated in control and in the presence of 10μM zinc are shown in figure 4.3. At -110mV the current amplitude was reduced from 500pA in control to 296pA in 10μM zinc. The effects of both cadmium and zinc were completely reversible upon wash as is shown by the lower traces in figures 4.2 and 4.3 respectively.

The mean current voltage relationships obtained in solutions containing the divalent cations are shown in figures 4.4a and 4.4c. The data presented are the mean ± sem, n = 4 for the cadmium data and n = 3 for the zinc data. The graphs indicate that both cadmium and zinc had effects on the current amplitude at all the potentials tested and this is further illustrated in figures 4.4b and 4.4d. In these figures the percentage inhibition of the control current caused by either 10μM cadmium or zinc is plotted against the command potential. Both ions were significantly more effective at the depolarised potentials than at the hyperpolarised potentials. In the presence of cadmium the current at -50mV was inhibited by 77.4 ± 6.7% but at -110mV the current was only reduced by 53.5 ± 3.5% ($p < 0.01$, paired t test). Similarly for zinc, the current was inhibited by 77.0 ± 3.1% at -60mV while at -110mV it was inhibited by only 27.3 ± 1.4% ($p < 0.02$, paired t test).

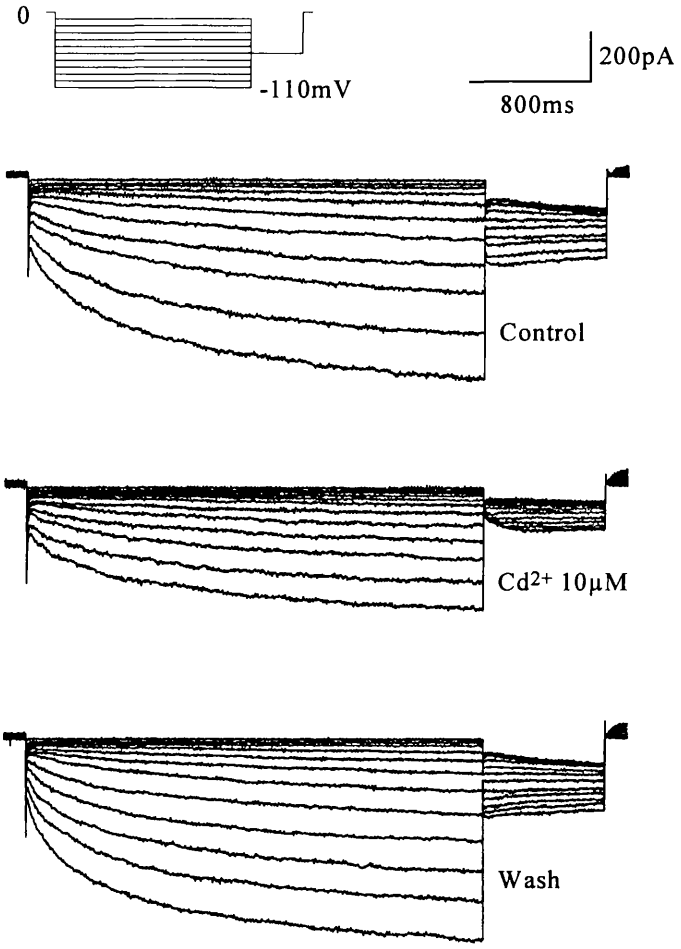

FIGURE 4.2. Effect of 10μM cadmium on the amplitude of $I_{Cl_{IR}}$. Current voltage relationships generated by hyperpolarising the membrane in 10mV steps to potentials between -10 and -110mV from a holding potential of 0mV. The currents were recorded in control and then in 10μM cadmium. The lower current traces were generated after cadmium had been washed out.

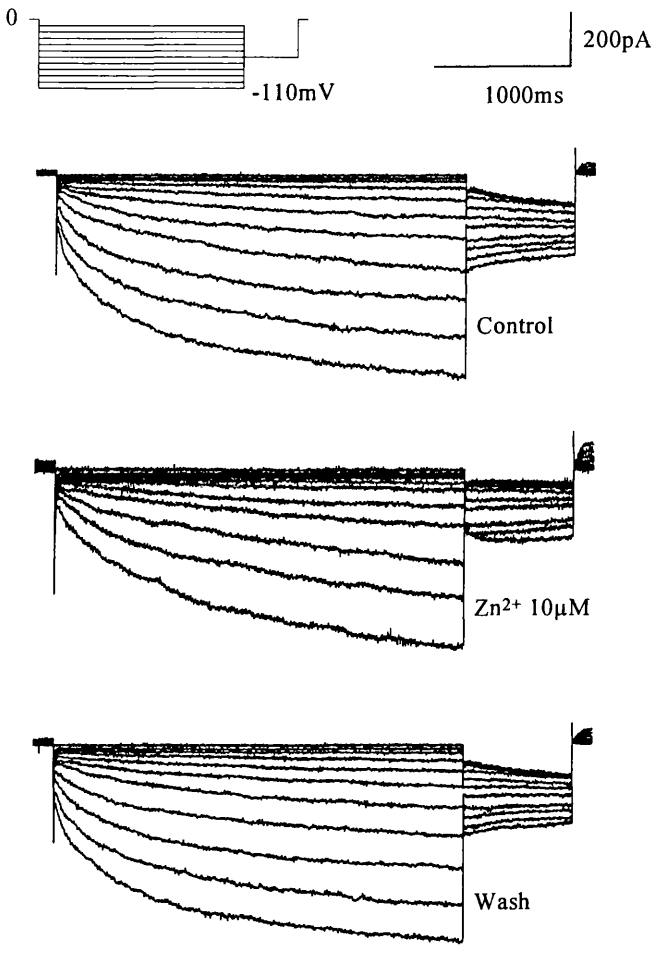

FIGURE 4.3. Effect of 10μM zinc on the amplitude of $I_{Cl_{IR}}$. Current voltage relationships were generated in control and then in the presence of 10μM zinc using the voltage protocol described for FIGURE 4.1. Currents recorded after zinc had been washed out are shown by the bottom group of data traces.

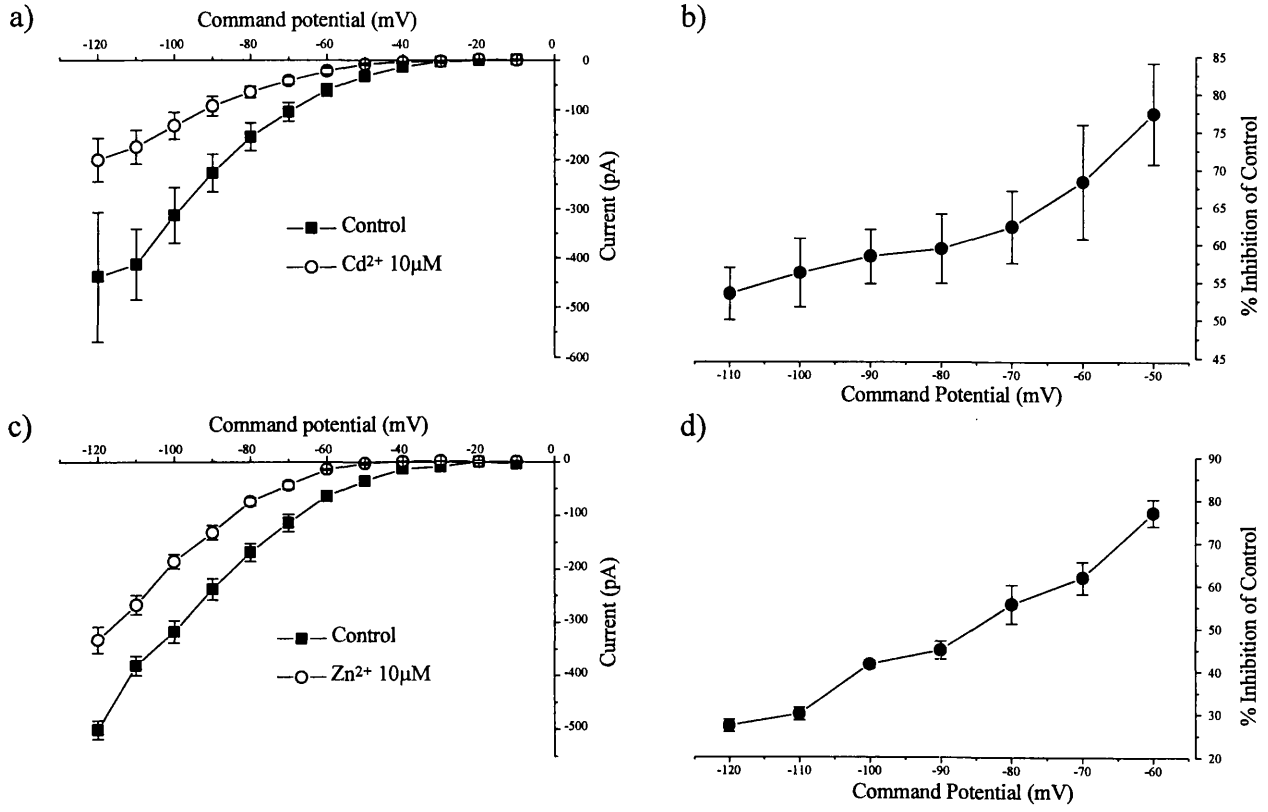

FIGURE 4.4. The effects of cadmium and zinc are voltage dependent. **(a)** Mean current voltage relationship obtained in 10µM cadmium is plotted together with the respective mean control current voltage relationship. **(b)** The mean percentage inhibition of the control current caused by 10µM cadmium is plotted against command potential. **(c)** Mean current voltage relationships generated in control and 10µM zinc. **(d)** Graph showing the mean percentage inhibition of the control current caused by 10µM zinc plotted against command potential. All data are the mean ± sem, n = 4 and n = 3 for the cadmium and zinc data respectively.

Effects of cadmium and zinc on the activation of $I_{Cl_{IR}}$.

The data in figure 4.4 indicate that cadmium and zinc are apparently acting in an analogous manner, in that the voltage dependence of the block is similar. Differences are, however, apparent in the effects of cadmium and zinc on the activation kinetics of the current. Figure 4.5 shows data traces generated at a command potential of -110mV. In figure 4.5a, a control trace recorded at this potential and the trace recorded in 10μM cadmium are shown. Figure 4.5b shows a control trace and the corresponding trace generated in 10μM zinc. The data were obtained from the same cell. In each case the current trace generated in the presence of the cation was scaled up to the maximum current amplitude (the current at the end of the voltage step) of the relevant control current trace. In figure 4.5a it can be seen that the scaled cadmium trace overlies the control data trace. This indicates that the activation kinetics of the current have not changed in the presence of cadmium. In contrast, the scaled zinc data trace does not, with the exception of a small portion of the trace at the end of the voltage step, superimpose onto the control current. It appears that the activation of $I_{Cl_{IR}}$ in the presence of zinc has been somewhat slowed compared to that in control.

Under control conditions the time constants of activation are slower at more depolarised potentials than at hyperpolarised potentials (see chapter 3). Therefore the control traces recorded at more depolarised command potentials were scaled to the zinc trace at -110mV to determine if the activation kinetics could be compared. The current traces are shown in figure 4.5b. It was found that the control trace recorded at a command potential of -70mV superimposed onto the zinc trace at -110mV. This suggests that the activation kinetics have been shifted in the hyperpolarised direction. The activation kinetics of $I_{Cl_{IR}}$ in other neurons were similarly affected, although the magnitude of the shift was not so

prominent as for the cell illustrated in figure 4.5b. The shift in the activation kinetics ranged from 20mV to 50mV (n = 3).

An alternative method of determining the effects of cadmium and zinc on the activation kinetics is to create conductance plots and then fit Boltzmann equations. A graph of the conductance in control and in the presence of 10μM zinc is shown in figure 4.6. The data indicates that there has been a shift in the activation kinetics but the conductance of neither the control or the zinc data reaches a maximum over the range of potentials applied. There is also no obvious point of inflection. To fit data with a Boltzmann equation a maximum and minimum conductance or a point of inflection are necessary. The lack of these for the data obtained meant that a Boltzmann equation could not be fitted. Therefore it was not possible to obtain a numerical value for the shift in the activation observed, by this method. The application of potentials hyperpolarised to -120mV was not generally possible since the cells became unstable.

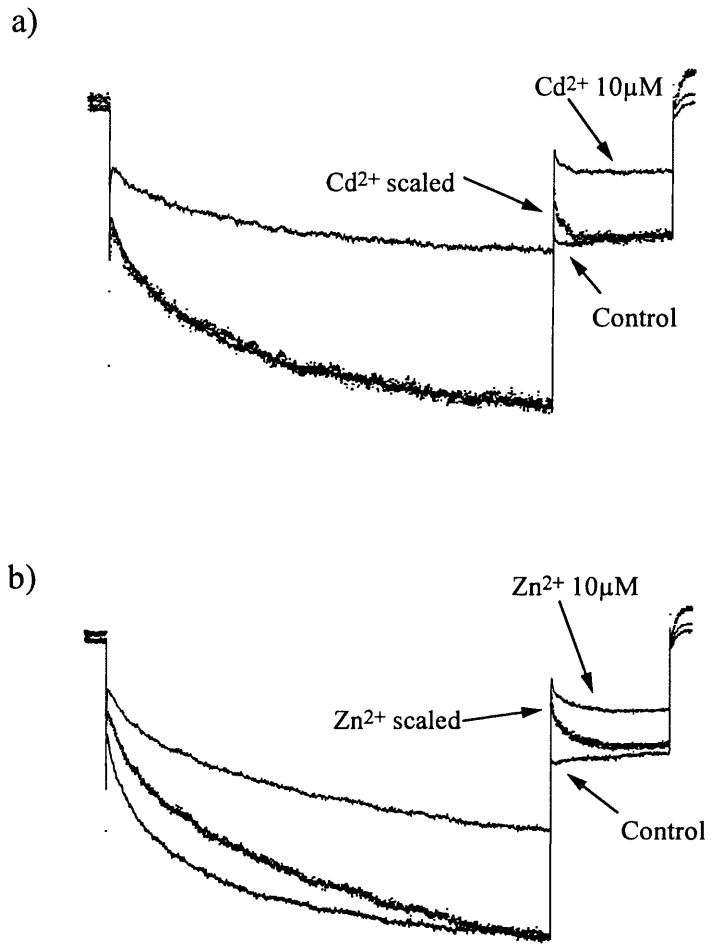

FIGURE 4.5. Effects of cadmium and zinc on the activation kinetics of the hyperpolarisation activated current. **(a)** Current traces generated by a command step to -110mV in control and in the presence of 10μM cadmium. The current trace in 10μM cadmium has been scaled to the maximum control current amplitude (open symbols). **(b)** Current traces obtained in control and 10μM zinc at a command potential of -110mV. The current trace obtained in 10μM zinc has been scaled to the maximum control current amplitude (open symbols).

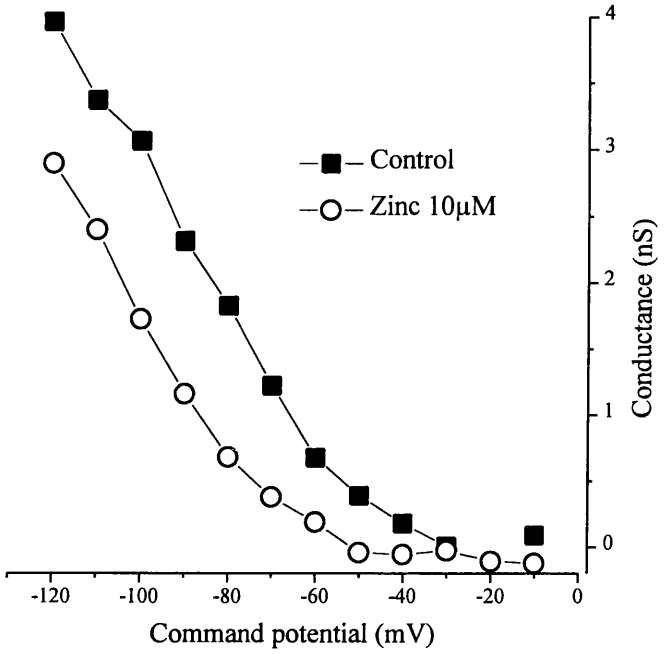

FIGURE 4.6. Graph showing the conductance of $I_{Cl_{IR}}$ in control and 10μM zinc. A current voltage relationship was generated in control and then in an external solution containing 10μM zinc. The conductance was then calculated assuming a reversal potential of 0mV and plotted against the command potential.

Effects of the divalent cations on the deactivation of $I_{Cl_{IR}}$.

The deactivation of the currents recorded in cadmium and zinc upon repolarisation of the membrane potential to -60mV from very hyperpolarised potentials (< 90mV) was markedly different to the deactivation of control currents. The tail currents generated in both cadmium and zinc consisted of an instantaneous current jump followed by an inward relaxation. This was in contrast to the instantaneous current jump followed by an outward relaxation observed for the control currents. The difference in the tails over the total potential range applied can be seen in figures 4.2 and 4.3 but it is particularly obvious in figure 4.4 where the cadmium and zinc data traces generated at -110mV have been scaled to the relevant control traces.

It is interesting that the effects of cadmium and zinc on the current deactivation appear to be the same while there are obvious differences in the effects of the two cations on the activation of the current.

The effects of cadmium and zinc are concentration dependent.

Figure 4.7 shows the effects of various concentrations of cadmium and zinc. In figure 4.7a the mean percentage inhibition of the control current recorded at -90mV caused by 10 and 30μM cadmium is shown. At 10μM, cadmium inhibited the current by 41.0 ± 2.8% (n = 5) while at 30μM the current was reduced by 72.7 ± 3.4% (n = 6). The data shown in figure 4.7a were obtained after holding the neurons at a potential of 0mV. Currents have, in addition, were also generated from a holding potential of -30mV in the presence of either 30 or 100μM cadmium. The current in 30μM cadmium was inhibited by 58.5 ± 16.6% (n = 3, data not shown) which is not significantly different to the inhibition caused by 30μM cadmium when a holding potential of 0mV was used ($p > 0.5$, unpaired

t-test). At a concentration of 100μM, cadmium substantially reduced the current at -90mV. The current in the presence of 100μM cadmium was blocked by 77.6 ± 4.4% (n = 13, data not shown).

Figure 4.7b is a graph showing the concentration dependent effects of zinc on the current at -90mV. The data shown are the mean ± sem, n = 3-4 and were obtained for concentrations of zinc between 1 and 1000μM. The data were fitted with a dose-response curve (shown by the dotted line) that had a slope value of unity. The fitted curve indicated that the concentration of zinc that produced half the maximal inhibitory effect (IC_{50}) was approximately 23μM. At concentrations of 300 and 1000μM, zinc completely abolished the current at -90mV but even at these high concentrations the block was fully reversible.

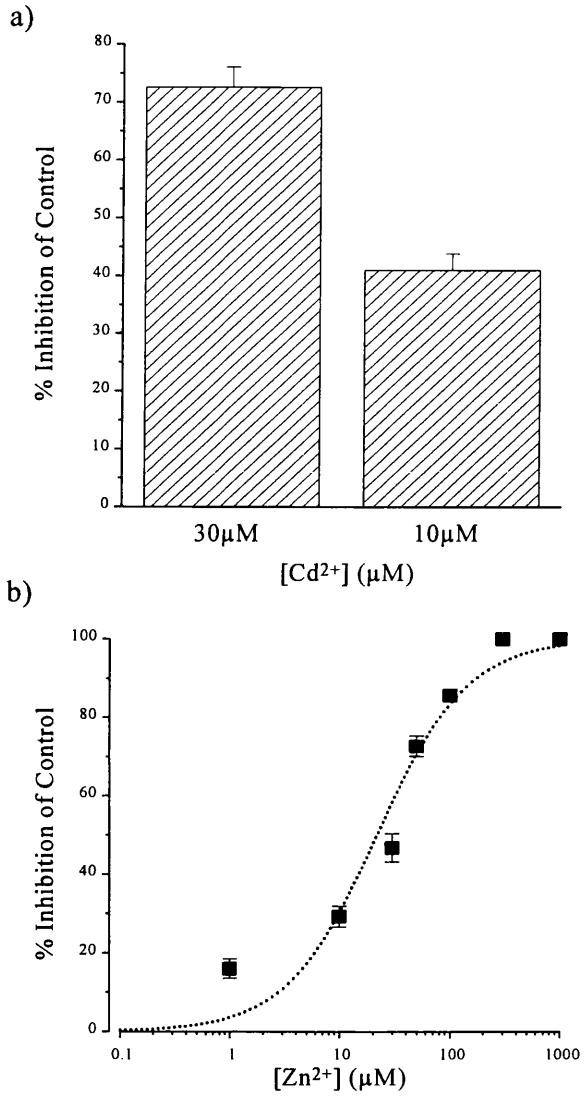

FIGURE 4.7. The effects of cadmium and zinc on $I_{Cl_{IR}}$ are concentration dependent. **(a)** Graph of the mean percentage inhibition of the control current at -90mV caused by 10 and 30μM cadmium. **(b)** Semi-logarithmic plot of the mean percentage inhibition of the control current at -90mV caused by concentrations of zinc between 1 and 1000μM zinc. The data are fitted by a dose response curve (dotted line) having a slope of unity.

Effect of internal BAPTA concentration on the block by zinc.

A recent report of a hyperpolarisation activated chloride current in hippocampal neurons (Staley, 1994) found a block by zinc but only when the internal calcium buffering was low. Since all the zinc experiments reported here were conducted using a 0.1mM BAPTA pipette solution further experiments were carried out using a pipette solution that contained 10mM BAPTA. The time constant for diffusion of BAPTA from the pipette was estimated to be approximately 5 minutes for the neurons studied (see Pusch and Neher, 1988; Stansfeld and Mathie, 1993).

In 7 cells where 300 μM zinc was applied between 5 and 17 minutes after obtaining the whole cell configuration, a full block was observed and this still occurred even when, in one cell, zinc was applied 32 minutes after going whole cell. Figure 4.8a shows the amplitude of $I_{Cl_{IR}}$ recorded at -90mV. Zinc was applied at approximately 17 minutes and 32 minutes into the recording. In both instances the current was rapidly and completely blocked. The relevant current traces are shown in figure 4.8b. The speed with which zinc was able to block $I_{Cl_{IR}}$ and the ability of zinc to block in the presence of a high internal BAPTA concentration suggest that zinc is not acting at an intracellular site.

a)

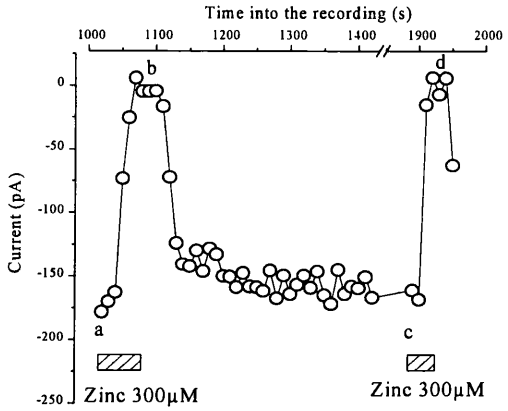

b)

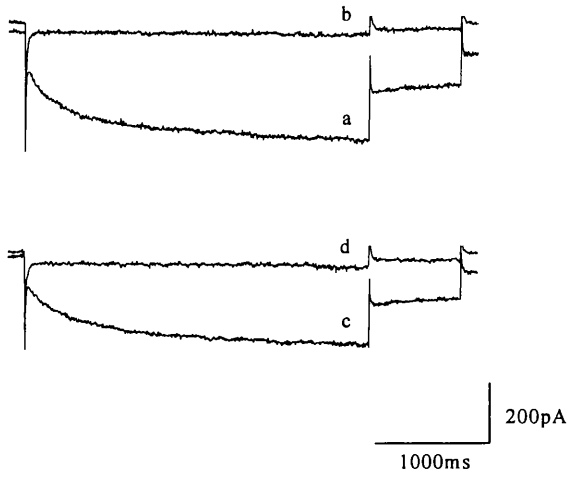

FIGURE 4.8. Effect of BAPTA concentration on the block of $I_{Cl_{IR}}$ by 300μM zinc. **(a)** The amplitude of $I_{Cl_{IR}}$ recorded at -90mV from a holding potential of -30mV was plotted against recording time. Zinc was applied at a concentration of 300μM at 17 and 32 minutes into the recording as indicated by the hatched bars. **(b)** Current traces a and b were recorded at the points indicated in (a). Current traces c and d were recorded immediately before and at the peak of the second application of zinc.

4-Acetamido-4'-isothiocyanato-stilbene-2,2'-disulfonic acid (SITS) and niflumic acid do not affect $I_{Cl_{IR}}$.

Current traces recorded in control external solution and in an external solution containing 1mM SITS are shown in figure 4.9a. The mean current voltage relationships obtained with the two solutions are shown in figure 4.8b. The data are the mean ± sem, n = 3. As can be seen from both the raw data traces and the current voltage relationship plots, 1mM SITS was without effect at any of the potentials tested. At -110mV the control current was -477.9 ± 39.6pA while that in 1mM SITS was -494.9 ± 56.7pA. This was not significantly different to control ($p > 0.5$, paired t test).

Figure 4.10a shows the amplitude of $I_{Cl_{IR}}$ at -90mV. The application of niflumic acid at a concentration of 10μM did not affect the current amplitude in this or a further 4 cells. Current traces obtained in control and 10μM niflumic acid are shown in figure 4.10b. The amplitude of the current in control was -68pA while that in niflumic acid was -82pA.

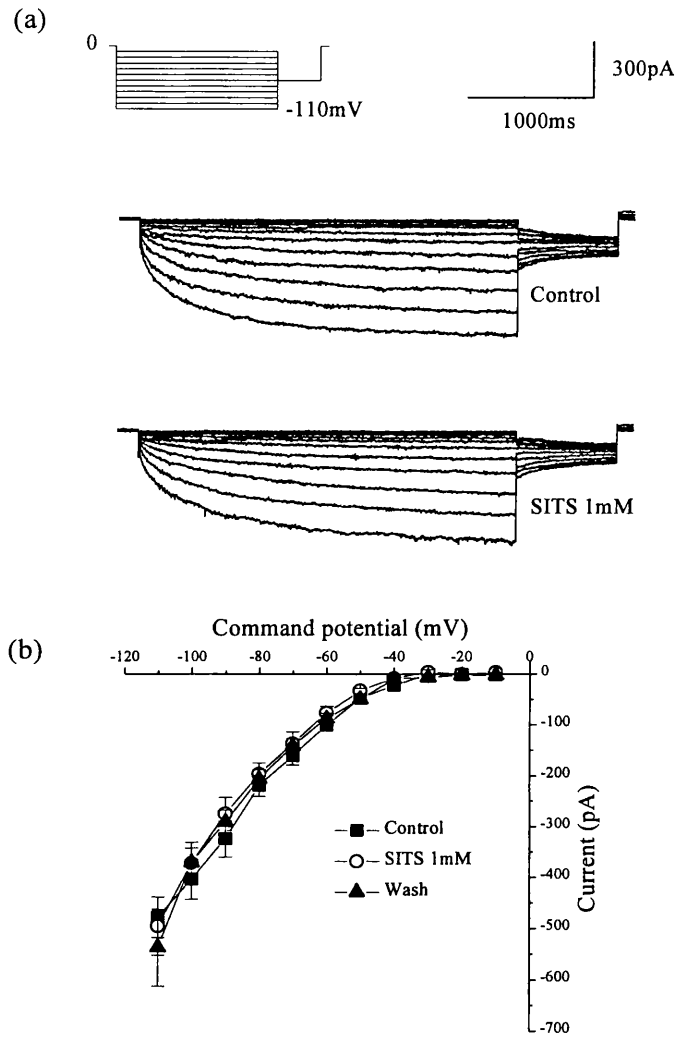

FIGURE 4.9. Effect of 4-Acetamido-4'-isothiocyanato-stilbene-2,2'-disulfonic acid (SITS). **(a)** Current voltage relationships generated by stepping in 10mV steps to between -10 and -110mV from a holding potential of 0mV in control and 1mM SITS. **(b)** Mean current voltage relationships generated in control and 1mM SITS. Data are mean ± sem (n = 3).

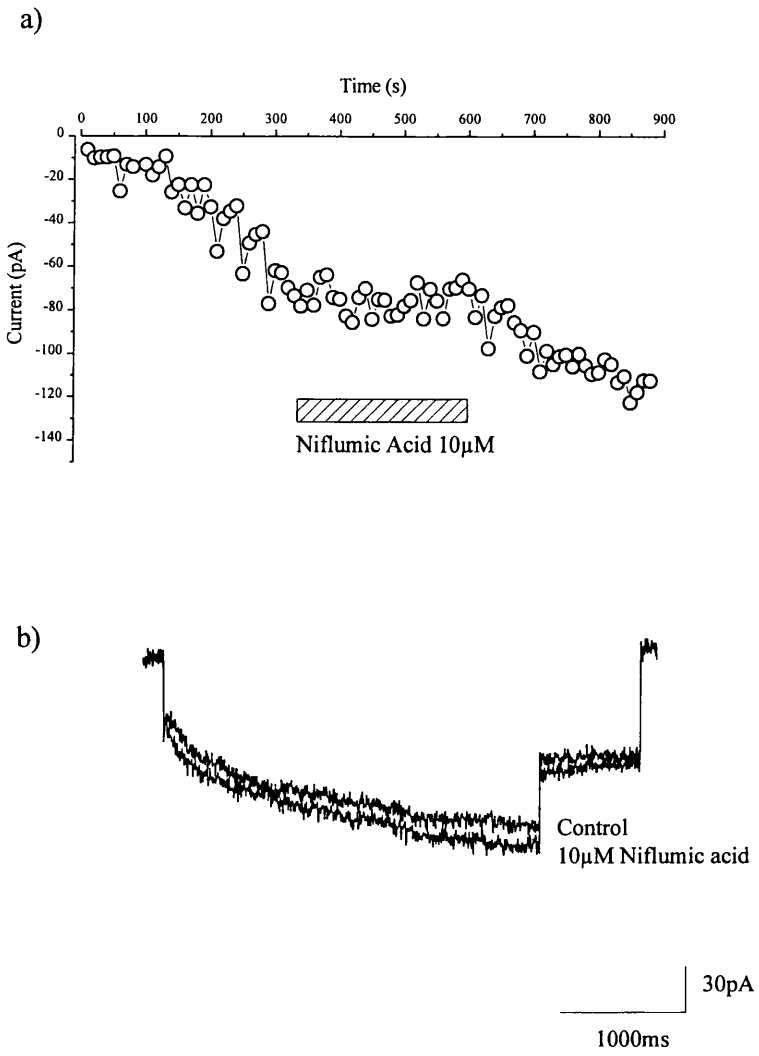

FIGURE 4.10. Effect of niflumic acid on $I_{Cl_{IR}}$ at -90mV. **(a)** The amplitude of $I_{Cl_{IR}}$ at -90mV was plotted against the time into the recording. Niflumic acid was applied at a concentration of 10μM as indicated by the hatched bar. **(b)** Current traces recorded at -90mV in control and in the presence of 10μM niflumic acid.

Effects of 4,4'-Diisothiocyanato-stilbene -2,2'-disulphonic acid (DIDS), antracene-9- carboxylic acid (9AC) and 5-Nitro-2-(3-phenylpropylamino) benzoic acid (NPPB).

In contrast to the lack of effect observed with SITS and niflumic acid; DIDS, 9AC and NPPB all were able to reduce the current amplitude. Figure 4.11 shows the amplitude of the current recorded at -90mV plotted against time. Figure 4.11a illustrates the effect of DIDS at a concentration of 1mM. DIDS in this example reduced the current by 50%. The mean inhibition of the current was 35.3 ± 6.1% (n = 3) and in this and all the neurons to which it was applied the effects were fully reversible.

9AC, also at a concentration of 1mM, reduced the current by about 40% and again the inhibition of the current was completely reversible upon wash (figure 4.11b). The mean reduction in the current at -90mV was 33.5 ± 6.8% (n = 5). In contrast to the onset of the effects of both DIDS and NPPB, the block by 9AC was slow to occur. In the example shown, the block by 9AC took almost 300s to reach maximal effect while the block by both DIDS and NPPB took less than 100s.

NPPB produced a substantial inhibition at a concentration of only 200μM. NPPB reduced the current shown by approximately 70% (figure 4.11c) and the mean inhibition was 58.6 ± 4.9% (n = 7). The effects of NPPB fully reversed.

Figure 4.12 shows plots of the mean current voltage relationships obtained in 1mM DIDS (figure 4.12a), 1mM 9AC (figure 4.12b) and 200μM NPPB (figure 4.12c), together with their respective controls. All three blockers were shown to reduce the current over the entire voltage range studied. The data shown in figure 4.12 are the mean ± sem and n = 3, 3 and 4 for DIDS, 9AC and NPPB

respectively. The voltage dependence of the inhibition caused by the compounds is shown in figure 4.13 where the percentage inhibition of the control current is plotted against the command potential. DIDS (figure 4.13a) and NPPB (figure 4.13c) both appeared to be more effective at blocking the current at the more depolarised command potentials. For DIDS there was a significant difference in the block at -60 and -110mV. The mean inhibition was 60.5 ± 1.7% ($n = 3$) at a potential of -60mV and at -110mV it was 21.9 ± 4.8% ($n = 3$) ($p < 0.01$, paired t test). NPPB caused a 83.5 ± 10.4% inhibition at -70mV but only a 52.5 ± 9.8% ($n = 4$) reduction at -110mV, this was not significantly different ($p < 0.09$, paired t test). In contrast the effect of 9AC (figure 4.12b) significantly increased with increasing hyperpolarisation so that at -60mV the current was inhibited by only 29.4 ± 3.9% ($n = 3$) while at -110mV the current was inhibited by 58.6 ± 2.5% ($n = 3$, $p < 0.05$, paired t test).

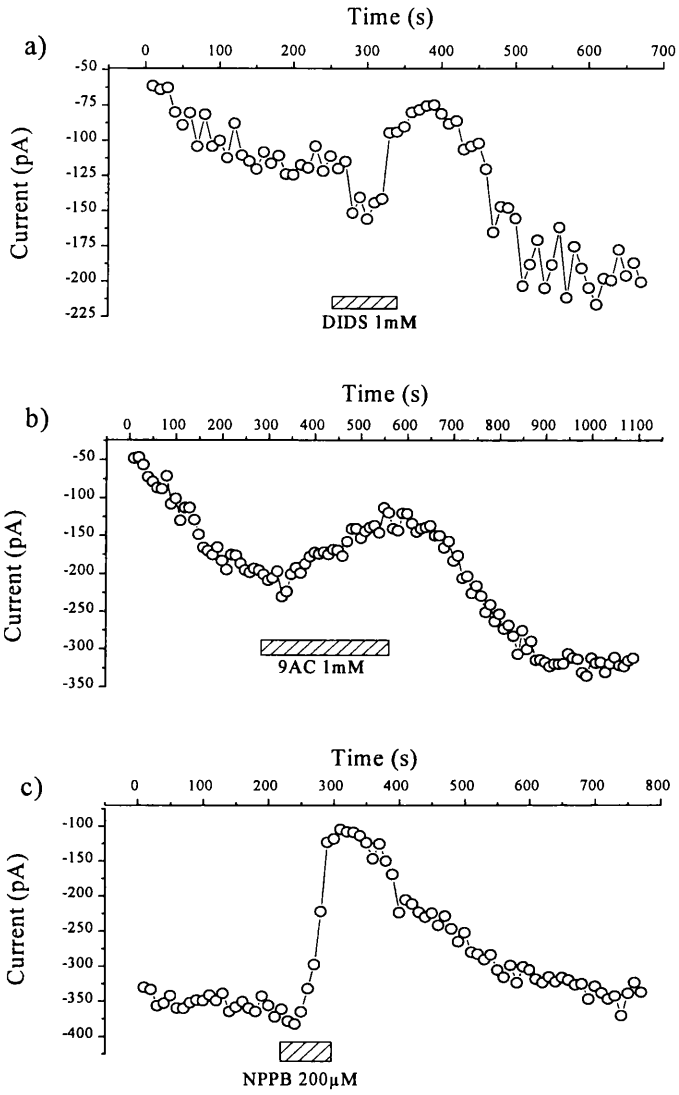

FIGURE 4.11. Effects of 4,4'-Diisothiocyanato-stilbene -2,2'-disulphonic acid (DIDS), antracene-9- carboxylic acid (9AC) and 5-Nitro-2-(3-phenylpropylamino) benzoic acid (NPPB). **(a)** Effect of 1mM DIDS on the current generated by a command potential of -90mV. **(b)** Graph of the effect of 1mM 9AC on the amplitude of the current generated at -90mV. **(c)** Effect of 200μM NPPB on the amplitude of the current recorded at -90mV.

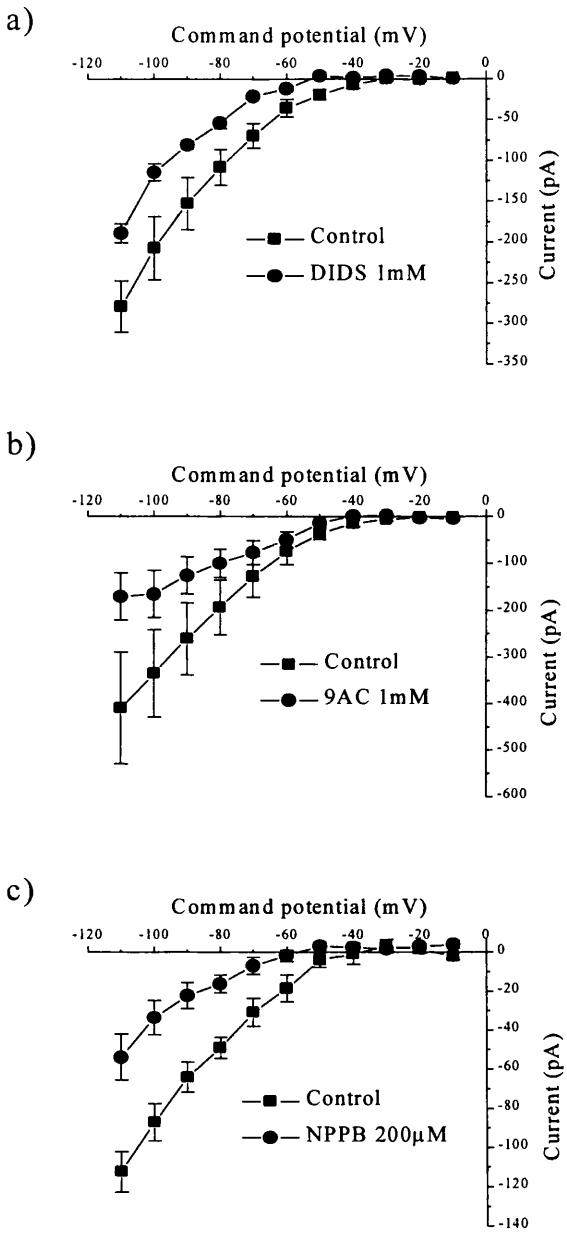

FIGURE 4.12. Current voltage relationships generated in DIDS, 9AC and NPPB. **(a)** Current voltage relationships recorded in control and 1mM DIDS by stepping to between -10 and -110mV from a holding potential of 0mV. **(b)** Effect of 1mM 9AC on the control current voltage relationship. **(c)** Current voltage relationships generated in control and then in the presence of 200μM NPPB. All data are the mean ± sem (n = 3, 3 and 4 for DIDS, 9AC and NPPB respectively).

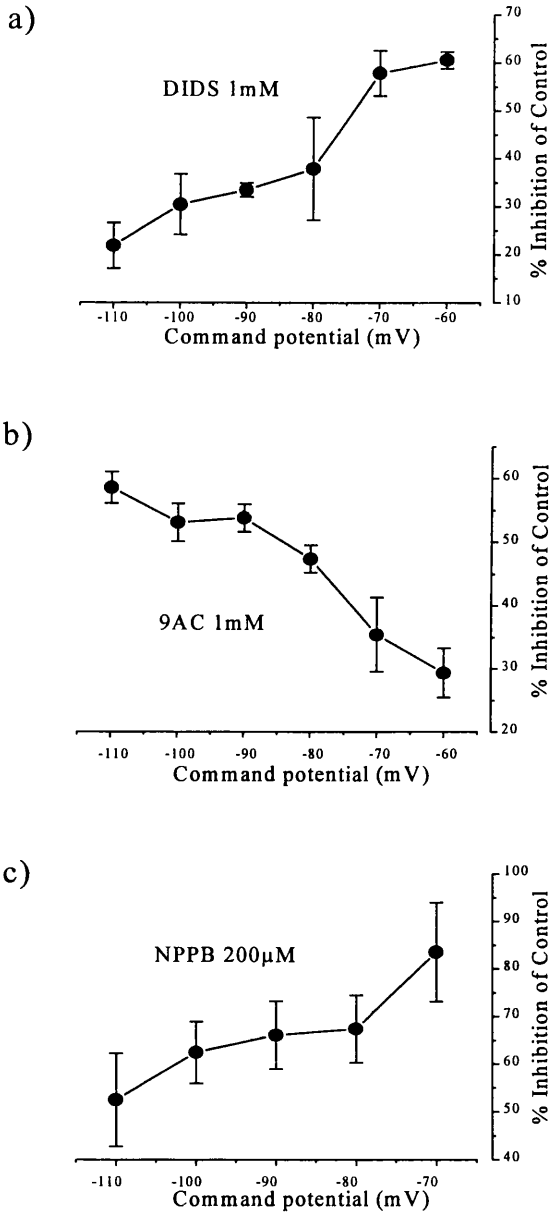

FIGURE 4.13. The effects of DIDS, 9AC and NPPB are voltage dependent. The percentage inhibition of the control current caused by **(a)** 1mM DIDS **(b)** 1mM 9AC and **(c)** 200µM NPPB are plotted against the command potential. The data are the mean ± sem and n = 3, 3 and 4 for DIDS, 9AC and NPPB respectively.

DISCUSSION.

The experiments presented in this chapter were carried out in order to obtain a pharmacological profile for $I_{Cl_{IR}}$ so that it could be compared with other voltage activated chloride currents. $I_{Cl_{IR}}$ was found to be blocked in a voltage and concentration dependent manner by the divalent cations cadmium and zinc. Also, a voltage dependent effect was observed for DIDS, NPPB and 9AC. In contrast neither SITS or niflumic acid appeared to have any effect on $I_{Cl_{IR}}$.

Block of $I_{Cl_{IR}}$ by the divalent cations cadmium and zinc.

Although both cadmium and zinc were able to inhibit $I_{Cl_{IR}}$, this can not be attributed to non specific effects of all divalents cations because barium had no effect on current amplitude (see chapter 3). Both cadmium and zinc are group IIB, transition metals whereas barium is a group IIA, alkaline earth metal and this may explain the difference in effects. Similar differential effects were observed in studies investigating the effects of divalent cations on I_A in neurons of the suprachiasmatic nucleus (Huang *et al.*, 1993) and $GABA_A$ gated chloride channels in SCG neurons (Smart and Constanti, 1990).

Cadmium and zinc were able to inhibit $I_{Cl_{IR}}$ in a concentration and voltage dependent manner. Cadmium appeared to be slightly more effective at inhibiting $I_{Cl_{IR}}$ at the concentrations applied but a full concentration response curve was not obtained and therefore a proper comparison can not be made between the two cations.

The inhibition caused by cadmium and zinc exhibited voltage dependence. This indicates that the inhibition is not due to a simple shift in the activation curve and therefore is probably not due, at least solely, to effects of the divalent cations on membrane surface charges. Such effects have been reported to account for the effects of zinc on sodium currents (Gilly and Armstrong, 1982; Hahin and Campbell, 1983). It was not possible however to fully investigate the effects of cadmium and zinc on the activation of $I_{Cl_{IR}}$ since a complete activation curve could not be obtained (see discussion, Chapter 3).

Although there have been other studies that have found an inhibitory effect of cadmium and zinc on hyperpolarisation activated chloride currents (Fritsch and Edelman, 1996; Chesnoy-Marchais and Fritsch, 1994; Staley, 1994; Selyanko, 1984; Madison *et al.*, 1986), there are none describing the voltage dependence of the inhibition. It is not exactly clear how cadmium and zinc are able to block $I_{Cl_{IR}}$ but the voltage dependence of the effect suggests that they are interacting with a region near the channel pore.

If cadmium and zinc are inhibiting $I_{Cl_{IR}}$ by blocking the pore of the channel they may be less effective at hyperpolarised potentials because there is a greater chloride conductance. The efflux of chloride ions can be envisaged to dislodge the cations from their binding sites. Several studies which have reported effects of zinc on ion channels have suggested that zinc may act at one or more histidine residues in the channel protein since the effects caused by zinc were altered by changing the pH (Huang *et al.*, 1993; Smart and Constanti, 1982). Therefore experiments looking at the effects of both changes in pH and the application of zinc on $I_{Cl_{IR}}$ may provide more information on the site of action of the divalent cations. It would also be interesting to determine if zinc and cadmium are acting at the same site.

The other interesting feature of the block by the divalent cations is that they have very obvious effects on the tail current produced upon repolarisation of the membrane potential to -60mV. In the presence of divalent cation, the instantaneous current jump observed at -60mV was followed by an inward relaxation rather than the usual outward relaxation. As mentioned above, the block by cadmium and zinc was more effective at depolarised potentials. Therefore it is possible that the repolarisation of the membrane potential, after the hyperpolarising voltage step, resulted in a rapid increase in the effectiveness of the cation block of the channel. The subsequent inward relaxation of the current is suggested to be due to outflow of chloride ions dislodging the cations from their binding sites, since at -60mV there is still a relatively large chloride conductance present. Interestingly, it appears that such tail currents are only observed after hyperpolarising voltage steps to -90mV and below.

Zinc has been shown to have a neuromodulatory role. It can be localised to synaptic vesicles of neurons in the central nervous system where the concentration of zinc is estimated to be as much as 300μM (Frederickson, 1989). It is also known that zinc can be released from synapses in a calcium dependent manner (Assaf and Chung, 1984) and that it can modulate ion channels (e.g. Smart and Constanti, 1990; Huang *et al.*, 1993). Therefore, although the block of $I_{Cl_{IR}}$ by cadmium is not likely to be of physiological importance the effects of zinc could be, especially since the concentration of zinc that can be released from synapses is high enough to completely block $I_{Cl_{IR}}$.

Effects of the organic chloride channel blockers on $I_{Cl_{IR}}$.

Cadmium is a well known inhibitor of calcium currents therefore the block of $I_{Cl_{IR}}$ by cadmium could perhaps suggest that $I_{Cl_{IR}}$ is calcium dependent. However, niflumic acid, which has been shown to block calcium activated chloride currents in many different cell types including rat SCG neurons (Sánchez-Vives and Gallego, 1994) had virtually no effect on $I_{Cl_{IR}}$. In addition the external calcium concentration is very low and would not be able to support a calcium current. Further more, Selyanko (1984) reported that the hyperpolarisation activated current of rat SCG neurons was unaffected by Co2+ and calcium free solutions. Similar results were also described for the hyperpolarisation activated chloride current present in hippocampal neurons (Madison *et al.*, 1986). The results obtained therefore indicate that $I_{Cl_{IR}}$ is not a calcium activated or calcium dependent chloride current.

DIDS, NPPB and 9AC were all able to inhibit $I_{Cl_{IR}}$. All three compounds reduced the amplitude of $I_{Cl_{IR}}$ in a voltage dependent manner but DIDS and NPPB exhibited a different voltage dependence to that of 9AC. Both DIDS and NPPB were more effective at depolarised potentials while 9AC produced a greater effect at hyperpolarised potentials. An additional difference is that 9AC appeared to have a much slower onset of action than the other two compounds.

A similar voltage dependent effect of DIDS was observed for the hyperpolarisation activated chloride current in rat osteoblastic cells, in that the current was completely blocked at -40mV but only partially blocked at -100mV (Chesnoy-Marchais and Fritsch, 1994). DIDS, although able to block other native hyperpolarisation activated chloride currents (Chesnoy-

Marchais and Fritsch, 1994; Chesnoy-Marchais, 1983; White and Miller, 1979), was reported to be ineffective at blocking ClC-2, the cloned chloride channel that results in a hyperpolarisation activated chloride current when expressed in *Xenopus* oocytes (Thiemann *et al.*, 1992). It is possible that an effect was missed however, because DIDS was only applied at very hyperpolarised potentials and as has been shown in this chapter and for rat osteoblastic cells (Chesnoy-Marchais and Fritsch, 1994), DIDS is more effective at depolarised potentials.

NPPB is the most potent of the carboxylic acid derivatives that has been synthesised to date. The presence of a carboxylate group in its structure means that it is anionic at physiological pH. In addition, it has an amino group and an apolar residue. The potency of NPPB seems to be due to the distance between the different groups since derivatives of NPPB, which have different spacing, are not as effective at blocking chloride channels (Wangemann *et al.*, 1986).

In rat SCG neurons the onset of the block by NPPB was very rapid especially when compared with the onset of the other compounds. This observation together with the results from other studies would seem to suggest that NPPB is acting at an extracellular site. Chloride channels, recorded in inside out patches of epithelial cells, were found to be blocked by NPPB but only after a delay, while those in outside out patches were blocked instantaneously. In addition, large macromolecules of NPPB, which are not membrane permeable were only able to block from the outside (Tilmann *et al.*, 1991). Since it appears that NPPB is acting at an extracellular site to block $I_{Cl_{IR}}$, it is possible to explain the greater potency observed at the more depolarised membrane potentials in a similar manner

to the block by cadmium and zinc. That is, the blocker is more effective at depolarised membrane potentials because there is less chloride efflux.

In contrast to NPPB, 9AC was not very effective at blocking $I_{Cl_{IR}}$, despite being applied at a higher concentration. The onset of effect was also much slower. The chloride current in the apical membrane of canine epithelium has also been shown to be only partially blocked by 9AC. This is despite the concentration of 9AC being far greater than that of NPPB required to completely blocked the current (Gögelein, 1988). In some other preparations 9AC has no effect at all (e.g. Komwatana *et al.*, 1994; Noulin and Joffre, 1993) and yet it is a potent blocker of skeletal muscle chloride channels both in the intact tissue (Bryant and Morales-Aguilera, 1971) and when ClC-1, the major skeletal muscle chloride channel, is expressed in *Xenopus* oocytes (Steinmeyer *et al.*, 1991b).

However, although the block by 9AC of ClC-1 is very potent (>80% block at 0.1mM), more than ten minutes are required to reach maximal effect (Jentsch, 1994). In addition, vesicles from skeletal muscle transverse tubules, incorporated into planar lipid bilayers, were only inhibited by 9AC when it was applied to the *cis* or cytoplasmic side of the membrane (Ide *et al.*, 1995). These data indicate that 9AC is probably acting at the cytoplasmic face of chloride channel proteins.

A similar mechanism of action would explain the slow onset of the 9AC induced inhibition of $I_{Cl_{IR}}$ and also the small reduction of current amplitude observed. Since the effects of 9AC are voltage dependent it can be postulated that 9AC inhibits $I_{Cl_{IR}}$ by binding to a site in the intracellular mouth of the channel pore. If this is the case, 9AC, which is an anion like NPPB at physiological pH (Wangemann *et al.*, 1986), may be more

effective at hyperpolarised potentials because at those potentials it is forced further into the channel pore.

The major problem with the chloride channel blockers that are available is that their ability to block is not determined by the type of chloride current being investigated. For example, DIDS is able to inhibit the hyperpolarisation activated chloride currents found in rat SCG neurons and rat osteoblasts (Chesnoy-Marchais and Fritsch, 1994) but not those of T84 epithelial cells (Fritsch and Edelman, 1996) or mouse mandibular gland cells (Komwatana *et al.*, 1994). Also in some preparations DIDS is only able to exert an effect when applied from the cytoplasmic side of the membrane (Chesnoy-Marchais, 1983; White and Miller, 1979). Similar differences in effect are seen for the other types of chloride channel blockers. Therefore it is not yet possible to identify chloride channels purely on the basis of their pharmacological profile. They must instead be characterised using electrophysiological and molecular biological techniques until more selective and potent compounds are available,.

CHAPTER 5

Effects of changes in the extracellular pH and a reduction in the external osmolarity on $I_{Cl_{IR}}$.

INTRODUCTION.

The aim of the first part of this chapter was to further characterise $I_{Cl_{IR}}$ by determining the sensitivity of the current to increases and decreases in the extracellular pH. Effects of changes in pH have been reported previously for a number of sodium, potassium and chloride currents and a variety of effects have been described.

The sodium conductance of the frog node of Ranvier is reduced by a reduction in extracellular pH (Woodhull, 1973). The reduction in conductance that occurred when the concentration of hydrogen ions was increased was believed to be caused by a combination of a shift in the activation kinetics and a block of the sodium channels. The shift was thought to be due to screening of surface charges (see also Hille *et al.*, 1975) and when corrected for, the block by the hydrogen ions was evident. This block which was found to be voltage dependent was explained as being due to hydrogen ions binding to a site within the channel pore and sensing the electric field. A block of epithelial chloride channels upon acidification has also been reported (Duszyk *et al.*, 1995) although it was the channel gating rather than the conductance that appeared to affected suggesting that the effects were due to hydrogen ions binding to a site some distance away from the pore of the channel.

Other studies have discovered that acidification of the extracellular pH results in an increase in current amplitude. Frog skeletal muscle chloride currents are activated by low pH (Warner, 1972). The volume activated chloride current of

rat parotid acinar cells is increased by external acidification (Arreola *et al.*, 1995), as is the hyperpolarisation activated chloride current of *Aplysia* neurons (Chesnoy - Marchais, 1983). The current recorded after expression of phospholemman is also sensitive to external acidification (Moorman *et al.*, 1994) but the endogenous hyperpolarisation activated chloride current of *Xenopus* oocytes is not (Kowdley *et al.*, 1994). Some currents are only affected by reducing the internal pH. The activity of neuronal potassium channels is reversible increased by decreasing the intracellular pH (Kim *et al.*, 1995), while the opening of chloride channels of the *Torpedo* electroplax tends to increase only when the pH on the *cis* side of the planar bilayers is altered (Hanke and Miller, 1983).

There are few reports on the effects of increasing the external pH and the effects appear to be variable. The hyperpolarisation activated chloride current of *Aplysia* neurons is reduced by high extracellular pH and there are also effects on the activation kinetics (Chesnoy-Marchais, 1983). The effect of high pH in these cells was more pronounced than a similar decrease in pH. A comparable effect of high external pH on the current recorded upon expression of ClC-2 has been described (Jentsch, personal communication) and it should be noted that this current is also increased by reducing the extracellular pH. Increasing the extracellular pH has been found to have no major effect on neuronal potassium currents (Kim *et al.*, 1995, Wooltorton and Mathie, 1995, Howe and Ritchie, 1991).

The second group of experiments in this chapter were designed to examine the sensitivity of $I_{Cl_{IR}}$ to changes in the external osmolarity. Most cell types are capable of regulating their volume when exposed to hypoosmotic conditions. Volume regulation is achieved by the activation of independent potassium and chloride conductances which results in the efflux of solutes and subsequently water. Volume sensitive chloride currents have been described for many different

cell types (see chapter 1, Ackerman *et al.*, 1994; Anderson *et al.*, 1992; Arreola *et al.*, 1995, 1996; Nilius *et al.*, 1994). These currents are typically rapidly activating, display outward rectification and are time dependently inactivated at depolarised potentials. They also tend to have a greater iodide than chloride permeability and a dependence on intracellular ATP (Jentsch, 1996; Ackerman *et al.*, 1994; Nilius *et al.*, 1994).

The current recorded after the expression of ClC-2, however, is also activated by external hypoosmolarity but it does not show any similarity to the typical volume sensitive chloride currents (Gründer *et al.*, 1992). ClC-2, which is slowly activated by strong hyperpolarisation, does not exhibit any time dependent inactivation and has a greater permeability for chloride than iodide (Thiemann *et al.*, 1992). Exposure of ClC-2 to hypotonic external media causes the voltage dependence of activation to be shifted in the depolarised direction. The activation threshold therefore becomes physiological under hypoosmotic conditions.

The hyperpolarisation activated chloride current in rat osteoblastic cells is sensitive to the external osmolarity as well but the sensitivity is anomalous. The current in these cells is reduced under hypotonic conditions but activated when exposed to hypertonic solution (Chesnoy-Marchais and Fritsch, 1994).

Experiments examining the effects of hypoosmotic external solution on $I_{Cl_{IR}}$ were initially, like experiments described in previous chapters, carried out using the whole cell method of the patch clamp technique. However, hypotonic external solution was found to have no apparent effect on $I_{Cl_{IR}}$ when it was recorded using this method. Whole cell patch clamping results in diffusional exchange between the pipette and the cell cytoplasm which can cause cell constituents such as enzymes and second messengers to be lost. It was therefore possible that the hypotonic external solution was not having any effect because a

cell cytoplasm constituent was missing. To overcome this problem the experiments were repeated using the amphotericin B perforated patch clamp technique (Rae *et al.*, 1991).

The first perforated patch recording of ionic currents was carried out by Lindau and Fernandez (1986) using ATP. ATP was found to increase the permeability of plasma membranes at a high concentration but the series resistance was very high and the technique was limited to a few cell types. The method was improved considerable by the use of the pore forming antibiotic nystatin (Horn and Marty, 1988) but the access resistances were again somewhat higher than conventional whole cell recording. The latest improvement is the use of another pore forming polyene antibiotic, amphotericin B. The access resistances obtained with amphotericin B are lower still than those obtained with nystatin (Rae *et al.*, 1991). Both of the polyene antibiotics are permeable to chloride and the monovalent cations but they do not allow the permeation of multivalent ions or nonelectrolytes. Therefore with amphotericin B the chloride concentration equilibrates across the plasma membrane but intracellular constituents that might be necessary for the hypotonic solution to affect $I_{Cl_{IR}}$ are not lost.

RESULTS

Effect of changes in the pH of the extracellular solution.

The extracellular pH was reduced by 0.5 or increased by 0.6 of a pH unit, from pH 7.4 to either pH 6.9 or pH 8.0. A typical example of the effect that a reduction in the extracellular pH had on $I_{Cl_{IR}}$ is shown in figure 5.1. Current traces generated in pH 6.9 were larger in magnitude than those recorded in control (pH 7.4). For the examples shown in figure 5.1, the current at -110mV was -612.8pA in control but in pH 6.9 it was -822.5pA. This increase in current amplitude was completely reversible upon wash as is shown by the lowermost current traces in figure 5.1. Similar enhancements were observed in a further four cells where the pH was decreased.

In contrast to the effect of a decrease in the extracellular pH, an increase in pH resulted in a reduction in current amplitude. Data traces recorded in control and then in an external solution having a pH of 8 are shown in figure 5.2. In the example illustrated the current at -110mV decreased from -619.9pA in control to -465.3pA in pH 8 and similar decreases in current were seen for three further cells. Like the effects of a decrease in the external pH, the effects caused by an increase in external pH were fully reversible upon wash. This is shown by the bottom current traces in figure 5.2.

The current traces shown in figures 5.1 and 5.2 were obtained from the same neuron and the corresponding current voltage relationships are plotted in figure 5.3a. Figure 5.3a shows that the current amplitudes recorded in control (closed squares) and after the two washes (closed triangles and closed diamonds, washes for pH 8 and pH 6.9 respectively) were not different. It also shows that increasing the extracellular pH caused a reduction in current amplitude at all

potentials while reducing the extracellular pH resulted in an increase in current at all potentials.

The effects of reducing or increasing the extracellular pH are voltage dependent.

The voltage dependence of the effects of changes in the external pH is shown in figures 5.3b and 5.3c respectively. In figure 5.3b the mean percentage inhibition of the control current caused by the pH 8 external solution is plotted against the command potential. pH 8 appeared to be more effective at the relatively more depolarised command potentials than at the hyperpolarised potentials. At -50mV the current was inhibited by 81.0 ± 7.9% while at -110mV it was inhibited by only 27.3 ± 4.2% ($n = 4$, for the data at -50mV and $n = 3$, for the data at -110mV). This reduction was not found to be significant ($p > 0.06$, paired t test) but if the reduction at -60 (68.3 ± 4.3%, $n = 4$) and -110mV were compared, then significance was found ($p < 0.003$, paired t test).

The effects of pH 6.9 were also found to be more potent at the more depolarised potentials. Figure 5.3c shows the mean percentage increase in current amplitude caused by pH 6.9 plotted against command potential. At -40mV the current amplitude was increased by 257.2 ± 15.2% but at -110mV it was only increased by 38.1 ± 10.7% ($n = 5$, at -40mV and $n = 3$, at -110mV). The effects at the two potentials were significantly different ($p < 0.02$, paired t test).

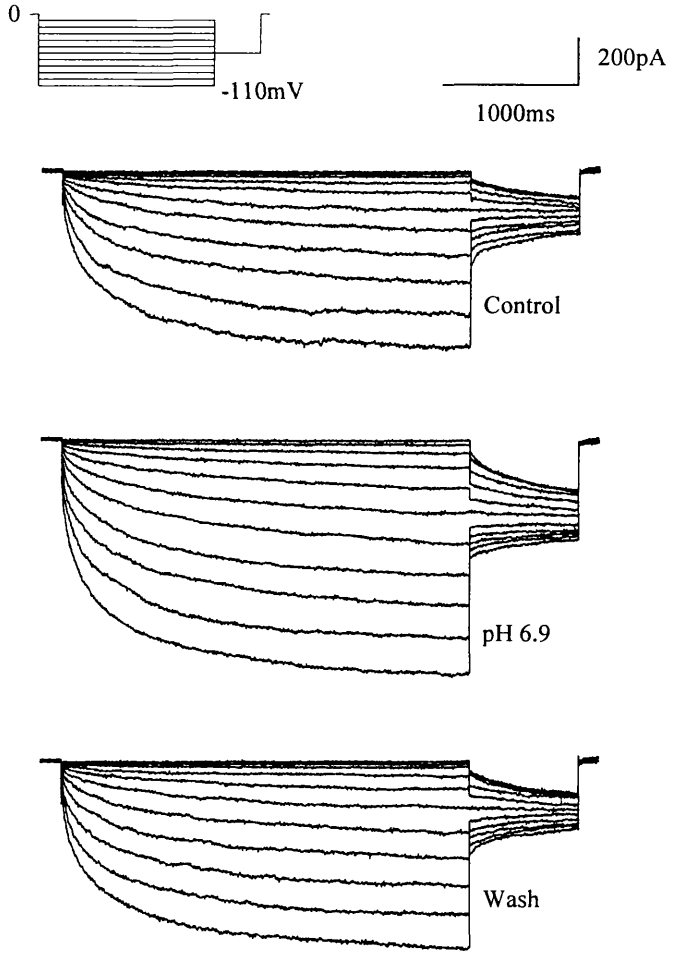

FIGURE 5.1. Effect of a reduction in extracellular pH. Current traces generated by stepping to between -10 and -110mV from a holding potential of 0mV. Traces were obtained in control (pH 7.4) and then in a pH 6.9 external. The lowermost current traces show that the effects of pH 6.9 were fully reversible upon wash.

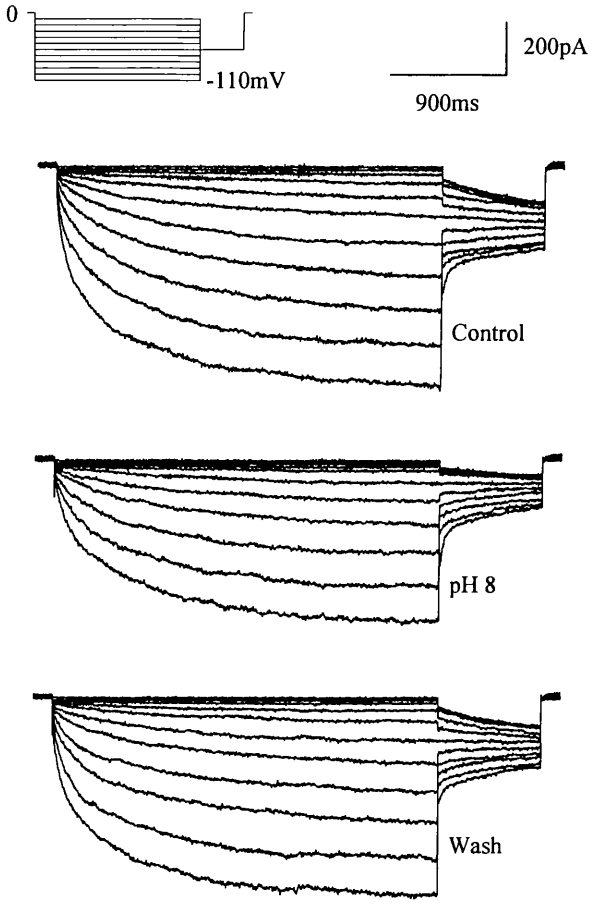

FIGURE 5.2. Effect of an increase in the extracellular pH. Current traces recorded in control (pH 7.4) and then pH 8 external by hyperpolarising the membrane potential in 10mV steps to between -10 and -110mV from a holding potential of 0mV. The lowermost traces show that the effects of pH 8 were fully reversible upon wash.

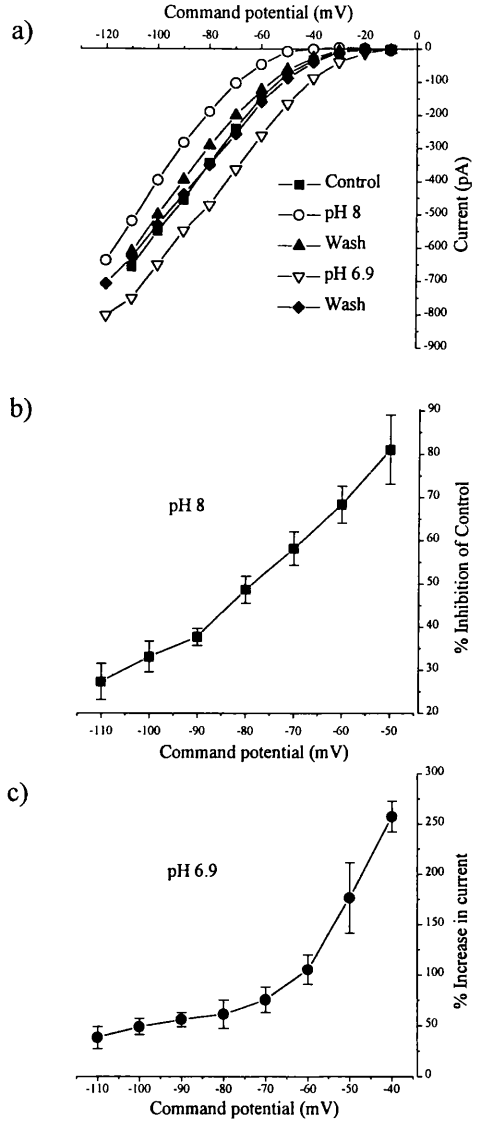

FIGURE 5.3. The effects of changes in external pH are voltage dependent. **(a)** Plots of the current voltage relationships shown in FIGURES 5.1. and 5.2. The control data is shown by closed squares, data in ph 8 external by open circles, the first wash by closed triangles, the pH 6.9 data by open triangles and the second wash by closed diamonds. **(b)** The mean percentage inhibition of current amplitude caused by pH 8 external solution is plotted against command potential. The data are the mean ± sem, n = 3 or 4. **(c)** The mean percentage increase in current amplitude caused by pH 6.9 external is plotted against command potential. The data are the mean ± sem, n = 3 - 5.

Effects of changes in extracellular pH on $I_{Cl_{IR}}$ activation kinetics.

Figure 5.4a shows single current traces obtained at -110mV in control and pH 6.9. The control trace at this potential has been scaled to the pH 6.9 current trace. The scaled control trace did not overlie the trace obtained in pH 6.9 and indicates that the activation of $I_{Cl_{IR}}$ in pH 6.9 is faster than in control. In figure 5.4b, data traces obtained from the same neuron as in figure 5.4a are shown. The pH 6.9 current trace which was recorded at -90mVwas found to have similar activation kinetics to the control current which was recorded at the more hyperpolarised potential of -110mV. This indicates that, for the example shown, reducing the pH of the external solution resulted in a depolarised shift in the activation kinetics of about 20mV. In a further two cells, pH 6.9 caused depolarised shifts in the activation kinetics of around 10 and 30mV. There were also, however, two cells in which pH 6.9 increased current amplitude but appeared to have no effect on the activation kinetics.

The effect of increasing the extracellular pH on the activation kinetics of $I_{Cl_{IR}}$ was also analysed. Figure 5.5a shows current traces obtained at -110mV in control and pH 8 external solutions. The pH 8 current trace has been scaled to the maximum amplitude of the control trace and as can be seen pH 8 appears to have caused a slowing in the activation kinetics. Figure 5.5b shows that the control trace recorded at -100mV can be scaled to the trace recorded in pH 8 at -110mV. This indicates that increasing the external pH caused a 10mV hyperpolarised shift in the activation kinetics of $I_{Cl_{IR}}$. In a further two cells pH 8 resulted in hyperpolarised shifts in the activation kinetics of around 10 and 15mV.

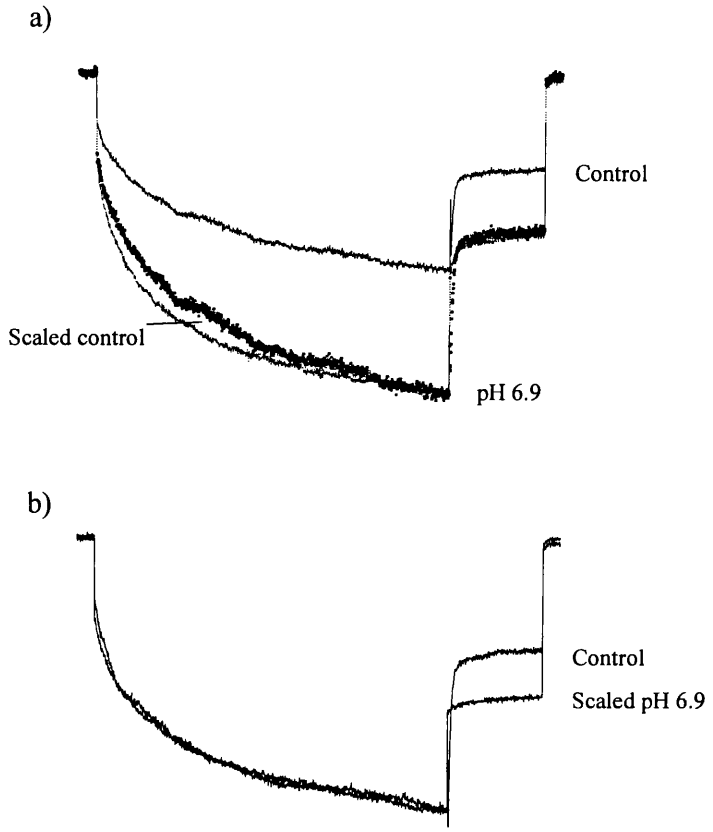

FIGURE 5.4. Effect of a reduction in external pH on the activation kinetics of $I_{Cl_{IR}}$. **(a)** Single current traces obtained at -110mV in control (pH 7.4) and pH 6.9 external solutions. The current trace obtained in control has been scaled to the maximum amplitude of the pH 6.9 current trace (closed squares). **(b)** Single current traces obtained in control at -110mV and in pH 6.9 external at -90mV. The trace obtained at pH 6.9 has been scaled to the maximum amplitude of the control current trace.

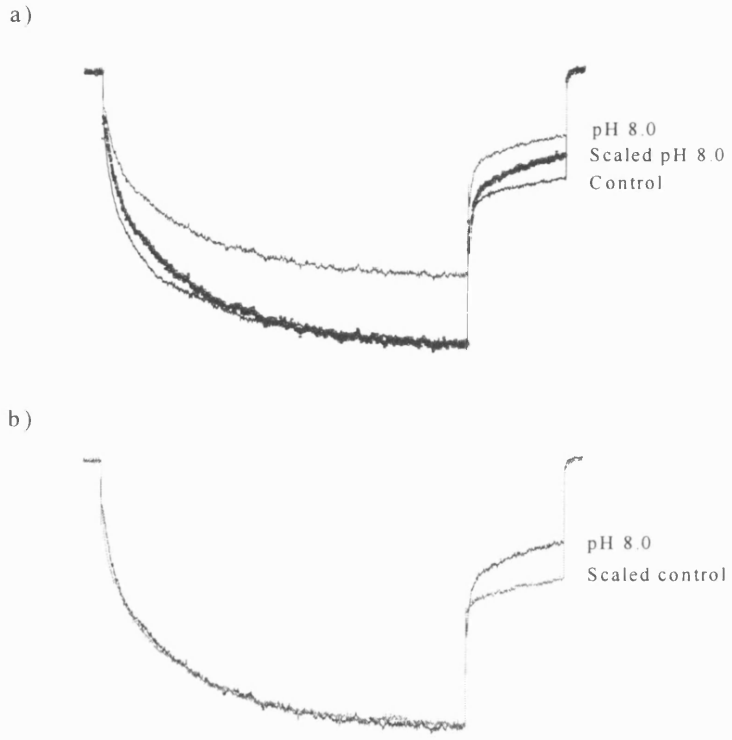

FIGURE 5.5. Effect of an increase in external pH on the activation kinetics of $I_{Cl_{IR^+}}$. **(a)** Single current traces obtained in control and pH 8 external solutions at -110mV. The pH 8 current trace has been scaled to the maximum control current amplitude (closed squares). **(b)** Current traces obtained in control at -100mV and pH 8 external at -110mV. The control trace has been scaled to the maximum pH 8 current amplitude.

Effect of changing the extracellular pH from pH 7.4 to pH 9.4.

The effects of greater changes in the extracellular pH were also investigated and it was found that raising the external pH from pH 7.4 to pH 9.4 resulted in a complete inhibition of the current amplitude. Figure 5.6a shows current traces recorded by stepping to -90 mV from a holding potential of -30mV, in control (pH 7.4) and then in high external pH (pH 9.4). The time dependent current amplitude in control was -42pA while that in pH 9.4 external was 0pA. Although the block by the pH 9.4 external was complete it was still, like smaller changes in pH, fully reversible upon returning to control solution (Figure 5.6a).

In figure 5.6b the mean current voltage relationships produced by a ramp voltage protocol in three cells are shown. The ramp protocol involved holding the cell at -30mV and then ramping the membrane potential from 0 to -120mV at a rate of 32.5 mV s^{-1}. This produced a current at -120mV whose amplitude was approximately equal to that of the steady state current recorded with a conventional voltage step to -120mV. To obtain the data shown in figure 5.6b the amplitude of the current produced by the ramp voltage protocol was measured at the appropriate points between 0 and -120mV. This gives a current voltage relationship which is in the same format as that obtained for a conventional current voltage relationship protocol. Figure 5.6b shows that high pH completely blocked the current at all potentials. The data for the pH 9.4 external were approximately linear and probably represented a leak conductance.

Attempts were also made to study the effect of a large reduction in the external pH from pH 7.4 to pH 5.4 but such a large change seemed to destabilise the membrane and this could not therefore be investigated.

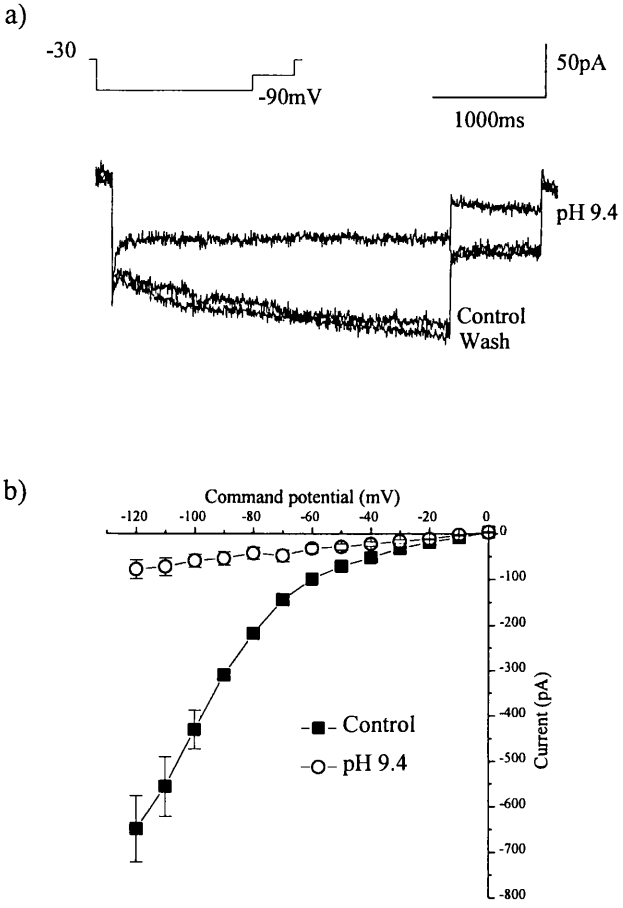

FIGURE 5.6. Effects of a pH 9.4 external solution on $I_{Cl_{IR}}$. **(a)** Current traces obtained in control and pH 9.4 external solutions by stepping to -90mV from a holding potential of -90mV. **(b)** Plots of mean current voltage relationships obtained in control (closed squares) and pH 9.4 (open circles) external solutions using a ramp voltage protocol (see text for details). The data are the mean ± sem, n = 3.

Effects of a reduction in external osmolarity on $I_{Cl_{IR}}$.

Figure 5.7a shows typical current traces obtained in control (osmolarity of between 310 and 320mmol/kg) and in hypotonic (osmolarity of between 250 and 260mmol/kg) external solutions. The current voltage relationships obtained in each of the solutions are shown in figure 5.7b. There was no difference in the current amplitudes measured in the two solutions at any potential tested. At -110mV the current in control was -636.7pA while that in hypotonic external was -645.5pA. The same lack of effect was observed in a further four cells. The hypotonic solution was applied for between 3.5 and 7 minutes.

Effects of a hypotonic external solution when recording $I_{Cl_{IR}}$ using the amphotericin B perforated patch clamp technique.

The currents shown in figure 5.7 were recorded using the conventional whole cell patch clamp method. It is well known that the conventional whole cell mode of patch clamping results in dialysis of the intracellular solution by the pipette solution and that this results in the loss of intracellular constituents. There are therefore two possible reasons why the hypotonic solution had no effect. The first is that a factor necessary for the hypotonic external to have an effect, was lost due to dialysis. The second was that dialysis mimics the effect of the hypotonic solution so that the current is already maximally activated and a challenge by hypotonic solution can have no further effect. Experiments investigating the effects of hypotonic solution were repeated using the amphotericin B perforated patch technique which allows exchange of monovalent ions but not large intracellular constituents.

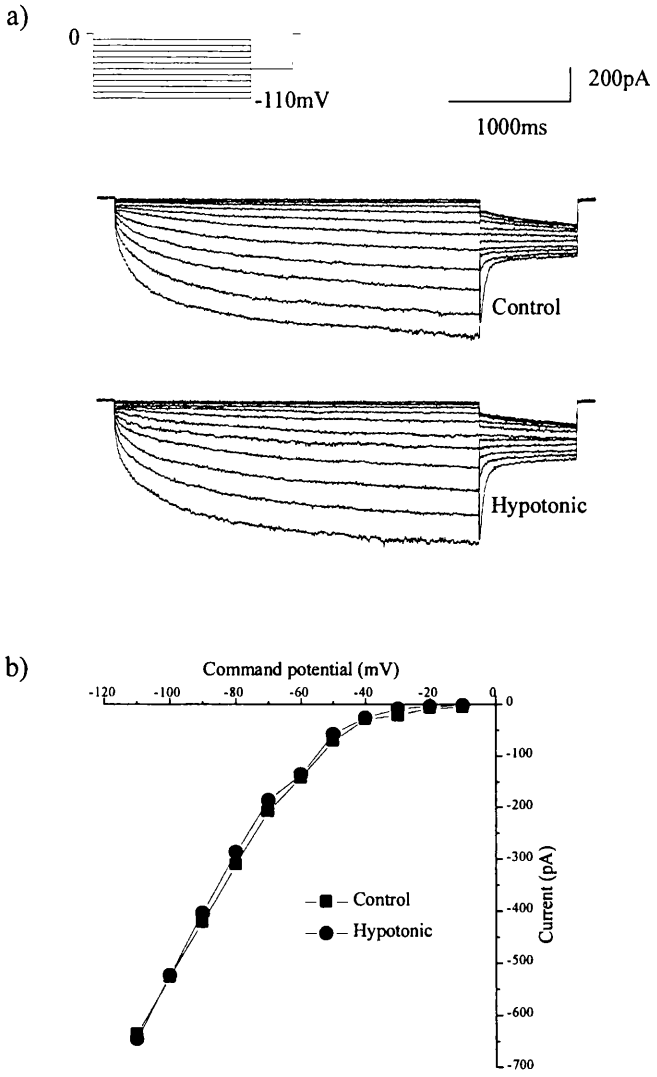

FIGURE 5.7. Effect of a hypotonic external solution on $I_{Cl_{IR}}$ recorded with the conventional whole cell patch clamp technique. **(a)** Current traces generated by stepping in 10mV steps to between -10 and -110mV from a holding potential of 0mV. Currents were recorded in control (310 - 320mmol/kg) and then hypotonic (250 - 260mmol/kg) external solutions. **(b)** Plots of the current voltage relationships obtained in control (closed squares) and hypotonic (open circles) external solutions.

Figure 5.8a shows the amplitude of a current recorded at -90mV using the amphotericin perforated patch clamp technique. In control there was little or no current present, the mean amplitude of the current recorded between 10 and 500s into the recording was -4.9 ± 0.8pA (n = 50 sample points). When the osmolarity of the external solution was reduced however, the current amplitude increased substantially. The amplitude of the current at the point indicated by ' b ' in figure 5.8a was -57.3pA. This increase in current amplitude was reversible upon returning to control external, indicated by ' c '. The mean current amplitude between 1250 and 1740s into the recording was -10.7 ± 1.0pA (n = 50 sample points). This increase in current amplitude could be repeated but the second exposure of the cell to hypotonic solution resulted in less of an increase in current amplitude than the first exposure (d, figure 5.8a). The current increased to only -46.2pA. It also appears from the data shown in figure 5.8a that the increase in current that occurred as a result of the second exposure was slower to occur. In figure 5.8b current traces, generated at the points in the recording indicated in figure 5.8a, are shown. A similar effect to that shown in figure 5.8 was seen in a further two cells, however, there were also four neurons which did not appear to respond to the change in extracellular osmolarity.

Characteristics of $I_{Cl_{IR}}$ recorded using the amphotericin B perforated patch clamp technique.

Using the amphotericin B perforated patch clamp method to record currents it was found that while some cells had little or no current present in control solution (-6.0 ± 1.0pA, n = 3) others did have relatively large currents (-44 ± 5.7pA, n = 4). Interestingly, it appeared that the cells that had $I_{Cl_{IR}}$ present under control conditions were the ones which did not respond with an increase in current amplitude upon the application of hypotonic external solution. For the cells which responded to hypotonic solution, the current amplitude was -55.7 ± 8.1pA (n = 3)

upon hypotonic challenge. The range of current amplitudes observed with the conventional whole cell mode of patch clamping is -20 to -310pA with a holding potential of -30mV. The current amplitudes observed with the amphotericin B perforated patch are therefore on the small side. The currents recorded using the amphotericin B perforated patch clamp technique were studied in more detail.

Figure 5.9 shows current traces generated using the conventional whole cell and the amphotericin B perforated patch clamp techniques. The current traces recorded using the amphotericin B perforated patch technique, like those recorded using the conventional whole cell method, activated slowly at hyperpolarised potentials and reached a steady state towards the end of the voltage step. For the example shown, the current trace obtained at the potential of -110mV was fitted with a double exponential function using the method of exponential peeling (for method see Chapter 3:Results). This gave values of 0.26s and 1.3s for τ_1 and τ_2 respectively. The corresponding amplitudes were 60.1pA and 65.9pA respectively. The time constants were close to those determined for currents recorded using the conventional whole cell method. τ_1 at -110mV was 0.20 ± 0.02s (n = 6) and τ_2 was 1.3 ± 0.1s, (n = 6) (see chapter 3:results).

Current voltage relationships were recorded in three cells using the amphotericin B perforated patch technique and a plot of the mean current voltage relationship is shown in figure 5.10. The threshold for activation was found to be approximately -40mV and the current showed strong inward rectification. Again these were comparable with currents recorded using the conventional whole cell method.

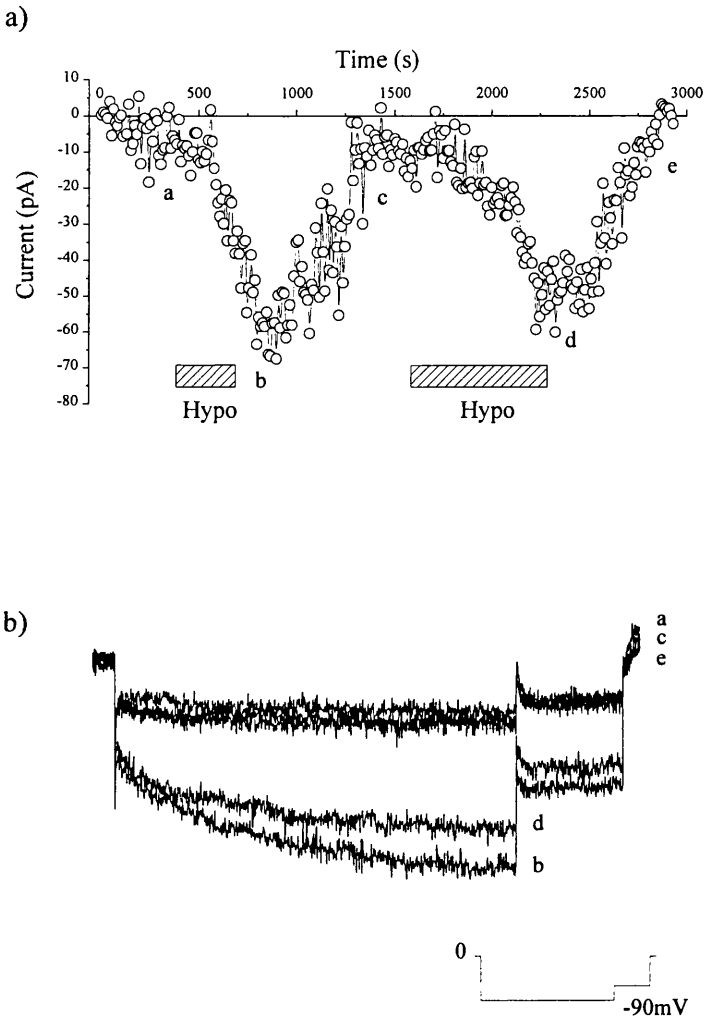

FIGURE 5.8. Effect of a hypotonic external solution on $I_{Cl_{IR}}$ recorded using the amphotericin B perforated patch technique. **(a)** The amplitude of $I_{Cl_{IR}}$ at -90mV plotted against recording time. Hypotonic external solution was applied at the points indicated by the hatched bars. **(b)** Current traces recorded in control, ' a '; during the first application of hypotonic solution, ' b '; after washout of the effects of hypotonic external, ' c '; during the second application of hypotonic solution, ' d ' and after washout of the effects of the second application of hypotonic external, ' e '.

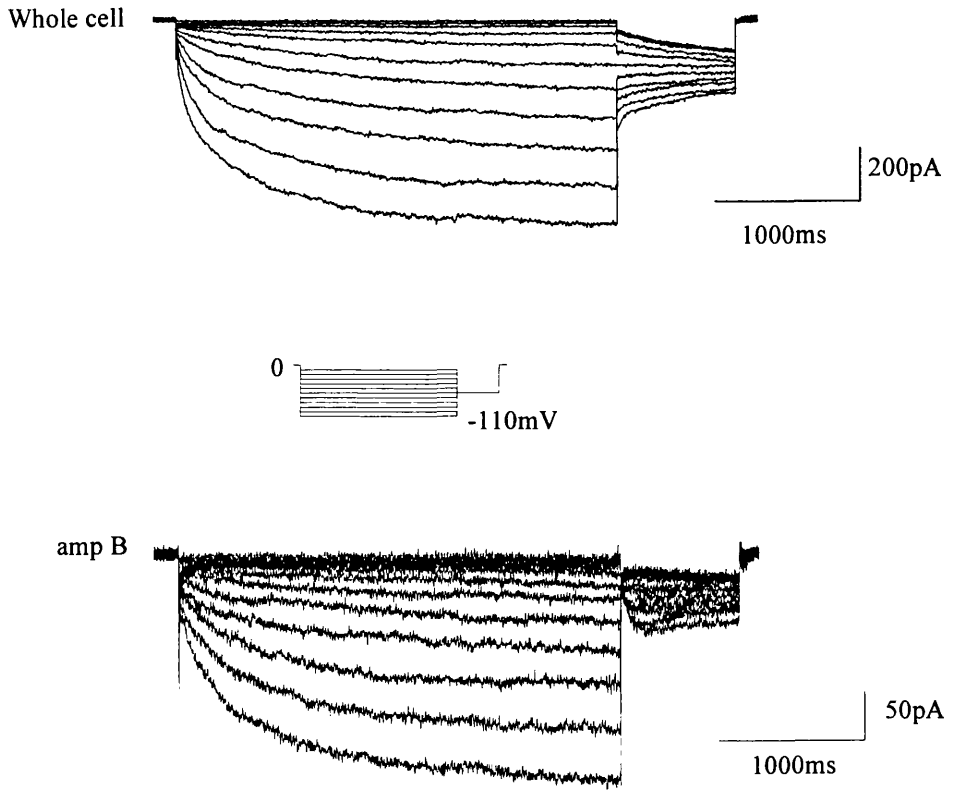

FIGURE 5.9. Comparison of current traces recorded using the whole cell and amphotericin B perforated patch clamp techniques. Current traces recorded using the conventional whole cell and Amphotericin B (amp B) perforated patch clamp techniques. Currents were generated by stepping to between -10 and -110mV in 10mV steps from a holding potential of 0mV. Both groups of current traces were recorded in control external solution. Note that the scale bars are different.

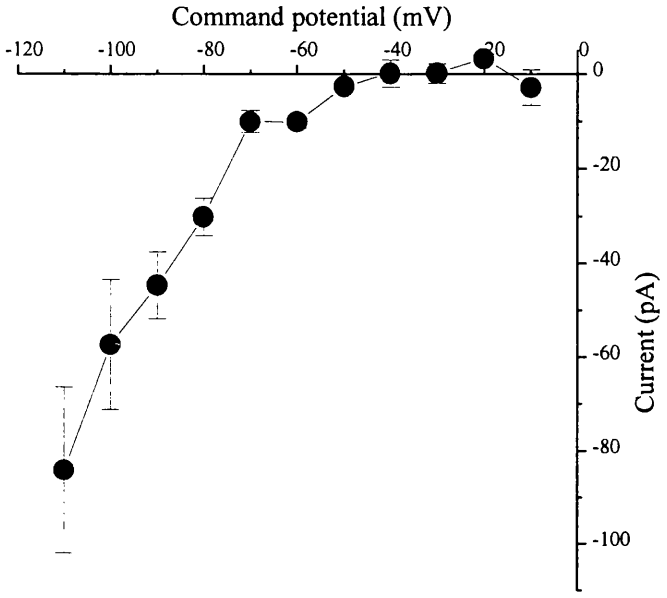

FIGURE 5.10. The current voltage relationship recorded using the amphotericin B perforated patch technique is similar to that recorded using the conventional whole cell method. Plot of the mean current voltage relationship recorded with the amphotericin B perforated patch. The current activates at potentials hyperpolarised to -40mV. The data are the mean ± sem, n = 3.

The deactivation of at -60mV of $I_{Cl_{IR}}$ is altered when recorded with the perforated patch rather than the conventional whole cell technique.

The activation of currents recorded using the amphotericin B perforated patch technique was found to be comparable to that seen with the conventional whole cell method of patch clamping. There were, however, differences found in the deactivation of the current observed upon repolarisation to -60mV (figure 5.9). At very hyperpolarised potentials, the deactivation of the current at -60mV, consisted of an instantaneous current jump followed by an inward relaxation. This is distinct to what is seen with conventional recording where the instantaneous current jump is followed by an outward relaxation. Interestingly the pattern of deactivation observed with the perforated patch is very similar to that observed after the application of either 10μM cadmium or 10μM zinc (chapter 4:results).

DISCUSSION

The results of this chapter show that $I_{Cl_{IR}}$ is sensitive to small changes of the external pH. A half pH unit acidification resulted in a voltage dependent increase in current amplitude. An alkalisation of 0.6 of a pH unit meanwhile caused a voltage dependent reduction in current amplitude. The effects of both increases and decreases in external pH were fully reversible. Experiments investigating the effects of reducing the external osmolarity were also conducted and it was found that the amplitude of $I_{Cl_{IR}}$ increased but only if it was recorded using the amphotericin B perforated patch clamp technique.

Effects of changes in external pH.

The effects of both a decrease and an increase in external pH had a very rapid onset. This suggests that the effects observed are not due to a change in the internal pH occurring subsequent to the change in the external pH, especially since the internal pH was buffered with HEPES. However, to confirm that this was not the cause of the effects, experiments with pipette solutions of different pH values should be carried out. A major problem though is that such experiments would be difficult to interpret since current amplitude, even under control conditions, is highly variable. An alternative method would be to combine fluorescent imaging techniques with electrophysiological recording to show whether changing the external pH is altering the internal pH under normal recording conditions.

It is possible that the changes in current amplitude observed were simply due to shifts of the current activation curve. The hyperpolarisation activated chloride current in *Aplysia* neurons was reported to exhibit the same sensitivity to external pH as was observed in these experiments and the effects observed were

apparently due to shifts in the activation curves (Chesnoy-Marchais, 1983). The activation threshold of $I_{Cl_{IR}}$ did appear shift when the external pH was both increased and decreased but the effects of changes in pH also displayed voltage dependence so it would therefore seem unlikely that the results observed were due solely to screening of surface charges. Unfortunately, the lack of current saturation, again meant that this could not be investigated in any detail.

A decrease in pH has been shown previously to inhibit sodium currents of frog nerve (Woodhull, 1973). This inhibition was, at least partially, due to a block of the sodium channels by hydrogen ions. It is more difficult to envisage why a decrease in pH should lead to an increase in current amplitude and an increase in pH should cause a decrease in current amplitude as has been observed in the studies presented here. There are a number of reports that have found similar effects for a decrease in the external pH. The magnitude of the inwardly rectifying potassium current of plant stomatal guard cells, which appears to be very similar to the inwardly rectifying potassium currents of animal cells, was found to be increased by acidification of the external media (Blatt, 1992). Also, a decrease in pH has been shown to increase the single channel conductance of cardiac sarcoplasmic reticulum chloride channels in lipid bilayers and this only occurred from the *trans* or external side of the membrane (Townsend and Rosenberg, 1995). In addition, the hyperpolarisation activated chloride current that can be recorded after expression of ClC-2 is also sensitive to both a decrease and an increase in external pH (Pusch and Jentsch, 1994).

There are a few possible explanations for the effects of a decrease in pH, at least for chloride channels. Ion permeation through a channel generally involves the permeating ion interacting with oppositely charged groups lining the channel pore. For chloride channels these groups would be expected to be positively charged so that increasing the hydrogen ion concentration may either add further

positive charges to these groups or possibly protonate neutral groups not normally involved in ion permeation. This could then increase the strength of the interaction with the permeating ion causing more ions to be 'pulled' through the channel. Alternatively, Arreola *et al.* (1995) have suggested that there may be negatively charged groups which, under control conditions normally restrict the flow of chloride ions, but which are neutralised by the decrease in pH. This latter explanation is not, however, consistent with the effects on SCG neurons observed with the increase in pH since it is not possible for a reduction in hydrogen ion concentration to make negative charges more negative. The most likely explanation for the effects of both a decrease and an increase in external pH, therefore seems to be protonation and deprotonation respectively, of positively charged groups that are found in the channel structure.

Since the amplitude of $I_{Cl_{IR}}$ is altered by relatively small changes in pH, the modulation could be of physiological importance. It is possible that the chloride efflux caused by activation of $I_{Cl_{IR}}$ may have a role in the regulation of intracellular pH. In addition, although not tested in the experiments presented in this Thesis, $I_{Cl_{IR}}$ may be permeable to bicarbonate ions as well. Electrophysiological recording together with fluorescent imaging of intracellular pH changes, would probably be the best method of determining any possible involvement of $I_{Cl_{IR}}$ in pH regulation.

Effect of a reduction in the external osmolarity on $I_{Cl_{IR}}$.

The effects of a change in the external osmolarity were determined by the method in which $I_{Cl_{IR}}$ was recorded. An increase in current amplitude was only apparent in those cells which were voltage clamped using the amphotericin B perforated patch variant of the patch clamp technique. Even using this method not all neurons responded to the osmotic challenge. The difference in the effect

observed with the two methods did not appear to be due to differences in $I_{Cl_{IR}}$ since the current, although smaller when recorded using amphotericin B, did not appear to exhibit any major differences. The mean activation threshold for the current was slightly more hyperpolarised when recorded using amphotericin B but this may simply be due to the difference in the number of neurons studied. Otherwise, the activation kinetics were within the range observed for the conventional whole cell patch and the currents appeared to be qualitatively alike.

It therefore appears that it was the method by which $I_{Cl_{IR}}$ was recorded that produced the differences in response. The perforated patch prevents the diffusion out of the cell of large intracellular constituents and it may be that the cell can only respond to hypoosmolarity when such constituents are intact. Interestingly only those neurons which did not possess a relatively large current under control conditions responded to the change in osmolarity with an increase in current amplitude. This suggests that the current in the other neurons was already fully activated.

With the whole cell mode of the patch clamp it has been postulated that the development of $I_{Cl_{IR}}$ is due either to (1) the increase in the cellular chloride concentration, (2) the loss of intracellular constituents or (3) osmotically induced changes in cell volume. Since, only some neurons which were voltage clamped using the perforated patch possessed the current under control conditions and only those neurons which did not have the current responded to the subsequent hypoosmolarity, a number of conclusions can be drawn. Firstly, an increase in chloride concentration can not be solely responsible for the development of $I_{Cl_{IR}}$ because not all neurons recorded with the perforated patch possessed the current, even though the chloride concentration would eventually have been the same in all neurons. Secondly, the presence of $I_{Cl_{IR}}$, under control conditions with the perforated patch, can not be due to loss of intracellular constituents and therefore

the development of $I_{Cl_{IR}}$ in the whole cell mode is probably not caused by that either. The smaller size of the currents recorded with the perforated patch does possibly indicate, however, that an additional process is occurring in the whole cell mode to produce the larger currents. The presence of $I_{Cl_{IR}}$ in amphotericin B patched neurons and the development of $I_{Cl_{IR}}$ in the whole cell mode can therefore probably be explained by osmotically induced changes in cell volume. This is despite the regulation of both the internal and external osmolarity with sucrose. It would be interesting to determine if the current, once developed under control conditions in the whole cell mode, can be reduced by an increase in the external osmolarity. Figure 5.8 shows that changing from a hypotonic solution to an isotonic one reduces current amplitude back to control levels.

Comparison of $I_{Cl_{IR}}$ with other osmotically sensitive chloride currents.

$I_{Cl_{IR}}$ is a chloride current that is slowly activated by hyperpolarising voltage steps and is sensitive to the external osmolarity. The characteristics of $I_{Cl_{IR}}$ however, are completely different to the typical volume activated chloride currents. Such currents are activated rapidly by depolarisation, display outward rectification, have a halide selectivity sequence of I > Br > Cl and require ATP (Ackerman *et al.*, 1994; Anderson *et al.*, 1992; Arreola *et al.*, 1995,1996; Nilius *et al.*, 1994). Of the currents which share common features with $I_{Cl_{IR}}$, there is only the hyperpolarisation activated chloride current of rat osteoblastic cells (Chesnoy-Marchais and Fritsch, 1994) and the ClC-2 induced chloride current (Thiemann *et al.*, 1992; Gründer *et al.*, 1992) which exhibit any sensitivity to the external osmolarity. However, while the current in rat osteoblastic cells is sensitive to a reduced external osmolarity, the effects of a hypoosmotic solution are opposite to those demonstrated for $I_{Cl_{IR}}$ in that the current in rat osteoblastic cells is reduced under hypoosmotic conditions. In contrast, both $I_{Cl_{IR}}$ and ClC-2 (Gründer *et al.*, 1992) are increased in magnitude by a reduction in the external osmolarity. The

only major difference between $I_{Cl_{IR}}$ in rat SCG neurons and ClC-2 induced chloride currents in *Xenopus* oocytes is that ClC-2 can only be activated by physiological voltages under hypoosmotic conditions while $I_{Cl_{IR}}$ is activated by physiological voltages in isotonic solutions.

CHAPTER 6

Is ClC-2 expressed in rat SCG neurons? Analysis of rat SCG neuron mRNA by RT-PCR.

INTRODUCTION.

The previous chapters have described the electrophysiological characterisation of the hyperpolarisation activated chloride found in rat SCG neurons. It has been found that $I_{Cl_{IR}}$ is activated slowly at potentials hyperpolarised to -20mV and does not show any time dependent inactivation. It is, in addition, blocked by divalent cations and a number of organic chloride channel blockers. $I_{Cl_{IR}}$ is sensitive to extracellular pH and when recorded using the amphotericin B perforated patch clamp technique, to hypotonic external solution as well. The characteristics that have been described for $I_{Cl_{IR}}$ appear to be virtually identical to those reported for the current recorded upon expression of ClC-2 in *Xenopus* oocytes (Thiemann *et al.*, 1992; Gründer *et al.*, 1992; Pusch and Jentsch, 1994; Jentsch, personal communication). It therefore seemed probable that the ClC-2 chloride channel underlies the hyperpolarisation activated chloride current recorded in rat SCG neurons. To determine if ClC-2 mRNA was indeed present in rat SCG neurons, experiments were conducted to analyse SCG mRNA using the technique of reverse transcription-polymerase reaction (RT-PCR).

The RT-PCR method.

RT-PCR is an adaptation of the polymerase chain reaction (Saiki *et al.*, 1985). In RT-PCR, mRNA acting as the starting template is reversed transcribed into cDNA (RT step) which is then amplified many times to give a detectable signal (PCR step, Powell *et al.*, 1987). To carry out RT-PCR two primers are

required. The different types that can be used are oligo(dT) primers, random hexamer primers and antisense primers (Sucher and Deitcher, 1995). Those used in the experiments presented here were antisense primers specific for ClC-2. That is one of the primers is antisense to the cDNA sequence of the protein of interest, the other is a sense primer and they are generated from parts of the sequence which are unique to the protein. The primers are generally between twenty and twenty four nucleotides in length and should have approximately the same C and G content so that they anneal at the same temperature.

In the RT step of the process the antisense primer is incubated with the mRNA, reverse transcriptase and the four deoxyribonucleoside triphosphates. The primer binds specifically to mRNA having the same but complementary sequence and transcribes only that mRNA into cDNA.

Once the cDNA has been made it is then amplified by the three step process of PCR. PCR requires large amounts of the four deoxyribonucleoside triphosphates, excess DNA polymerase and a pair of primers. The segment of DNA which is amplified is defined by the 5' ends of the primers. A diagrammatic illustration of the PCR process is shown in figure 6.1. The first step of PCR is the heat denaturation of the double stranded DNA template into single strands (step 1, cycle 1, Figure 6.1). The denaturation step is followed by the annealing of the two oligonucleotide primers to their complementary sequences on the cDNA strands (step 2, cycle 1, Figure 6.1). The final step is the extension of the annealed primers by the DNA polymerase to yield a complementary second strand of DNA (step 3, cycle 1, Figure 6.1). After the extension of the primers the temperature is raised again to denature the newly formed double stranded DNA and enable the whole process to be repeated.

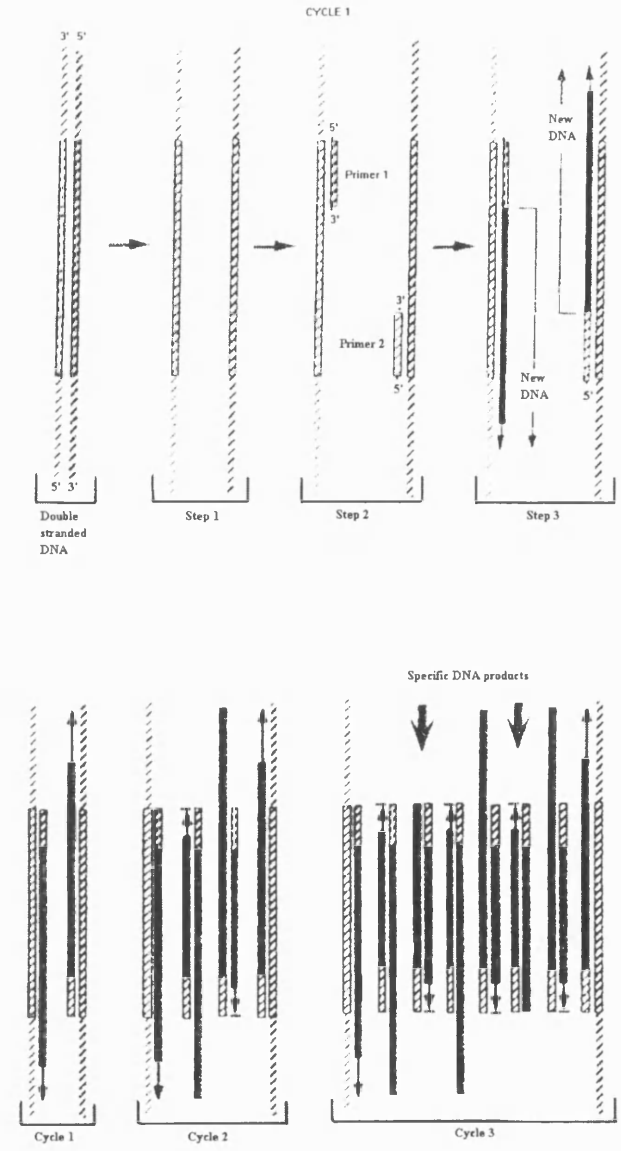

FIGURE 6.1. Diagrammatic representation of the PCR process. **Cycle 1, step 1**, double stranded DNA incorporating the segment of DNA to be amplified (hatched box) is heat denatured. This gives two single, complementary strands of DNA. **Step 2**, The temperature is lowered and the two oligonucleotide primers (primers 1 and 2) are annealed to their complementary sequences. **Step 3**, The temperature is raised slightly and the primers are extended to form new DNA by the DNA polymerase. The formation of new DNA occurs in the 5' to 3' direction (shown by the arrows). At the end of the first cycle the temperature is raised again and the newly formed DNA is heat denatured. **Cycle 2**, Each of the four strands of DNA present at the end of the first cycle can act as a template for the next cycle. The primers anneal to each of the strands and are extended to form four more strands of DNA (denoted by filled boxes). **Cycle 3**, The first double stranded DNA of the required sequence is formed (specific DNA products). The length of these products is defined by the distance between the 5' ends of the two primers. As each of the strands of DNA acts as a template, the number of copies of these specific DNA products increases exponentially in subsequent cycles until the number of templates exceeds that which the polymerase can extend in the given time.

Each of the newly formed strands of DNA, provided it is long enough, is able to form a template for subsequent PCR cycles (cycle 2, figure 6.1). It is not until the third cycle, however, that DNA strands of the correct length are formed (cycle 3, Figure 6.1). After the third cycle there is an exponential growth in the number of copies of specific DNA but this exponential accumulation is not a limitless process since eventually the amount of template exceeds that which the polymerase can extend in the time provided. Once this stage is reached the accumulation of DNA copies becomes linear.

RT-PCR can be carried out using separate enzymes for the two stages but in the experiments presented in this chapter a single enzyme has been used for both the RT and PCR steps. This enzyme, rTth, is a thermostable DNA polymerase originally isolated from *Thermus Therophilus*. rTth functions as a reverse transcriptase in the presence of manganese and as a DNA polymerase after the edition of magnesium (and the chelation of the manganese with EGTA) (Meyers and Gelfand, 1991). The advantage of using a single enzyme is that there is a reduction in the number of sample manipulations and the whole reaction can be carried out in a single reaction tube.

RESULTS

Optimisation of the RT-PCR reaction.

The initial aim of the experiments performed using the RT-PCR technique was to determine the optimum magnesium concentration that would maximise the amplification of mRNA from the SCG neurons. Both the reverse transcription of the mRNA into cDNA and the subsequent amplification of the cDNA were carried out using the thermal stable enzyme, rTth. rTth acts as a DNA polymerase in the presence of magnesium but it is very sensitive to the concentration (Meyers and Gelfand, 1991). The concentration of magnesium therefore had to be optimised to obtain the highest possible enzyme activity. RT-PCR was carried out using the reaction mixtures and cycling protocols described in the methods section.

Figure 6.2 firstly shows that ClC-2 mRNA is indeed expressed in rat SCG neurons. It also shows that increasing the magnesium concentration from 1.5mM (control) to 1.8mM prevented the amplification and hence detection of that mRNA. The reaction was carried out using the larger ClC primers that were predicted to give a reaction product that was 765 base pairs long. In the first lane of the gel a sample taken from the reaction mixture containing high magnesium was run while a sample from the control reaction mixture was run in the second lane. In the figure only the second lane shows a DNA band. That band is relatively faint but is of the correct size as judged by the 100bp size markers which are shown on the left side of the image. Since increasing the magnesium concentration appeared to prevent the amplification of mRNA all further experiments were carried out using a magnesium concentration of 1.5mM.

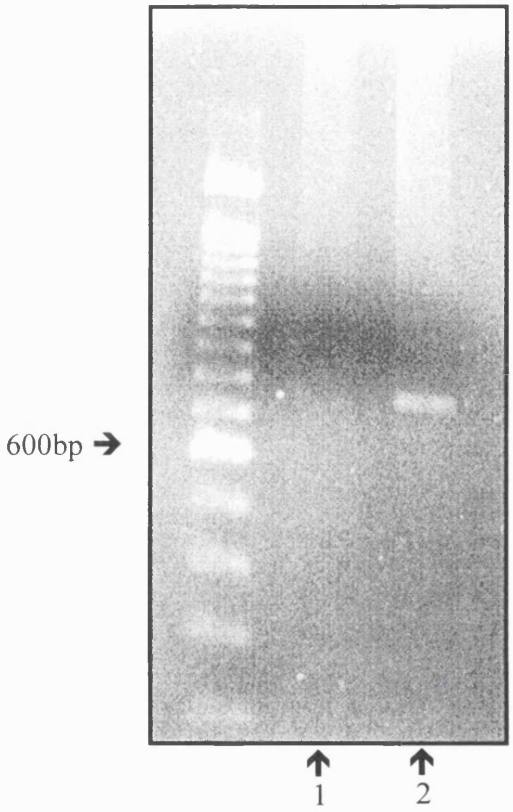

FIGURE 6.2. Image of gel showing the effect of an increase in the magnesium concentration on the amplification of mRNA from SCG neurons by RT-PCR using ClC primers. Lane 1 was obtained using 1.8mM $MgCl_2$ (high $MgCl_2$) while lane 2 was obtained using 1.5mM $MgCl_2$ (control).

Comparison of the expression of ClC-2 and actin mRNA in both SCG and cerebellar granule neurons.

Cerebellar granule neurons have been shown, by *in situ* hybridisation, not to express ClC-2 (Smith *et al.*, 1995). The RT-PCR of mRNA from these cells using primers for ClC-2 was therefore carried out as a negative control. In lanes 1 and 3 of figure 6.3 mRNA from SCG and CG neurons respectively has been amplified by RT-PCR using the longer ClC primers. A DNA band is visible in lane 1 but not lane 3 indicating that while CG neurons do not have ClC-2 mRNA as expected, SCG neurons do.

It is of course possible that no band is visible in lane 3 because there was no starting material. This is controlled for however, by two additional reactions. In lanes 2 and 4 respectively mRNA from both SCG and CG neurons was amplified using primers for actin. Actin is a ubiquitously expressed protein and therefore acts as a positive control since it should be detected in both SCG and CG neurons. DNA bands were observed in both lanes 2 and 4 therefore indicating that the lack of signal observed with ClC-2 primers in lane 3 was due to ClC-2 not being expressed in CG neurons.

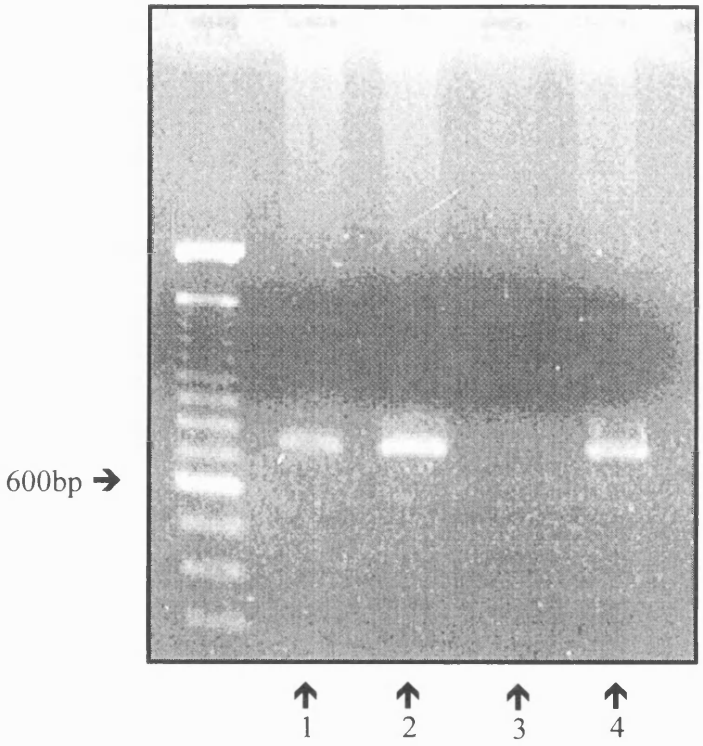

FIGURE 6.3. Image of a gel showing DNA bands obtained from SCG and granule neurons by RT-PCR using probes for ClC and actin. Lanes 1 and 2 were obtained from SCG neurons and Lanes 3 and 4 were obtained from granule neurons. Actin is present in both SCG and granule neurons (Lanes 2 and 4) but ClC is present only in SCG neurons (compare Lanes 1 and 3). The size markers are 100bp fragments.

Detection of ClC-2 and actin mRNA in the same tube.

Ideally for actin to act as a positive control its mRNA should be amplified in the same tube as the mRNA of interest. However, as is shown in figure 6.3 the DNA products produced by the primers for ClC-2 and actin were of approximately the same size (755bp and 763bp respectively). This similarity in size meant that if the two reactions were carried out in the same tube it would not have been possible to determine accurately what was present.

Further experiments were therefore performed using a second set of ClC-2 primers (ClCS) which were generated against a section of ClC-2 sequence carboxy terminal to that detected by the previous primers and which produced a smaller product of 238bp. Figure 6.4 shows the image of a gel on which two samples from separate tubes have been run. Both samples are from SCG neurons and in each case the mRNA has been probed with the short primers. Both lanes 1 and 2 show a DNA band of the correct size as determined by the 100bp size markers on the left hand size.

Having determined that the short ClC-2 primers were able to detect mRNA of the correct size, transcription and amplification of ClC-2 and actin mRNA was attempted in the same tube. In the same experiment it was ascertained whether the time at which samples were normally taken, that is after 25 cycles, was on the exponential phase of the PCR amplification curve (see introduction). Figure 6.5 shows a gel on which five samples, from the reaction tube have been run. The lanes 1 to 5 were obtained after 10, 20, 25, 35 and 45 PCR cycles respectively and both actin and ClC-2 primers were used in the same tube. As can be seen from figure 6.5, DNA bands were only detected in lanes 3-5 (25-45 cycles). The sample at 25 cycles is relatively faint and the intensity of the next

two bands is greater therefore indicating that the PCR process is still exponential at the points sampled.

Two rows of DNA bands were obtained in this experiment. While the upper and lower sets of bands are thought to relate to the presence of actin and ClC-2 mRNA respectively, the size markers indicate that the DNA bands produced are not of the correct size. The predicted size of the products was 238 and 763bp respectively for the ClC-2 and actin primers, however the upper bands are approximately 270bp while the lower bands are around 120bp. Similar results were obtained in a further three experiments. Such results may occur if there is insufficient enzyme present or the extension step of the cycle is not long enough to enable complete replication of the DNA sequence but changes were made to these parameters and no change in the results was observed. It was therefore not possible to accurately detect actin and ClC-2 mRNA in SCG neurons, in the same tube and experiments comparing the expression of the two mRNAs in SCG and CG neurons were as a result not performed.

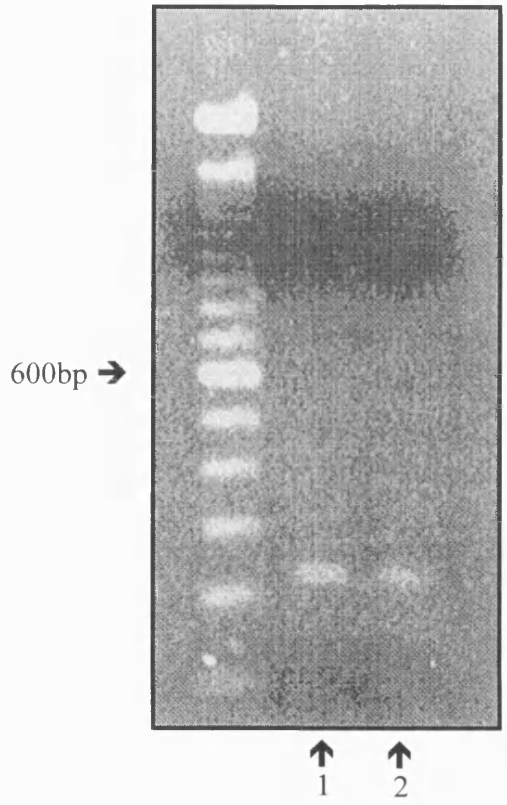

FIGURE 6.4. Image of a gel showing DNA bands obtained from SCG neurons by RT-PCR of SCG mRNA using the short ClC primers (ClCS). The oringinal starting material was divided into two to give the two lanes (Lanes 1 and 2). The size markers are 100bp fragments.

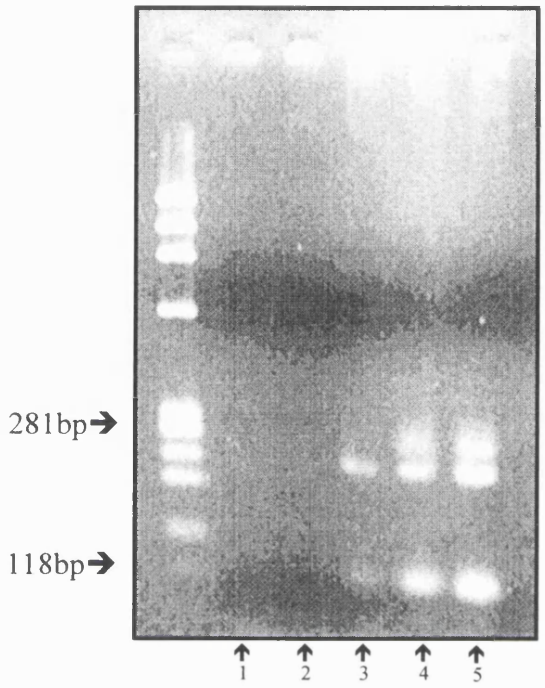

FIGURE 6.5. Image of a gel showing DNA bands generated by RT-PCR of mRNA from SCG neurons using the short ClC (ClCS) and Actin primers in the same tube. Lanes 1 to 5 are samples of the reaction mixture taken after 10, 20, 25, 35 and 45 PCR cycles respectively.

Electrophysiological comparison of SCG and CG neurons.

Using the whole cell patch clamp technique and the same recording solutions as were used to record $I_{Cl_{IR}}$ in SCG neurons, currents were recorded in CG neurons. Figure 6.6 compares currents generated by the same voltage protocol in SCG and CG neurons. Figure 6.6a shows a typical current produced in CG neurons by a single step to -90mV from a holding potential of 0mV. A typical current generated by the same protocol in SCG neurons is shown in figure 6.6b. While in SCG neurons this protocol produced a time dependent inward current, in CG neurons there was no obvious current detected. A similar apparent lack of current was observed for a further 3 cells. The absence of a hyperpolarisation activated chloride current in CG neurons is further illustrated in figure 6.6c which shows a group of current traces generated using the current voltage relationship protocol (see methods section). Voltage steps up to -110mV failed to reveal a current.

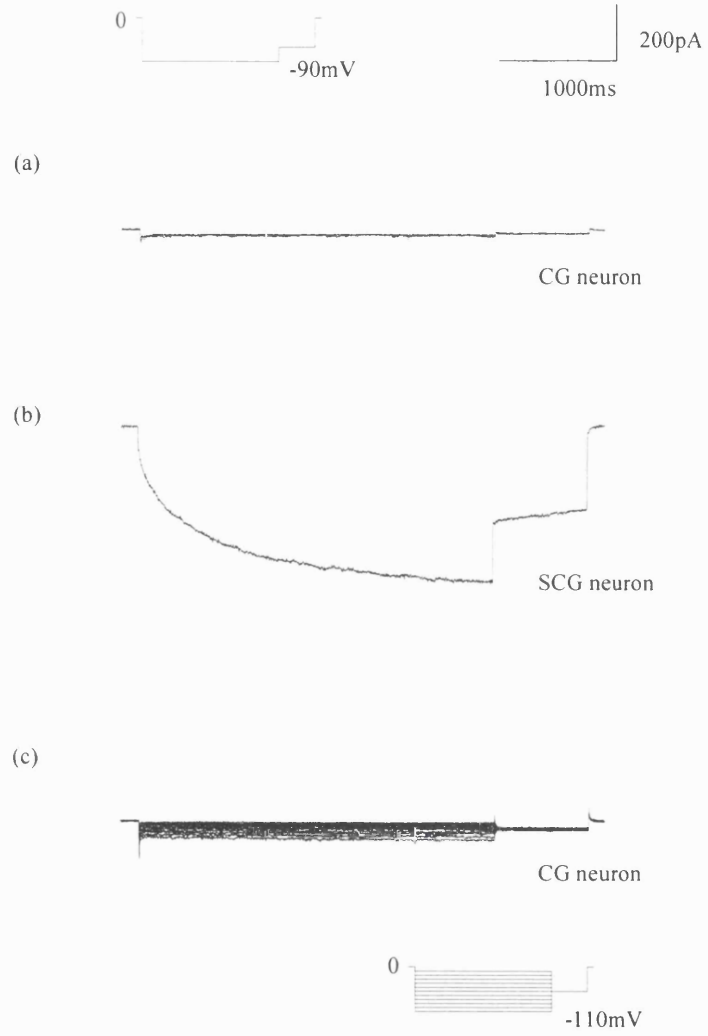

FIGURE 6.6. Comparison of currents recorded from SCG and CG neurons. **(a)** Typical current trace recorded from a CG neuron by stepping to -90mV from a holding potential of 0mV. **(b)** A current trace recorded from a SCG neuron using the same voltage protocol. **(c)** Typical current traces recorded from a CG neuron by stepping between -10 and -110mV in 10mV steps from a holding potential of 0mV. All current traces are to the same scale.

DISCUSSION

The results of the experiments that have been presented in this chapter indicate that mRNA for ClC-2 is expressed in rat SCG but not rat CG neurons. The presence of ClC-2 mRNA corresponded with the ability to record a hyperpolarisation activated chloride current and indicates, together with the electrophysiological data presented in previous chapters, that the ClC-2 channel underlies the hyperpolarisation activated chloride current that is present in rat SCG neurons.

All the RT-PCR experiments that were carried out were conducted on dissociated whole ganglia. There is therefore a possibility that the ClC-2 mRNA detected, came from cell types other than neurons. To show conclusively that ClC-2 mRNA is expressed in SCG neurons, the mRNA from single SCG neurons will have to be probed with the ClC-2 primers. In addition, to correlate the presence of $I_{Cl_{IR}}$ with the expression of ClC-2 mRNA, $I_{Cl_{IR}}$ should be recorded electrophysiologically before the mRNA is collected and analysed by RT-PCR.

Single cell RT-PCR was first described by Rappolee *et al.* (1989) and it has since been used in a wide range of studies such as determination of the subunit composition of glutamate gated channels (Lambolez *et al.*, 1992; Bochet *et al.*, 1994; Jonas *et al.*, 1994) and determination of dopamine subtype localisation (Surmeier *et al.*, 1990). Two strategies have been shown to lead to successful analysis of mRNA following electrophysiological characterisation. The first involves harvesting the total cell contents into the recording pipette by applying suction. The contents are then expelled into a PCR tube where the RT-PCR process is carried out

(e.g. Lambolez *et al.*, 1992). To obtain sufficient cDNA for visualisation on a gel two rounds of the PCR step are generally required. The second round being carried out with a small sample taken from the first round.

The second method of mRNA analysis results in amplification of the total cell mRNA which can then be furthered analysed to determine the presence of a specific mRNA (Van Gelder *et al.*, 1990; Eberwine *et al.*, 1992). In this method the recording pipette contains all the reagents required to synthesise cDNA from the mRNAs present in the cell. The reagents passively diffuse into the cell and once sufficient time has elapsed to allow synthesis of cDNA the cell contents are aspirated into the pipette. The single stranded cDNA obtained is then made double stranded and is used as a template for subsequent synthesis and amplification of antisense RNA. Since the original mRNA is transcribed into cDNA within the cell there is a reduced chance of degradation of the mRNA by RNAses and also loss due to non specific binding to plastic and glass. This increases the efficiency of the reverse transcription process.

RT-PCR of mRNA from SCG neurons resulted in DNA bands of the correct size being detected upon visualisation of the gel. The primers used were the same as those used by Smith *et al.* (1995) to detect ClC-2 by *in situ* hybridisation and were taken from different parts of the published ClC-2 cDNA sequence (Thiemann *et al.*, 1992). Although the products were of the size expected it is possible that their sequences were incorrect. This can occur if annealing temperatures are not quite optimal and the primers are therefore able to bind non specifically to the target DNA. To determine if the product sequence is the same as that of the original ClC-2 cDNA sequence it will be necessary to do a southern hybridisation analysis of a gel. Southern blotting is process where DNA is transferred from the gel to a nitrocellulose filter. In order to transfer the DNA, it is first depurinated and denatured by incubation in acid and alkali solutions.

Capillary diffusion of a high salt solution then draws the DNA from the gel onto the nitrocellulose filter where it is immobilised by baking. Nucleotide probes having the same sequence as the expected products and labelled with ^{32}P are hybridised to the DNA at a raised temperature and the filter is then visualised by autoradiography (Dyson, 1991).

Finally, the presence of mRNA for ClC-2 does not necessarily mean that the channel is functionally expressed. That can only be determined by immunohistochemical studies using antibodies against ClC-2. Unfortunately such antibodies have not as yet been successfully generated (Jentsch, personal communication) and therefore the experiments at the moment can not be performed.

GENERAL DISCUSSION.

Characteristics of $I_{Cl_{IR}}$.

The previous chapters have described the results of experiments designed to characterise some of the properties of $I_{Cl_{IR}}$, a hyperpolarisation activated chloride current that can be recorded from rat SCG neurons. $I_{Cl_{IR}}$ was activated by potentials hyperpolarised to -20mV in a manner that was best described, at membrane potentials between -80 and -110mV, by a double exponential function. The two activation time constants exhibited voltage dependence with both of them becoming faster with increasing hyperpolarisation. Activation of $I_{Cl_{IR}}$ was slow so that it only just reached a steady state level towards the end of the 3 to 4s voltage steps that were typically used. $I_{Cl_{IR}}$, however, once activated did not display any time dependent inactivation at any of the potentials tested.

$I_{Cl_{IR}}$ did not have any of the characteristics of the hyperpolarisation activated cation currents such as I_Q (Halliwell and Adams, 1982) or the inwardly rectifying potassium currents (e.g. Constanti and Galvin, 1983). However, it reversed at 0mV which agrees with the chloride equilibrium potential calculated for the recording conditions used. The halide selectivity sequence of $I_{Cl_{IR}}$ was found to be $Cl \geq Br > I$.

$I_{Cl_{IR}}$ was reduced by a number of putative chloride channel blockers in a voltage dependent manner. The divalent cations, cadmium and zinc, also inhibited $I_{Cl_{IR}}$ in concentration dependent manner. It was concluded that this was not subsequent to block of calcium currents since the low calcium concentration was unlikely to have been sufficient to support a calcium conductance and niflumic acid, a blocker of calcium activated chloride currents (White and Aylwin, 1990), was ineffective. DIDS, NPPB and 9AC voltage dependently reduced $I_{Cl_{IR}}$ but

while both DIDS and NPPB were more effective at depolarised potentials, 9AC had a greater effect at hyperpolarised potentials. This is thought to reflect the sites of action of the different agents. SITS, although structurally similar to DIDS had no effect.

$I_{Cl_{IR}}$ was found to be sensitive to both acidification and alkalisation of the external recording solution. A half pH unit decrease in pH resulted in an increase in current amplitude while a 0.6 of a pH unit increase in pH decreased the amplitude of $I_{Cl_{IR}}$. These effects, like those of the chloride channel blockers, were also voltage dependent which indicates that the effects are occurring at a site within the electric field of the membrane. A possible explanation is that the decrease and increase in pH are causing protonation and deprotonation respectively of positively charged groups in the channel.

A reduction in the external osmolarity caused an increase in current amplitude that was fully reversible. This only occurred, however, when $I_{Cl_{IR}}$ was recorded using the amphotericin perforated patch clamp technique and then only in neurons which did not display an appreciable current under control conditions. The lack of effect of hypotonic solutions on neurons already possessing $I_{Cl_{IR}}$ under control conditions, in both the whole cell mode and perforated patch, would seem to indicate that $I_{Cl_{IR}}$ is already fully activated in those neurons.

Comparison of $I_{Cl_{IR}}$ and ClC-2.

ClC-2, when expressed in *Xenopus* oocytes results in a hyperpolarisation activated chloride current (Thiemann *et al.*, 1992). The ClC-2 induced current has a similar sensitivity to cadmium, zinc and 9AC as $I_{Cl_{IR}}$ (Jentsch, personal communication; Thiemann *et al.*, 1992). In addition, it is increased in amplitude by a reduction in the external pH (Pusch and Jentsch, 1994) and is activated by a

reduction in the external osmolarity (Gründer *et al.*, 1992). ClC-2 differs from $I_{Cl_{IR}}$ in that it has been reported to be insensitive to the application of DIDS (Thiemann *et al.*, 1992). However, it is possible that an effect of DIDS was not apparent because it was only applied at very hyperpolarised potentials. DIDS produced a greater inhibition of $I_{Cl_{IR}}$ at -60mV than at -110mV. Another difference between the two currents is that ClC-2 can only be activated by physiological voltages in hypoosmotic conditions. The reason for this discrepancy is not apparent but perhaps it reflects differences in the cell processing of the protein.

Since the characteristics of ClC-2 and $I_{Cl_{IR}}$ have been found to be virtually identical it seems highly probable that the ClC-2 chloride channel underlies $I_{Cl_{IR}}$. Further evidence for this comes from experiments using the RT-PCR technique which demonstrated that mRNA for ClC-2 was expressed in rat SCG neurons.

Putative physiological functions of $I_{Cl_{IR}}$ in rat SCG neurons.

$I_{Cl_{IR}}$ is activated at potentials hyperpolarised to -20mV. It is therefore likely that $I_{Cl_{IR}}$ will be active at the resting membrane potential which has been previously reported to be approximately -60mV in these neurons (Adams and Harper, 1995). An internal chloride concentration of between 20 and 30mM has been found for these neurons (Woodward et al., 1969; Ballanyi and Grafe, 1985). At such concentrations the chloride reversal potential is predicted to be approximately -50mV in intact neurons. The current amplitude would therefore not be very large at the resting membrane potential and so it would contribute little if anything to the resting membrane potential itself.

The slow activation and lack of inactivation of $I_{Cl_{IR}}$ suggests that it may have a regulatory function. The amplitude of $I_{Cl_{IR}}$ is altered by relatively small

changes in the external pH. If $I_{Cl_{IR}}$ is permeable to bicarbonate ions then it may have a role in the regulation of intracellular pH, which can change as a result of changes in the external pH. Also, the sensitivity of $I_{Cl_{IR}}$ to hypoosmotic conditions could indicate a function in volume regulation. An increase in chloride efflux is known to be an important part of regulatory volume decrease and hypoosmotic conditions have been shown to increase the activation of $I_{Cl_{IR}}$, thereby increasing chloride efflux. A similar role has been suggested for ClC-2, the channel thought to underlie $I_{Cl_{IR}}$ (Gründer *et al.*, 1992).

Hippocampal pyramidal neurons possess a hyperpolarisation activated chloride current that has characteristics very similar to those described for $I_{Cl_{IR}}$ (Staley, 1994). It has been proposed that the current maintains the relationship between the chloride equilibrium potential and the resting membrane potential and therefore determines the direction of chloride flux upon activation of $GABA_A$ receptors. These receptors normally mediate an influx of chloride which causes hyperpolarisation of the membrane potential and inhibition of neuronal firing. However, if the hyperpolarisation activated chloride current is blocked by the application of phorbol esters then activation of the $GABA_A$ receptors eventually leads to chloride accumulation. An increase in the internal chloride concentration causes a positive shift in the chloride equilibrium potential and this results in a paradoxical depolarisation upon further activation of the $GABA_A$ receptors.

The electrophysiological effects of GABA acting at $GABA_A$ receptors, on rat SCG neurons have been described in numerous reports (Adams and Brown, 1975; Smart and Constanti, 1990; Smart, 1992; Aguayo and Alarcón, 1993) and evidence indicates that GABA may be a neurotransmitter within the SCG. GABA immunoreactivity has been localised to fibres entering the SCG from the preganglionic nerve trunk (Dobó *et al.*, 1989) and fibres that are positive for GABA have been shown to form basket like structures around and presumably

innervate some of the principal neurons of the SCG (Párducz *et al.*, 1992). Small immunoreactive neurons are also located within the ganglia itself (Wolff *et al.*, 1986). In addition, ^{3}H-GABA can be released from SCG neurons by potassium induced depolarisation and taken up into neurons and glia by low and high affinity uptake systems (Burgos *et al.*, 1992).

Therefore, a role in the regulation of the internal chloride concentration and consequently the chloride flux caused by activation of $GABA_A$ receptors is conceivable for $I_{Cl_{IR}}$. The application of GABA has been reported to cause both depolarisation and hyperpolarisation of the membrane potential of SCG neurons (Adams and Brown, 1975). In addition Eugène (1987) has shown that GABA can mediate fast depolarising postsynaptic potentials in rat SCG neurons. The precise effect was dependent on whether the resting membrane potential was positive or negative to the chloride equilibrium potential. $I_{Cl_{IR}}$ was present in all neurons studied in the experiments presented here but its amplitude was highly variable. Perhaps the magnitude of $I_{Cl_{IR}}$ determines the internal chloride concentration and hence the response of SCG neurons to GABA.

Appendix 1.

Liquid Junction Potentials.

Liquid junction potentials develop at the interface between solutions which have different compositions and are due to disparities in ion mobility. In patch clamp measurements liquid junction potentials can be particularly problematic since the concentrations of ions in pipette solutions are relative low and they frequently have very different mobilities. During patch recording, errors due to junction potentials may erroneously be assumed to be compensated for when the normal zeroing procedures are performed. During zeroing of the amplifier before seal formation, the junction potential is balanced by an equal and opposite potential within the circuitry. Once the pipette is sealed against the membrane the junction potential is no longer present as there is now no interface between the pipette solution and the bath solution. The potential used to balance it, is still, however, present within the circuitry. A correction is therefore necessary to accurately determine the potential being applied to the membrane. The junction potential correction, for the whole cell recording configuration is given by the following equation,

Equation 1.

$$V_m = V_p - L_j$$

(Where Vm is the actual membrane potential, Vp is the pipette potential and Lj is the liquid junction potential.)

When the cell membrane is ruptured for whole cell recording, there is a second junction potential generated between the pipette solution and the cell cytoplasm but this does not cause the same problems since the cell contents

become dialysed by the pipette solution so that the second potential tends towards zero with time.

As previously mentioned the effects of changes in solution were generally observed after 50 to 150s. This period of time was not sufficient for the solution distal to the cell, that is close to the bath ground, to have been completely exchanged. This incomplete exchange meant that a liquid junction potential was generated at the interface between the first and second external solutions. A correction for this junction potential was therefore required and is given by the following equation,

Equation 2.

$$V_m = V_p - L_{j1} - L_{j2}$$

(where V_m is the actual membrane potential, V_p is the pipette potential, L_{j1} is the liquid junction potential between the pipette solution and external solution and L_{j2} is the liquid junction potential between the first and second external solutions.)

Determination of liquid junction potentials.

Liquid junction potentials can be measured experimentally or they can be calculated. Once the magnitude and polarity of the junction potential have been determined it can then be compensated for at the time of the experiment or at some point during analysis.

The method used to measure the liquid junction potentials experimentally has been described by Neher (1992). To measure junction potentials accurately there are certain conditions which have to be fulfilled. The first is the requirement for a salt bridge that provides an abrupt boundary between 3M KCl and the test solution. The salt bridge which is usually manufactured from pipette glass filled

with KCl-agar has a chlorided silver wire inside it and is used to ground the bath. This must be the only ground connection. The second condition is that there is no drift in the pipette potential. This in ensured by rechloriding the silver wire within the pipette holder. The third condition is that there is a small but steady outflow of solution from both the recording pipette and the salt bridge. This ensures that there are no secondary junction potentials generated at the interfaces between the pipettes and the bath solution. Once all of these conditions have been satisfied a patch pipette filled with the test solution is mounted onto the headstage of the patch clamp setup. The bath is then filled with the same solution as that present in the pipette. The amplifier is switched to current clamp mode and the voltage output is zeroed. After this the bath solution is exchanged for the reference solution and the voltage output once stabilised is noted. The value obtained can then be used for correction of the applied membrane potential.

While the magnitude of the junction potential can be measured by the above means, the requirement for two electrodes and the necessity of fulfilling all the conditions often mean that it is simpler to calculate the junction potential using the generalised Henderson equation (equation 3). To obtain a very accurate estimate of junction potentials using the generalised Henderson equation it is necessary to use ion activity values. However, if ion concentrations are used instead there is, in most cases, little difference between the values obtained (Barry and Lynch, 1991).

The liquid junction potentials generated between the solutions used in the experiments described here, were calculated where possible using ion concentrations and the generalised Henderson equation (see table 1). The exception to this was the cyclamate substituted external. There is no published value for the mobility of cyclamate and therefore the junction potential could not be calculated.

Equation 3.

$$L_j = \left(RT/F\right) S_F \ln\left\{\frac{\sum_{i=1}^{N} z_i^2 u_i a_i^p}{\sum_{i=1}^{N} z_i^2 u_i a_i^s}\right\} \quad \text{where,} \quad S_F = \frac{\sum_{i=1}^{N}\left[\left(z_i u_i\right)\left(a_i^s - a_i^p\right)\right]}{\sum_{i=1}^{N}\left[\left(z_i^2 u_i\right)\left(a_i^s - a_i^p\right)\right]}$$

and where u, a and z are the mobility, activity and valency of each ion respectively. Lj (liquid junction potential), p (pipette), s (external solution), i (ion). R, T and F have their usual meanings.

Solution 1	Solution 2	Solution 1 vs CsCl pipette ($-Lj_1$)	Solution 1 vs solution 2 (Lj_2)	Total junction potential ($-Lj_1-Lj_2$)
External 2	-	-4.6	-	-4.6
External 3	-	-4.7	-	-4.7
External 2	NMDG	-4.6	5.3	-9.9
External 2	25mM K^+	-4.6	-0.8	-3.8
External 3	NaBr	-4.7	0.3	-5.0
External 3	NaI	-4.7	0.1	-4.8

Table 1. Liquid junction potentials calculated using the generalised Henderson equation. The liquid junction potentials generated between the solutions indicated in the left hand column are shown. Where a change in external solution occurred the liquid junction potential between the first external solution and the pipette solution ($-L_{j1}$) and the liquid junction potential between the two external solutions (L_{j2}) is shown. The sum of the two ($-Lj_1-Lj_2$) which can be put into equation 2 to calculate the necessary potential correction is given in the right hand column.

REFERENCES.

Ackerman M.J., Krapivinsky G.B., Gordon E., Krapivinsky L. and Clapham D.C. (1994). Characterisation of a native swelling-induced chloride current, IClswell, and its regulatory protein, pI_{Cln}, in *Xenopus* oocytes. J. Jap. Physiol. **44**: s17-s24.

Ackerman M.J., Wickman K.D. and Clapham D.E. (1994). Hypotonicity activates a native chloride current in *Xenopus* oocytes. J. Gen. Physiol. **103**: 153-179.

Adachi S., Uchida S., Ito H., Hata M., Hiroe M., Marumo F. and Sasaki S. (1994). Two isoforms of a chloride channel predominantly expressed in thick ascending limb of Henle's loop and collecting ducts of rat kidney. J. Biol. Chem. **269**: 17677-17683.

Adams D.J. and Harper A.A. (1995). Electrophysiological properties of autonomic ganglion neurons. Chapter 5. p 153-212 in The autonomic nervous system. Vol. 6 Autonomic ganglia. Ed. E.M. McLachlan.

Adams P.R. and Brown D.A. (1975). Actions of gamma-aminobutyric acid on sympathetic ganglion cells. J. Physiol. **250**: 85-120.

Aguayo L.G. and Alarcón J.M. (1993). Modulation of the developing rat sympathetic GABA receptor by Zn, benzodiazepines, barbituates and ethanol. J. Pharm. and Exp. Ther. **267**: 1414-1422.

Anderson M. P., Sheppard D.N., Berger H.A. and Welsh M.J. (1992). Chloride channels in the apical membrane of normal and cystic fibrosis airway and intestinal epithelia. Am. J. Physiol. **263**: L1-L14.

Anderson M.P., Berger H.A., Rich D.P., Gregory R.J., Smith A.E. and Welsh M.J. (1991). Nucleoside triphosphates are required to open the CFTR chloride channel. Cell **67**: 775-784.

Araque A. and Buño W. (1994). Novel hyperpolarisation-activated K^+ current mediates anomalous rectification in crayfish muscle. J. Neurosci. **14**: 399-408.

Arreola J., Melvin J.E. and Begenisich T. (1995). Volume-activated chloride channels in rat parotid acinar cells. J. Physiol. **484**: 677-687.

Arreola J., Park K., Melvin J.E. and Begenisich T. (1996). Three distinct chloride channels control anion movements in rat parotid acinar cells. J. Physiol. **490**: 351-362.

Assaf S.Y. and Chung S-H. (1984). Release of endogenous Zn^{2+} from brain tissue during activity. Nature **308**: 734-738.

Bader C.R., Bertrand D. and Schwartz E.A. (1982). Voltage-activated and calcium-activated currents studied in solitary rod inner segments from the salamander retina. J. Physiol. **331**: 253-284.

Bakhramov A., Fenech C. and Bolton T.B. (1995). Chloride current activated by hypotonicity in cultured human astrocytoma cells. Exp. Physiol. **80**: 373-389.

Ballanyi K. and Grafe P. (1985). An intracellular analysis of γ-aminobutyric acid-associated ion movements in rat sympathetic neurons. J. Physiol. **365**: 41-58.

Barish M.E. (1983). A transient calcium-dependant chloride current in the immature *Xenopus* oocyte. J. Physiol. **342**: 309-325.

Baron A., Pacaud P., Loirand G., Mironneau C. and Mironneau J.(1991). Pharmacological block of Ca^{2+}-activated Cl^- current in rat vascular smooth muscle cells in short-term primary culture. Pflügers Arch. **419**: 553-558.

Barry P.H. and Lynch J.W. (1991). Liquid junction potentials and small cell effects in patch-clamp analysis. J. Mem. Biol. **121**: 101-117.

Bauer C.K., Steinmeyer K., Schwarz J.R. and Jentsch T.J. (1991). Completely functional double-barrelled chloride channel expressed from single *Torpedo* cDNA. Proc. Natl. Acad. Sci. USA **88**: 11052-11056.

Beech D.J., Bernheim L., Mathie A. and Hille B. (1991). Intracellular Ca^{2+} buffers disrupt muscarinic suppression of Ca^{2+} current and M current in rat sympathetic neurons. Proc. Natl. Acad. Sci. USA **88**: 652-656.

Belluzzi O., Sacchi O. and Wanke E. (1985). Identification of delayed potassium and calcium currents in the rat sympathetic neurone under voltage clamp. J. Physiol. **358**: 109-129.

Belluzzi O., Sacchi O. and Wanke E. (1985). A fast transient outward current in the rat sympathetic neurone studied under voltage-clamp conditions. J. Physiol. **358**: 91-108.

Betz H. (1990). Ligand-gated ion channels in the brain: the amino acid receptor superfamily. Neuron **5**: 383-392.

Betz H. (1991). Glycine receptors: Heterogeneous and widespread in the mammalian brain. TINS **14**: 458-461.

Betz H., Langosch D., Rundstrom N., Bormann J., Kuryatov A., Kushse J., Schmeiden V., Matzenbach B. and Kirsch J. (1993). Structure and biology of inhibitory glycine receptors. Annals N.Y. Acad. Sci. USA **707**: 109-115.

Blatt M.R. (1992). K^+ channels of stomatal guard cells. Characteristics of the inward rectifier and its control by pH. J. Gen. Physiol. **99**: 615-644.

Bochet P., Audinat E., Lambolez B., Crepel F., Rossier J., Lino M., Tsuzuki K. and Ozawa S. (1994). Subunit composition at the single-cell level explains functional properties of a glutamate-gated channel. Neuron **12**: 383-388.

Bormann J. (1988). Electrophysiology of $GABA_A$ and $GABA_B$ receptor subtypes. TINS **11**: 112-116.

Bormann J., Hamill O.P. and Sakmann B. (1987). Mechanism of anion permeation through channels gated by glycine and gamma-aminobutyric acid in mouse cultured spinal neurons. J. Physiol. **385**: 243-286.

Brandt S. and Jentsch T.J. (1995). ClC-6 and ClC-7 are two novel broadly expressed members of the CLC chloride channel family. FEBS Lett. **377**: 15-20.

Bretag A.H. (1987). Muscle chloride channels. Physiol. Rev. **67**: 618-724.

Brown D.A. and Adams P.R. (1980). Muscarinic suppression of a novel voltage-sensitive K^+ current in a vertebrate neurone. Nature **283**: 673-676.

Brown H. and DiFrancesco D. (1980). Voltage-clamp investigation of membrane currents underlying pace-maker activity in rabbit sino-atrial node. J. Physiol. **308**: 331-351.

Bryant S.H. and Conte-Camerino D. (1991). Chloride channel regulation in the skeletal muscle of normal and myotonic goats. Pflügers Arch. **417**: 605-610.

Bryant S.H. and Morales-Aguilera A. (1971). Chloride conductance in normal and myotonic muscle fibres and the action of monocarboxylic aromatic acids. J. Physiol. **219**: 367-383.

Burgos G.G., Rosenstein R.E. and Cardinali D.P. (1992). Neurochemical evidence for a neuronal GABAergic system in the rat sympathetic superior cervical ganglion. J. Neural Trans. **89**: 27-40.

Burt D.R. (1994). $GABA_A$ receptor-activated chloride channels. Current topics in membrane transport **42**: 215-263.

Burt D.R. and Kamatchi G.L. (1991). $GABA_A$ receptor subtypes: from pharmacology to molecular biology. FASEB J. **5**: 2916-2923.

Caulfield M.P., Jones S., Vallis Y., Buckley N.J., Kim G-D., Milligan G. and Brown D.A. (1994). Muscarinic M-current inhibition via $G_{\alpha q/11}$ and α-adrenoceptor inhibition of Ca^{2+} current via $G_{\alpha o}$ in rat sympathetic neurones. J. Physiol. **477**: 415-422.

Cheng S.H., Rich D.P., Marshall J., Gregory R.J., Welsh M.J. and Smith A.E. (1991). Phosphorylation of the R domain by cAMP-dependent protein kinase regulates the CFTR chloride channel. Cell **66**: 1027-1036.

Chesnoy-Marchais D. (1982). A Cl^- conductance activated by hyperpolarisation in *Aplysia* neurones. Nature **299**: 359-360.

Chesnoy-Marchais D. (1983). Characterisation of a chloride conductances activated by hyperpolarisation in *Aplysia* Neurones. J. Physiol. **342**: 277-308.

Chesnoy-Marchais D. and Evans (1986). Chloride channels activated by hyperpolarisation in *Aplysia* neurones. Pflügers Arch. **407**: 694-696.

Chesnoy-Marchais D. and Fritsch J. (1994). Activation by hyperpolarisation and atypical osmosensitivity of a Cl^- current in rat osteoblastic cells. J. Mem. Biol. **140**: 173-188.

Constanti A. and Brown D.A. (1981). M-currents in voltage-clamped mammalian sympathetic neurones. Neurosci. Lett. **24**: 289-294.

Constanti A. and Galvan M. (1983). Fast inward-rectifying current accounts for anomalous rectification in olfactory cortex neurons. J. Physiol. **335**: 153-178.

Conti Camerino D., De Luca A., Mambrini M. and Vrbova G. (1989). Membrane ionic conductances in normal and denervated skeletal muscle of the rat during development. Pflügers Arch. **413**: 568-570.

Crepel F. and Penit-Soria J. (1986). Inward rectification and low threshold calcium conductance in rat cerebellar purkinje cells. An *in vitro* study. J. Physiol. **372**: 1-23.

Cull-Candy S.G. and Mathie A. (1986). Ion channels activated by acetylcholine and γ-aminobutyric acid in freshly dissociated sympathetic neurones of the rat. Neurosci. Lett. **66**: 275-280.

Currie K.P.M., Wootton J.F. and Scott R.H. (1995). Activation of Ca^{2+}-dependant Cl^- currents in cultured rat sensory neurones by flash photolysis of DM-nitrophen. J. Physiol. **482**: 291-307.

Delorey T.M. and Olsen R.W. (1992). Gamma-aminobutyric acid A receptor structure and function. J. Biol. Chem. **267**: 16747-16750.

DiFrancesco D. (1982). Block and activation of the pace-maker channel in calf purkinje fibres: effects of potassium, caesium and rubidium. J. Physiol. **329**: 485-507.

Dinudom A., Young J.A. and Cook D.I. (1993). Na^+ and Cl^- conductances are controlled by cytosolic Cl^- concentration in the intralobular duct cells of mouse mandibular glands. J. Mem. Biol. **135**: 289-295.

Dobó E., Kása P., Wenthold R.J. and Wolff J.R. (1989). Evidence for GABAergic fibers entering the superior cervical ganglion of rat from the preganglionic nerve trunk. Histochem. **92**: 133-136.

Drew C.A., Johnston G.A.R. and Weatherby R.P. (1984). Bicuculline-insensitive GABA receptors: studies on the binding of (-)-baclofen to rat cerebellar membranes. Neurosci. Lett. **52**: 317-321.

Duszyk M., Liu D., French A.S. and Man S.F.P. (1995). Evidence that pH-titratable groups control the activity of a large epithelial chloride channel. Biochem. and Biophys. Res. Comm. **215**: 355-360.

Dyson N. J. (1991). Essential molecular biology. A practical approach II. Ed. Brown T.A.

Eberwine J., Yeh H., Miyashiro K., Cao Y., Nair S., Finnell R., Zettel M. and Coleman P. (1992). Analysis of gene expression in single live neurons. Proc. Natl. Acad. Sci. USA **89**: 3010-3014.

Eugéne D. (1987). Fast non-Cholinergic depolarising postsynaptic potentials in neurons of rat superior cervical ganglia. Neurosci. Lett. **78**: 51-56.

Evans M.G. and Marty A. (1986). Calcium-dependent chloride currents in isolated cells from rat lacrimal glands. J. Physiol. **378**: 437-460.

Falke J.J. and Chan S.I. (1986). Molecular mechanisms of band 3 inhibitors. 2. Channel blockers. Biochem. **25**: 7895-7898.

Ferroni S., Marchini C., Schubert P. and Rapisarda C. (1995). Two distinct inwardly rectifying conductances are expressed in long term bibutyryl-cyclic-AMP treated rat cultured cortical astrocytes. FEBS Lett. **367**: 319-325.

Fisher S.E., Black G.C.M., Lloyd S.E., Hatchwell E., Wrong O., Thakker R.V. and Craig L.W. (1994). Isolation and partial characterisation of a chloride channel gene which is expressed in kidney and is a candidate for Dents disease (an x-linked hereditary nephrolithiasis). Hum. Mol. Genet. **3**: 2053-2059.

Frederickson C.J. (1989). Neurobiology of zinc and zinc-containing neurons. Int. Rev. Neurobiology **31**: 145-238.

Fritsch J. and Edelman A. (1996). Modulation of the hyperpolarisation-activated Cl^- current in human intestinal T_{84} epithelial cells by phosphorylation. J. Physiol. **490**: 115-128.

Fujita N., Mori H., Yura T. and Ishihama A. (1994). Systematic sequencing of the Escherichia coli genome: analysis of the 2.4-4.1 min (110,917-193,643bp) region. Nuc. Acids Res. **22**: 1637-1639.

Fuller C.M. and Benos D.J. (1992). CFTR! Am. J. Physiol. **263**: c267-c286.

Galzi J-L., Devillers-Thiéry A., Hussy N., Bertrand S., Changeux J-P and Bertrand D. (1992). Mutations in the channel domain of a neuronal nicotinic receptor convert ion selectivity from cationic to anionic. Nature **359**: 500-505.

Gay L.A. and Stanfield P.R. (1977). Cs^+ causes a voltage-dependent blockade of inward K currents in resting skeletal muscle fibres. Nature **267**: 169-170.

Gill D.R., Hyde S.C., Higgins C.F., Valverde M.A., Mintenig G.M. and Sepulveda F.V. (1992). Separation of drug transport and chloride channel functions of the human multidrug resistance P-glycoprotein. Cell **71**: 23-32.

Gilly W.M.F. and Armstrong C.M. (1982). Slowing of sodium channel opening kinetics in squid axon by extracellular zinc. J. Gen. Physiol. **79**: 935-964.

Gögelein H. (1988). Chloride channels in epithelia. Biochem. et Biophys. Acta **947**: 521-547.

Greene J.R., Brown N.H., DiDomenico B.J., Kaplan J. and Eide D.J. (1993). The GEF-1 gene of Saccharomyces cerevisiae encodes an integral membrane protein; mutations in which have effects on respiration and iron-limited growth. Mol. Gen. Genet. **241**: 542-553.

Gründer S., Thiemann A., Pusch M. and Jentsch T.J. (1992). Regions involved in the opening of ClC-2 chloride channel by voltage and cell volume. Nature **360**: 759-762.

Gschwentner M., Nagl U.O. Woll E., Schmarda A., Ritter M. and Paulmichl M. (1995). Antisense oligonucleotides suppress cell-volume-induced activation of chloride channels. Pflügers Arch. **430**: 464-470.

Hagiwara S., Miyazaki S., Moody W. and Patlak J. (1978). Blocking effects of barium and hydrogen ions on the potassium current during anomalous rectification in the starfish egg. J. Physiol. **279**: 167-185.

Hahin R. and Campbell D.T. (1983). Simple shifts in the voltage dependence of sodium channel gating caused by divalent cations. J. Gen. Physiol. **82**: 785-805.

Hall S.K., Zhang J. and Lieberman M. (1995). Cyclic AMP prevents activation of a swelling-induced chloride-sensitive conductance in chick heart cells. J. Physiol. **488**: 359-369.

Halliwell J.V. and Adams P.R. (1982). Voltage-clamp analysis of muscarinic excitation in hippocampal neurons. Brain Res. **250**: 71-92.

Hamill O.P., Marty A., Sakmann B. and Sigworth F.J. (1981). Improved Patch-clamp techniques for high resolution current recording from cells and cell-free membrane patches. Pflügers Arch. **391**: 85-100.

Hanke W. and Miller C. (1983). Single chloride channels from *Torpedo* electroplax. J. Gen. Physiol. **82**: 25-45.

Hardy S.P., Goodfellow H.R., Valverde M.A., Gill D.R., Sepulveda F.V. and Higgins C.F. (1995). Protein kinase C-mediated phosphorylation of the human multidrug resistance P-glycoprotein regulates cell volume-activated chloride channels. EMBO J. **14**: 68-75.

Herbert S.C. (1996). Crystal-clear chloride channels. Nature **379**: 398-399.

Higgins C.F. (1995). Volume-activated chloride currents associated with the multidrug resistance P-glycoprotein. J. Physiol. **482P**: 31S-36S.

Hille B. (1992). Ionic channels in excitable membranes. 2nd edition. Sinauer Associates inc. Sunderland Massachusetts.

Hille B., Beech D.J., Bernheim L., Mathie A., Shapiro M.S. and Wollmuth L.P. (1995). Multiple G-protein coupled pathways inhibit N-type Ca channels of neurons. Life Sci. **56**: 989-992.

Hille B., Woodhull A.M. and Shapiro B.I. (1975). Negative surface charge near sodium channels of nerve: divalent cations, monovalent ions and pH. Phil. Trans. R. Soc. Lond. B. **270**: 301-318.

Hodgkin A.L. and Horowicz P. (1959). The influence of potassium and chloride ions on the membrane potential of single muscle fibres. J. Physiol. **148**: 127-160.

Hogg R.C., Wang Q. and Large W.A. (1993). Time course of spontaneous calcium-activated chloride currents in smooth muscle cells from the rabbit portal vein. J. Physiol. **464**: 15-31.

Hogg R.C., Wang Q. and Large W.A. (1994). Effects of Cl channel blockers on Ca-activated chloride and potassium currents in smooth muscle cells from rabbit portal vein. Br. J. Pharmacol. **111**: 1333-1341.

Horn R. and Marty A. (1988). Muscarinic activation of ionic currents measured by a new recording method. J. Gen. Physiol. **92**: 145-159.

Howe J.R. and Richie J.M. (1991). On the active form of 4-aminopyridine: block of K^+ currents in rabbit Schwann cells. J. Physiol. **433**: 183-206.

Huang R-C., Peng Y-W. and Yau K-W. (1993). Zinc modulation of a transient potassium current and histochemical localisation of the metal in neurons of the suprachiasmatic nucleus. Proc. Natl. Acad. Sci. USA **90**: 11806-11810.

Hyde S.C., Emsley P., Hartshorn M.J., Mimmack M.M., Gileadi U., Pearce S.R., Gallager M.P., Gill D.R., Hubbard R.E. and Higgins C.F. (1990). Structural model of ATP-binding proteins associated with cystic fibrosis, multidrug resistance and bacterial transport. Nature **346**: 362-365.

Ide T., Hidaka J. and Kasai M. (1995). An anion channel from transverse tubular membranes incorporated into planar bilayers. Biochem. et Biophys. Acta **1237**: 115-120.

Ikeda S.R. (1996). Voltage-dependent modulation of N-type calcium channels by G-protein βγ subunits. Nature **380**: 255-258.

Ishikawa T. and Cook D.I. (1993). A Ca^{2+} activated Cl^- current in sheep parotid secretary cells. J. Mem. Biol. **135**: 261-271.

Janssen L.J. and Sims S.M. (1994). Spontaneous transient inward currents and rhythmicity in canine and ginea-pig tracheal smooth muscle cells. Pflügers Arch. **427**: 473-480.

Janssen L.J. and Sims S.M. (1995). $Ca^{(2+)}$-dependent Cl^- current in canine tracheal smooth muscle cells. Am. J. Physiol. **269**: C163-C169.

Jentsch T. (1996). Chloride channels: a molecular perspective. Curr. Opin. Neurobiol. **6**: 303-310.

Jentsch T.J. (1994). Molecular biology of voltage-gated chloride channels. Current topics in membrane transport **42**: 35-57.

Jentsch T.J. (1994). Structure and function of ClC chloride channel. J. Jap. Physiol. **44**: S1-S2.

Jentsch T.J., Gunther W., Pusch M. and Schwappach B. (1995). Properties of voltage-gated chloride channels of the CIC gene family. J. Physiol. **482P**: 19S-25S.

Jentsch T.J., Steinmeyer K. and Schwarz G. (1990). Primary structure of *Torpedo* marmorata chloride channel isolated by expression cloning in *Xenopus* oocytes. Nature **348**: 510-514.

Jonas P., Racca C., Sakmann B., Seeburg P.H. and Monyer H. (1994). Differences in Ca^{2+} permeability of AMPA type glutamate receptor channels in neocortical neurons caused by differential GluR-B subunit expression. Neuron **12**: 1281-1289.

Katz B. (1949). Les constantes electriques de la membrane du muscle. Archs Sci. Physiol. **3**: 285-299.

Kawasaki M., Susuki M., Uchida S., Sasaki S. and Marumo F. (1995). Stable and functional expression of the ClC-3 chloride channel in somatic cell lines. Neuron **14**: 1285-1291.

Kawasaki M., Uchida S., Monkawa T., Miyawaki A., Mikoshiba K., Marumo F. and Sasaki S. (1994). Cloning and expression of a protein kinase C-regulated chloride channel abundantly expressed in rat brain neuronal cells. Neuron **12**: 597-604.

Kelly M.E., Dixon S.J. and Sims S.M. (1994). Outwardly rectifying chloride current in rabbit osteoclasts is activated by hyposmotic stimulation. J. Physiol. **475**: 377-389.

Kieferle S., Fong P., Bens M., Vandewalle A. and Jentsch T.J. (1994). Two highly homologous members of the CIC chloride channel family in both rat and human kidney. Proc. Natl. Acad. Sci. USA **91**: 6943-6947.

Kim D., Sladek C.D., Aguado-Valasco C. and Mathiasen J.R. (1995). Arachidonic acid activation of a new family of K^+ channels in cultured rat neuronal cells. J. Physiol. **484**: 643-660.

Koch M.C., Ricker K., Otto M., Wolf F., Zoll B., Lorenz C., Steinmeyer K. and Jentsch T.J. (1993). Evidence for genetic homogeneity in autosomal recessive generalised myotonia (Becker). J. Med. Genet. **30**: 914-917.

Komwatana P., Dinudom A., Young J.A. and Cook D.I. (1994). Characterisation of the Cl^- conductance in the granular duct cells of the mouse mandibular glands. Pflügers Arch. **428**: 641-647.

Korn S.J., Bolden A. and Horn R. (1991). Control of action potential and Ca^{2+} influx by the Ca^{2+}-dependent chloride current in mouse pituitary cells. J. Physiol. **439**: 423-437.

Kowdley G.C., Ackerman S.J., John J.E., Jones L.R. and Moorman J.R. (1994). Hyperpolarisation-activated chloride currents in *Xenopus* Oocytes. J. Gen. Physiol. **103**: 217-230.

Krapivinsky G.B., Ackerman M.J., Gordan E.A., Krapivinsky L.D. and Clapham D.C. (1994). Molecular characterisation of ICln protein: identification as a swelling-induced chloride conductance regulator. Cell **76**: 439-448.

Kubo Y., Baldwin T.J., Jan Y. N. and Jan L.Y. (1993). Primary structure and functional expression of a mouse inward rectifier potassium channel. Nature **362**: 127-133.

Lambolez B., Audinat E., Bochet P., Crepel F. and Rossier J. (1992). AMPA receptor subunits expressed by single purkinje cells. Neuron **9**: 247-258.

Lindau M. and Fernadez J.M. (1986). IgE-mediated degranulation of mast cells does not require opening of ion channels. Nature **319**: 150-153.

Lloyd S.E., Pearce S.H.S., Fisher S.E., Steinmeyer K., Schwappach B., Scheinman S.J., Harding B., Bolino A., Devoto M., Goodyer P., Rigden S.P., Wrong O., Jentsch T.J., Craig I.W. and Thakker R.V. (1996). A common molecular basis for three inherited kidney stone diseases. Nature **379**: 445-49.

Lotshaw D.P. and Levitan I.B. (1987). Serotonin and forskolin modulation of a chloride conductance in cultured identified *Aplysia* neurons. J. Neurophysiol. **58**: 922-939.

Madison D.V., Malenka R.C. and Nicoll R.A. (1986). Phorbol esters block a voltage-sensitive chloride current in hippocampal pyramidal cells. Nature **321**: 695-697.

Makhina E.N., Kelly A.J., Lopatin A.N., Mercer R.W. and Nichols C.G. (1994). Cloning and expression of a novel human brain inward rectifier potassium channel. J. Biol. Chem. **32**: 20468-20474.

Marsh S.J., Trouslard J., Leaney J.L. and Brown D.A. (1995). Synergistic regulation of a neuronal chloride current by intracellular calcium and muscarinic receptor activation: a role for protein kinase C. Neuron **15**:729-737.

Matthews G., Neher E. and Penner R. (1989). Chloride conductance activated by external agonists and internal messengers in rat peritoneal mast cells. J. Physiol. **418**: 131-144.

Mayer M.L. and Westbrook G.L. (1983). A voltage-clamp analysis of inward (anomalous) rectification in mouse spinal sensory ganglion neurones. J. Physiol. **340**: 19-45.

Mehrke G., Brinkmeier H. and Jockusch H. (1988). The myotonic mouse mutant adr: electrophysiology of the muscle fiber. Muscle Nerve **11**: 440-446.

Miledi R. (1982). A calcium-dependent transient outward current in *Xenopus* laevis oocytes. Proc. Royal Soc. B **315**: 491-497.

Miller C. (1982). Open-state substructure of single chloride channels from *Torpedo* electroplax. Phil. Trans. R. Soc. B **299**: 401-411.

Miller C. and White M. (1984). Dimeric structure of single chloride channels from *Torpedo* electroplax. Proc. Natl. Acad. Sci. USA **81**: 2772-2775.

Miyazaki S., Takahashi K., Tsuda K. and Yoshi M. (1974). Analysis of non-linearity observed in the current-voltage relation of the tunicate embryo. J. Physiol. **238**: 55-77.

Moorman J.R., Ackerman S.J., Kowdley G.C., Griffin M.P., Mounsey J.P., Chen Z., Cala S.E., O'brian J.J., Szabo G. and Jones L.R. (1995). Unitary anion currents through phospholemman channel molecules. Nature **377**: 737-40.

Moorman J.R., Palmer C.J., John J.E., Durieux M.E. and Jones L.R. (1992). Phospholemman expression induces a hyperpolarisation activated chloride current in *Xenopus* oocytes. J. Biol. Chem. **267**: 14551-14554.

Myers T.W. and Gelfand D.H. (1991). Reverse transcription and DNA amplification by a *Thermus therophilus* DNA polymerase. Biochem. **30**: 7661-7666.

Neher E. (1992). Correction for liquid junction potentials in patch clamp experiments. Methods in Enzymol. **207**: 123-131.

Nilius B., Sehrer J., Viana F., De Greef C., Raeymaekers L., Eggermont J., Droogmans G. (1994). Volume activated Cl^- currents in different mammalian non-excitable cell types. Pflügers Arch. **428**: 364-371.

Noulin J-F. and Joffre M. (1993). Characterisation and cyclic AMP dependence of a hyperpolarisation activated chloride conductance in leydig cells from mature rat testes. J. Mem. Biol. **133**: 1-15.

O' Neill G.P., Grygorczyk R., Adam M. and Ford-Hutchinson A.W. (1991). The nucleotide sequence of a voltage-gated chloride channel from the electric organ of *Torpedo* californica. Biochem. et Biophys. Acta **1129**: 131-134.

Oberleithner H., Ritter M., Lang F. and Guggino W. (1983). Antracene-9-carboxylic acid inhibits renal chloride reabsorption. Pflügers Arch. **398**: 172-174.

Olsen R.W. and Tobin A.J. (1990). Molecular biology of $GABA_A$ receptors. FASEB J. **4**: 1469-1480.

Pacaud P., Loirand G., Lavie J.L. and Mironneau J. (1989). Calcium-activated chloride current in rat vascular smooth muscle cells in short term primary culture. Pflügers Arch. **413**: 629-636.

Palade P.T. and Barchi R.L. (1977). Characteristics of the chloride conductance in muscle fibers of the rat diaphragm. J. Gen. Physiol. **69**: 325-342.

Palmer C.J., Scott B.T. and Jones L.R.(1991). Purification and complete sequence determination of the major plasma membrane substrate for cAMP- dependent protein kinase and protein kinase C in myocardium. J. Biol. Chem. **266**: 11126-11130.

Parducz A., Dobo E., Joo F. and Wolff J.R. (1992). Termination pattern and fine structural characteristics of GABA- and [Met]enkephalin-containing nerve fibers and synapses in the superior cervical ganglion of adult rat. Neurosci. **49**: 963-971.

Parker I. and Miledi R. (1988). A calcium-independent chloride current activated by hyperpolarisation in *Xenopus* oocytes. Proc. Royal Soc. B **233**: 191-199.

Passow H. (1986). Molecular aspects of band 3 protein-mediated anion transport across the red blood cell membrane. Rev. Physiol. Biochem. Pharmacol. **103**: 62-123.

Paulmichl M., Wickman K., Ackerman M., Peralta E. and Clapham D. (1992). New mammalian chloride channel identified by expression cloning. Nature **356**: 238-241.

Peres A. and Bernardini G. (1983). A hyperpolarisation-activated chloride current in *Xenopus* laevis oocytes under voltage-clamp. Pflügers Arch. **399**: 157-159.

Perier F., Radeke C.M. and Vandenberg C.A. (1994). Primary structure and characterisation of a small-conductance inwardly rectifying potassium channel from human hippocampus. Proc. Natl. Acad. Sci. USA **91**: 6240-6244.

Pfieffer F., Graham D. and Betz H. (1982). Purification by affinity chromatography of the glycine receptor of rat spinal cord. J. Biol. Chem. **257**: 818-823.

Plummer M.R., Logothetis D.E. and Hess P. (1989). Elementary properties and pharmacological sensitivities of calcium channels in mammalian peripheral neurons. Neuron **2**: 1453-1463.

Powell L.M., Wallis S.C., Pease R.J., Edwards Y.H., Knott T.J. and Scott J. (1987). A novel form of tissue-specific RNA processing produces apolipoprotein-B48 in intestine. Cell **50**: 831-840.

Pritchett D.B., Sontheimer H., Shivers B.D., Ymer S., Kettenmann H., Schofield P.R. and Seeburg P.H. (1989). Importance of a novel $GABA_A$ receptor subunit for benzodiazepine pharmacology. Nature **338**: 582-585.

Pusch M. and Jentsch T.J. (1994). Molecular physiology of voltage-gated chloride channels. Physiol. Rev. **74**: 813-827.

Pusch M. and Neher E. (1988). Rates of diffusional exchange between small cells and a measuring patch pipette. Pflügers Arch. **411**: 204-211.

Pusch M., Ludewig U., Rehfeldt and Jentsch T.J. (1995). Gating of the voltage-dependent chloride channel ClC-0 by the permeant anion. Nature **373**: 527-531.

Pusch M., Steinmeyer K. and Jentsch T.J. (1994). Low single channel conductance of the major skeletal muscle chloride channel, CIC-1. Biophysical J. **66**: 149-152.

Rae J., Cooper K., Gates P. and Watsky M. (1991). Low access resistance perforated patch recordings using amphotericin B. J. Neurosci. Meth. **37**: 15-26.

Rappolee D.A., Wang A., Mark D. and Werb Z. (1989). Novel method for studying mRNA phenotypes in single or small numbers of cells. J. Cell Biochem. **39**: 1-11.

Regan L.J., Sah D.W.Y. and Bean B.P. (1991). Ca^{2+} channels in rat central and peripheral neurons: high-threshold current resistant to dihydropyridine blockers and ω-conotoxin. Neuron **6**: 269-280.

Richard E.A. and Miller C. (1990). Steady state coupling of the ion channel conformations to a transmembrane ion gradient. Science **247**: 1208-1210.

Riordan J.R., Rommens J.M., Kerem B., Alon N., Rozmahel R., Grzelczak Z., Zielenski J., Lok S., Plasvic N., Chou J.L., Drumm M.C. (1989). Identification of the cystic fibrosis gene: cloning and characterisation of complementary DNA. Science **245**: 1066-1073.

Saiki R.K. Scharf S., Faloona F., Mullis K., Horn G., Erlich H. and Arnheim N. (1985). Enzymatic amplification of beta-globin genomic sequences and restriction site analysis for diagnosis of sickle cell anemia. Science **230**: 1350-1354.

Sanchez-Vives M.V. and Gallego R. (1994). Calcium-dependant chloride current induced by axotomy in rat sympathetic neurons. J. Physiol. **475**: 391-400.

Sansom S.C., Bao-Quoc LA and Carosi S.L. (1990). Double-barrelled chloride channels of collecting duct basolateral membrane. Am. J. Physiol. **259**: F46-F52.

Sarkadi B. and Parker J.C. (1991). Activation of ion transport pathways by changes in cell volume. Biochem. et Biophys. Acta. **1071**: 407-427.

Schofield P.R., Darlison M.G., Fujita N., Burt D.R., Stephenson F.A., Rodriguez H., Rhee L., Ramachandran J., Reale V., Glencourse T.A. (1987). Sequence and functional expression of the $GABA_A$ receptor shows a ligand-gated receptor superfamily. Nature **328**: 221-227.

Scott R.H., Sutton K.G., Griffin A., Stapleton S.R. and Currie K.P.M. (1995). Aspects of calcium-activated chloride currents: A neuronal perspective. Pharmacol. Thera. **66**: 535-565.

Selyanko A.A. (1984). Cd^{2+} suppresses a time-dependant Cl^- current in rat sympathetic neurone. J. Physiol. **350**: 49P.

Singh A.K., Afink G.B., Venglarik C.J., Wang R. and Bridges R.J. (1991). Colonic Cl channel blockade by three classes of compounds. Am. J. Physiol. **261**: C51-C63.

Smart T.G. (1992). A novel modulatory binding site for zinc on the $GABA_A$ receptor complex in cultured rat neurones. J. Physiol. **447**: 587-625.

Smart T.G. and Constanti A. (1990). Differential effect of zinc on the vertebrate $GABA_A$ receptor complex. Br. J. Pharmacol. **99**: 643-654.

Smith R.L., Clayton G.H., Wilcox C.L., Escudero K.W. and Staley K.J. (1995). Differential expression of an inwardly rectifying chloride conductance in rat brain neurons: A possible mechanism for cell -specific modulation of postsynaptic inhibition. J. Neurosci. **15**: 4057-4067.

Spain W.J., Schwindt P.C. and Crill W.E. (1987). Anomalous rectification in neurons from cat sensorimoter cortex *In Vitro*. J. Neurophysiol. **57**: 1555-1576.

Spalding B.C., Taber P., Swift J.G. and Horowicz P. (1990). Zinc inhibition of chloride efflux from skeletal muscle of *Rana* pipiens and its modification by external pH and chloride activity. J. Mem. Biol. **116**: 195-214.

Staley K. (1994). The role of the inwardly rectifying chloride conductance in postsynaptic inhibition. J. Neurophysiol. **72**: 273-284.

Staley K.J., Soldo B.L. and Proctor W.R. (1995). Ionic mechanisms of neuronal excitation by inhibitory $GABA_A$ receptors. Science **269**: 977-981.

Stansfeld C. and Mathie A. (1993). Recording membrane currents of peripheral neurones in short-term culture. pg. 3-28 in Electrophysiology: A practical approach. Ed. Wallis D.I. Oxford IRL Press .

Steinmeyer K., Klocke R., Ortland C., Gronemeier M., Jockusch H., Gründer S. and Jentsch T.J. (1991a). Inactivation of muscle chloride channel by transposon insertion in myotonic mice. Nature **354**: 304-308.

Steinmeyer K., Lorenz C., Pusch M., Koch M. C. and Jentsch T.J. (1994). Multimeric structure of CIC-1 chloride channel revealed by mutations in dominant myotonia congenita (Thompson). EMBO J. **13**: 737-743.

Steinmeyer K., Ortland C. and Jentsch T.J. (1991b). Primary structure and functional expression of a developmentally regulated skeletal muscle chloride channel. Nature **354**: 301-304.

Steinmeyer K., Schwappach B., Bens M. and Vandewalle A. (1995). Cloning and functional expression of rat ClC-5, a chloride channel related to kidney disease. J. Biol. Chem. **270**: 31172-31177.

Sucher N.J. and Deitcher D.L. (1995). PCR and patch clamp analysis of single neurons. Neuron **14**: 1095-1100.

Surmeier D.J., Eberwine J.H., Wilson C.J., Cao Y., Stefani A. and Kitai S.T. (1992). Dopamine receptor subtypes colocalise in rat striatalnigral neurons. Proc. Natl. Acad. Sci. USA **89**: 10178-10182.

Tabcharani J.A., Rommens J.M., Hou Y-X., Chang X-B., Tsul L-C., Riordan J.R. and Hanrahan J.W. (1993). Multi-ion pore behaviour in the CFTR chloride channel. Nature **366**: 79-82.

Thiemann A., Gründer S., Pusch M. and Jentsch T.J. (1992). A chloride channel widely expressed in epithelial and non-epithelial cells. Nature **356**: 57-60.

Tilmann M., Kunzelmann K., Frobe U., Cabantchik I., Lang H.J., Englert H.C. and Greger R. (1991). Different types of blockers of the intermediate-conductance outwardly rectifying chloride channel in epithelia. Pflügers Arch. **418**: 556-563.

Tominaga M., Tominaga T., Miwa A. and Okada Y. (1995). Volume-sensitive chloride channel activity does not depend on endogenous P-glycoprotein. J. Biol. Chem. **270**: 27887-27893.

Townsend C. and Rosenberg R.L. (1995). Characterisation of a chloride channel reconstituted from cardiac sarcoplasmic reticulum. J. Mem. Biol. **147**: 121-136.

Uchida S., Sasaki S., Furukawa T., Hiraoka M., Imai T., Hirata Y. and Maramo F. (1993). Molecular cloning of a chloride channel that is regulated by dehydration and expressed predominantly in Kidney medulla. J. Biol. Chem. **268**: 3821-3824.

Valverde M.A., Diaz M., Sepulveda F.V., Gill D.R., Hyde S.C. and Higgins C.F. (1992). Volume regulated chloride channels associated with the multidrug-resistance P-glycoprotein. Nature **355**: 830-833.

Van Gelder R.N., Von Zastrow M.E., Yool A., Dement W.C., Barchas J.D. and Eberwine J.H. (1990). Amplified RNA synthesised from limited quantities of heterogeneous cDNA. Proc. Natl. Acad. Sci. USA **87**: 1663-1667.

Van Slegtenhorst M.A., Bassi M.T., Borsani G., Wapenar M.C., Ferrero G.B., De Concilis L., Rugarli E.L. Grillo A., Franco B., Zog (1994). A gene from the Xp22.3 region shares homology with voltage-gated chloride channels. Hum. Mol. Genet. **3**: 547-552.

Voets T., Buyse G., Tytgat J., Droogmans G., Eggermont J. and Nilius B. (1996). The chloride current induced by expression of the protein pI_{cln} in *Xenopus* oocytes differs from the endogenous volume-sensitive chloride current. J. Physiol. **495**: 441-447.

Wang H.-S. and Mckinnon D. (1995). Potassium currents in rat prevertebral and paravertebral sympathetic neurones: control of firing properties. J. Physiol. **485**: 319-335.

Wang H-S. and McKinnon D. (1996). Modulation of inwardly rectifying currents in rat sympathetic neurons by muscarinic receptors. J. Physiol. **492**: 467-478.

Wangemann P., Wittner M., Di Stefano A., Englert H.C., Lang H.J., Schlatter E. and Greger R. (1986). Cl^--channel blockers in the thick ascending limb of the loop of Henle. Structure activity relationship. Pflügers Arch. **407**: S128-S141.

Warner A.E. (1972). Kinetic properties of the chloride conductance of frog muscle. J. Physiol. **227**: 291-312.

Watkins C.S. and Mathie A. (1994). Modulation of the gating of the transient outward potassium current of rat isolated cerebellar granule neurones by lanthanum. Pflügers Arch. **428**: 209-216.

Watkins C.S. and Mathie A. (1996). A non-inactivating K^+ current sensitive to muscarinic receptor activation in rat cultured cerebellar granule neurons. J. Physiol. **491**: 401-412.

Welsh M.J., Anderson M.P., Rich D.P., Berger H.A. and Sheppard D.N. (1994). The CFTR chloride channel. Current topics in membrane transport **42**: 153-171.

White M.M and Miller C. (1979). A voltage-gated anion channel from the electric organ of *Torpedo* californica. J. Biol. Chem. **254**: 10161-10166.

White M.M. and Aylwin M. (1990). Niflumic and flufenamic acids are potent reversible blockers of $Ca^{2(+)}$-activated Cl^- channels in *Xenopus* oocytes. Mol. Pharmacol. **37**: 720-724.

Wolff J.R., Joó F., Kása P., Storm-Mathison J., Toldi J. and Balcar V. (1986). Presence of neurons with GABA-like immunoreactivity in the superior cervical ganglion of the rat. Neurosci. Lett. **71**: 157-162.

Woodhull A.M. (1973). Ionic blockage of sodium channels in nerve. J. Gen. Physiol. **61**: 687-708.

Woodward J.K., Bianchi C.P. and Erulkar S.D. (1969). Electrolyte distribution in rabbit superior cervical ganglion. J. Neurochem. **16**: 289-299.

Wooltorton J.R.A. and Mathie A. (1995). Potent block of potassium currents in rat isolated sympathetic neurones by the uncharged form of the amitriptyline and related tricyclic compounds. Br. J. Pharmacol. **116**: 2191-2200.

Acknowledgements

I would like to express my gratitude to Dr. Alistair Mathie for being a supportive and helpful supervisor. Thanks to Dr. Chris Watkins for his ever ready assistance in the lab and to Dr. Maureen Docherty for her technical assistance with the RT-PCR experiments. I am grateful also to everybody else in the department who gave their help and friendship during the last three years. Financial support, provided by the MRC, was gratefully received. I would like to dedicate this Thesis to my friends for always being there.